CONTROL OF MECHANICAL JOINTS THAT HAVE JOINT CLEARANCE

A Thesis Submitted to the
Graduate School of Engineering and Sciences of
İzmir Institute of Technology
in Partial Fulfillment of the Requirements for the Degree of

MASTER OF SCIENCE

in Mechanical Engineering

By
Gün GÜNDÜZALP

March 2015
İZMİR

We approve the thesis of **Gün GÜNDÜZALP**

Examining Committee Members:

Assist. Prof. Dr. Mehmet İsmet Can DEDE
Department of Mechanical Engineering, Izmir Institute of Technology

Assist. Prof. Dr. Gökhan KİPER
Department of Mechanical Engineering, Izmir Institute of Technology

Assoc. Prof. Dr. Enver TATLICIOĞLU
Department of Electrical and Electronics Engineering, Izmir Institute of Technology

Prof. Dr. Serhan ÖZDEMİR
Department of Mechanical Engineering, İzmir Institute of Technology

Assist. Prof. Dr. Onursal ÖNEN
Department of Mechanical Engineering, Izmir Institute of Technology

19 March 2015

Assist. Prof. Dr. Mehmet İsmet Can DEDE
Supervisor,
Department of Mechanical Engineering,
İzmir Institute of Technology

Assist. Prof. Dr. Gökhan KİPER
Supervisor,
Department of Mechanical Engineering,
İzmir Institute of Technology

Prof.Dr. Metin TANOĞLU
Head of the Department of
Mechanical Engineering

Prof.Dr. Bilge KARAÇALI
Dean of the Graduate School of
Engineering and Sciences

ABSTRACT

CONTROL OF MECHANICAL JOINTS THAT HAVE JOINT CLEARANCE

Joint clearance is a defect that is present in all mechanical joints in every mechanism. Joint clearances for revolute joints result from the relatively small difference between the dimensions of diameters of two concentric bodies which interrelated to each other. Manufacturing errors, tolerances, wear, and material deformation lead to joint clearances. Due to these unavoidable reasons, joint clearance is inevitable and has negative impact on the dynamic response on the whole system. There are numerous previous studies to compensate for the effects of joint clearance. Input shaping method is used to reduce residual vibrations in computer controlled mechanical systems. This method operates by changing the shape of the input. The aim of this study is to adapt input shaping method to the controller of a mechanical joint, that have joint clearance to compensate for the negative effects of the joint clearance, especially residual vibrations. The input shaping method is a model-based approach and therefore, exact knowledge of the system model is required. In this thesis, the first work is carried out to identify the system model. This is accomplished in two stages for the system without joint clearance and with joint clearance. Later, the input shaping method is implemented and tested on the simulation model of the mechanical joint with joint clearance. After receiving acceptable results in simulation tests, the method is implemented on the experimental system and system response is evaluated for a variety of inputs. The experimental test results indicated that the input shaping method applied to the controller of a mechanical joint with joint clearance makes the system free of residual vibrations especially for the inputs with relatively higher acceleration and jerk profiles.

ÖZET

MAFSAL BOŞLUKLARI OLAN MEKANİK EKLEMLERİN DENETİMİ

Mafsal boşlukları her bir mekanizmanın tüm mekanik eklemlerinde bulunan hatalardır. Dönel mafsalların boşlukları, eş merkezli olarak birbirine bağlanan iki parçanın çaplarının birbirinin aynı olmamasından kaynaklanmaktadır. Boşlukların görülme sebeplerinden bazıları üretim hataları, işleme toleransları, parçada meydana gelen aşınmalar ve malzeme deformasyonlarıdır. Bu sebepler kaçınılamaz olduklarından, mafsal boşlukları tamamıyla giderilememektedirler ve tüm sistemin dinamik tepkisini olumsuz etkilemektedirler. Mafsal boşluklarının etkilerini azaltmak için birçok çalışma yapılmıştır. Şekillendirilmiş girdi yöntemi bilgisayar kontrollü sistemlerde artık titreşimleri azaltan bir yöntemdir. Bu yöntem, girdi komutunun şeklini değiştirme esasına dayalı olarak çalışmaktadır. Bu çalışmanın amacı, mafsal boşluklarının mekanizma üzerinde yarattığı özellikle istenmeyen artık titreşimler gibi negatif etkileri azaltmak için sisteme şekillendirilmiş girdi yöntemini uygulamaktır. Şekillendirilmiş girdi, model-temelli bir yaklaşım olduğu için sistem modeli ile ilgili kesin bilgiye ihtiyaç duyulmaktadır. Bu tezde ilk çalışma, sistem modelinin ortaya çıkarılması üzerine yapılmıştır. Sistem modeli çalışması mafsal boşluklu ve mafsal boşluksuz olarak iki kısımda yapılmıştır. Daha sonra şekillendirilmiş girdi mafsal boşluklu model üzerinde benzetim ortamında uygulanmış ve test edilmiştir. Benzetim ortamında kabul edilebilir sonuçlar alındıktan sonra şekillendirilmiş girdi metodu deneysel sistem üzerinde test edilmiş ve sistem tepkisi çeşitli girdiler için sınanmıştır. Deneysel test sonuçlarına göre, şekillendirilmiş girdi yönteminin özellikle yüksek ivme ve ivmelenme profillerine sahip girdiler uygulandığında sistemdeki mafsal boşluklarından kaynaklanan artık titreşimleri azaltmak için kullanılabileceği ortaya çıkmıştır.

TABLE OF CONTENTS

LIST OF FIGURES

Figure **Page**

LIST OF TABLES

CHAPTER 1

INTRODUCTION

Based on working conditions and the competitive environment, excellence and quality are important assets in business. Companies use robots to improve the quality, provide standard production and decrease labor and material costs. Furthermore, robots save people from monotonous jobs such as welding, painting and other tiring jobs. For all these reasons, robots have become one of the vital machines in industry. A robot is a re-programmable, controllable, multipurpose electro-mechanic machine designed to perform different duties (Craig 2005). Robots are used in different areas such as;

Mechanical production

- Pick and placement, alignment
- Assembly
- Tool and workpiece attachment
- Burnishing and polishing
- Measurement and control
- Storage
- Painting and welding
- Cutting

Space and sea researches

- Put the satellite into orbit
- Make an observation about benthos researchers

Nuclear plant

- Nuclear fuel load
- Nuclear damage control

Military defence area

- Observation and destruction robots

Medical area

Entertainment area

Industrial robots are widely used in mechanical production. A pick and place robot is shown in Figure 1.1. Such robots take and transport the part to the desired place fast and safely. Because of these properties, these robots are generally used in assembly lines (Ammattikorkeakoulu 2011).

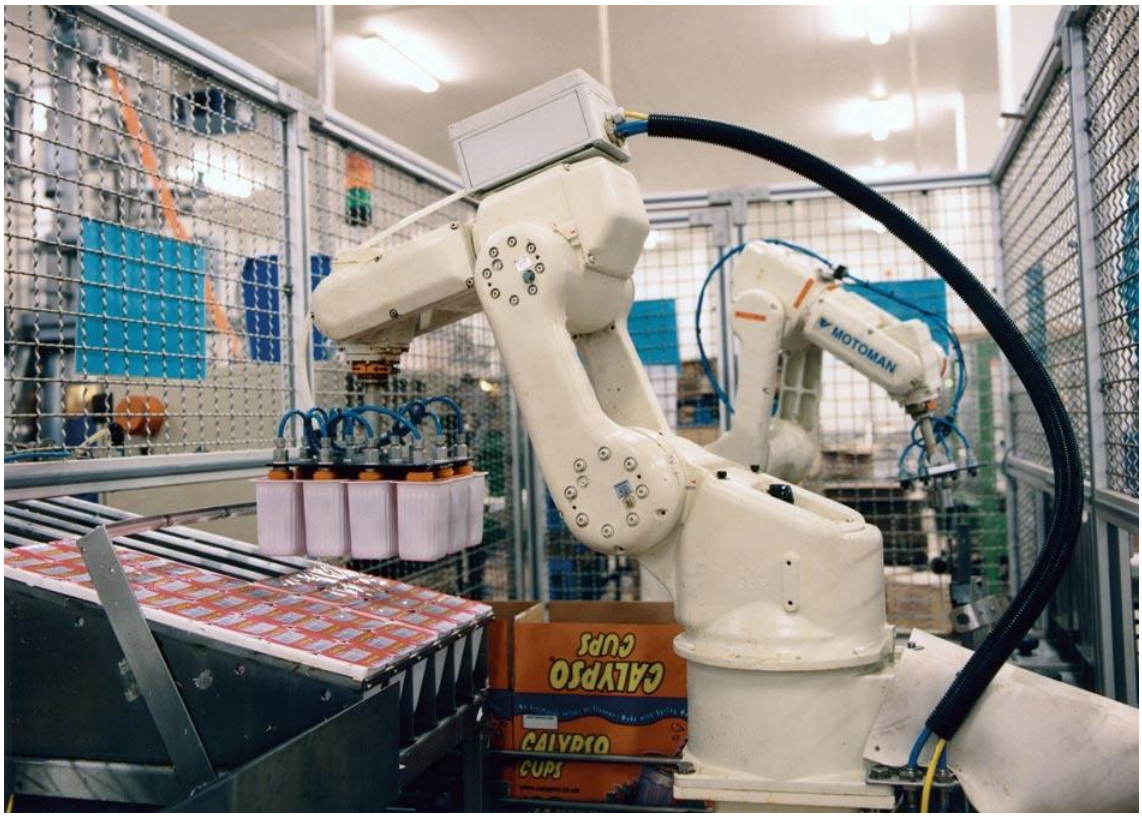

Figure 1.1. A pick and place robot
(Source: Robot palletizing 2015)

Robots are also used in automotive industry for painting and welding. Painting and welding are jobs that require extreme care and attention. Especially in welding robot position accuracy is vital (Ammattikorkeakoulu 2011). A welding robot is shown in Figure 1.2.

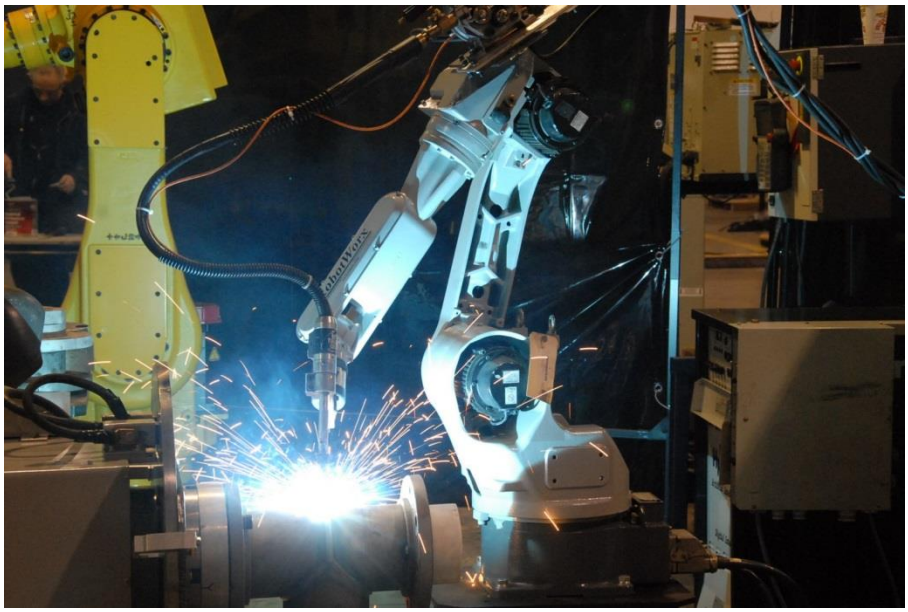

Figure 1.2. A welding robot
(Source: Robots 2015)

Robots are also used for laser cutting. The robots which are used for this task, require high accuracy and precision because of the sensitivity of the task. A laser cutting robot is displayed in Figure 1.3.

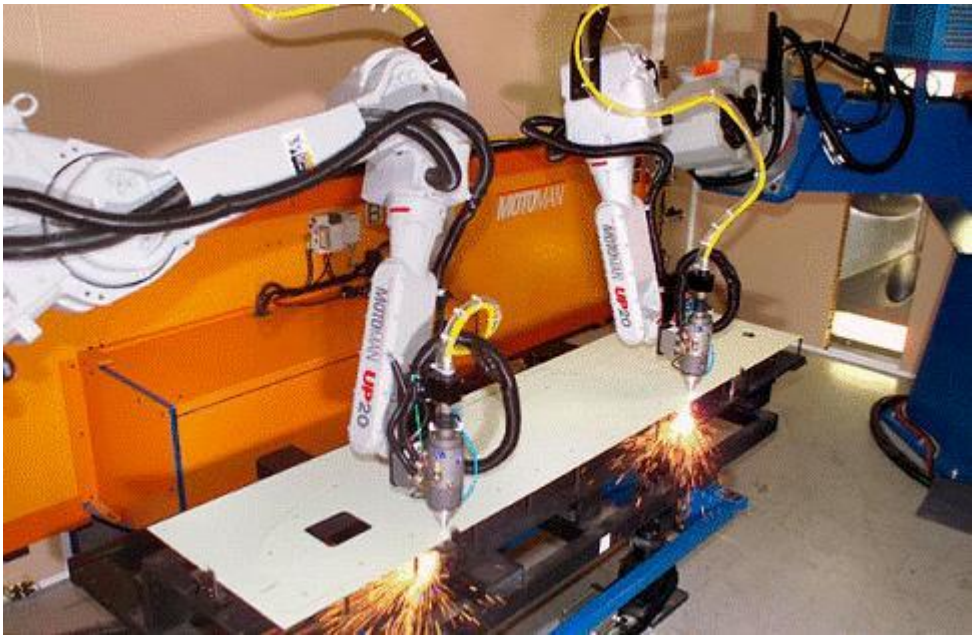

Figure 1.3. Laser cutting robots
(Source: Subsea World News 2015)

In assembly lines, especially in automotive area, robots are of great significance. Robots which are used in assembly lines do not only work fast but also accurately as demonstrated in Figure 1.4 (Ammattikorkeakoulu 2011).

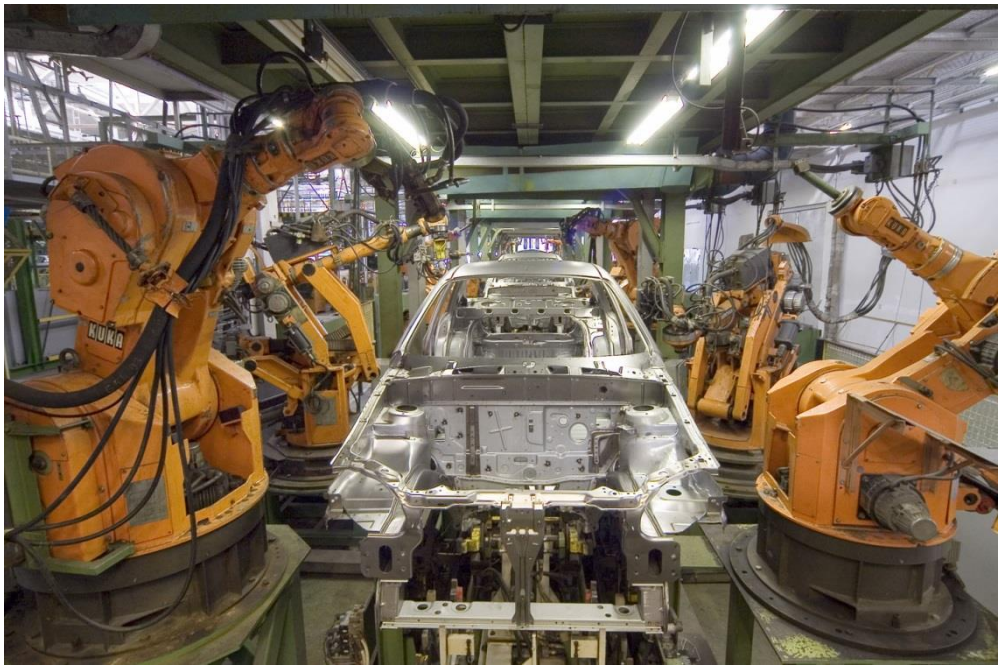

Figure 1.4. Assembly robots
(Source: Robots 2015)

Recently, robots have been increasingly used in medical area. Both rehabilitation robots and surgery robots are used in this field (Ammattikorkeakoulu 2011). A rehabilitation robot is shown in Figure 1.5.

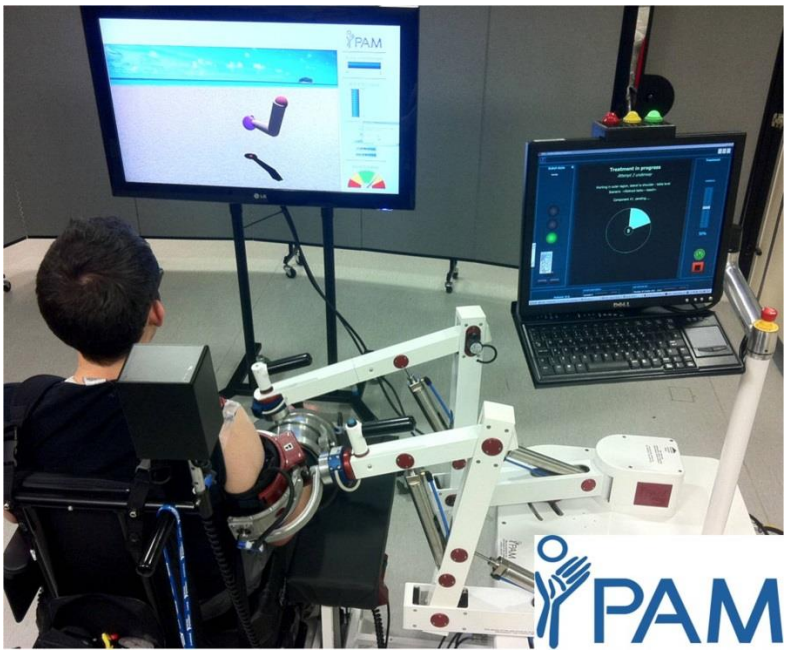

Figure 1.5. A rehabilitation robot
(Source: University of Leeds 2015)

1.1. Components of Industrial Robots

Industrial robotic manipulators contain 5 main components

- Controller
- Arm
- Drives
- End-Effector
- Sensors

Controller is the brain of an industrial robots and works like a computer. Controller manages the industrial robots and connects all systems together to work properly. Robot arm is a part that performs mechanical motion. Moreover industrial robot arm specifies the positioning of the end-effector. Most of the robot arms are produced to imitate human arms and have parts such as shoulder and wrist. Also, robot arm includes the end-effector and sensors on it. Drives are the actuators of the industrial robots. In industrial robots, drives are powered by electricity, hydraulics or pneumatics. The most common power type is electricity. If the robot is small, then pneumatic drive is better due to practical usage. On the other hand, if the system needs more power, hydraulic drive may be good option. End-effector is the hand of the industrial robot.

There are some variations with respect to their end task. Gripper, vacuum pump, magnets, welding and painting torches are some of the types of the end-effector. Sensors are special devices that allow the industrial robot to receive feedback about its surroundings. Sensors collect information from the environment and send this information back to the controller. A commonly used sensor is called an encoder which provides position information from the drives. Also sensors can be used in the field of computer vision and object recognition. For instance vision sensors allow a pick and place robot to differentiate between items to choose and items to ignore (Ammattikorkeakoulu 2011).

1.2. Classification of Robot Manipulators

Robots can be classified according to different criteria. Most common classification methods are;

Degree of Freedom

Kinematic Structure

- Serial Manipulator
- Parallel Manipulator
- Hybrid Manipulator

Workspace Geometry

- Cartesian
- Cylindrical
- Spherical
- Jointed Arm
- SCARA

1.2.1. Degree of Freedom

One of the classification criterion for robot manipulators is the degree of freedom (DoF). DoF of mechanical systems is described as a number of independent parameters which is used to characterize the system (Ammattikorkeakoulu 2011). Since

driving parts depend on the number of independent inputs, DoF has an important role in describing the mechanical system.

The capacity of a robot manipulator motion is determined by the motion capacity of the end-effector. Some of the motion axes are constraints, but the others are free. These free directions of motions indicate the DoF of the robot manipulators. If a robot manipulator has just one axis to rotate or translate, then it is a called single DoF mechanism. However, if a robot manipulator has multiple axes to rotate and/or translate, then the number of free directions describes the number of DoF of robot manipulator.

In a plane an unconstrained rigid body has three DoF. One of them is used for rotation and the others are used for translation.

Robot manipulators need six DoF in three-dimensional space. These six DoF consist of three rotations and three translations.

1.2.2. Kinematic Structure

Robots can be also classified according to their kinematic structure. Serial manipulators are the most common robot manipulators in industry (Figure 1.6). These robots are designed as a series of links connected by motor actuated joints that extend from a base to an end effector. A serial manipulator consists of an open loop chain comprising a number of rigid links connected with joints. The advantages of serial manipulators over other types of manipulators can be listed as (Angeles 2003):

- simplicity in manufacturing
- easy to control
- have a large workspace with respect to the size of robot
- floor space it occupies is smaller

On the other hand serial manipulators also have some drawbacks such as;

- low stiffness because of the open loop chain
- manages low effective load
- errors cumulate when the number of links increase

Figure 1.6. Serial manipulator
(Source: Innova 2015)

A parallel manipulator is a system that uses several serial chains to support a platform or several platforms. It comprises closed loop chains. Two well-known parallel manipulators are the Stewart platform and the Delta robot. The advantages of parallel manipulators over serial manipulators can be listed as (Angeles 2003):

- rigid against undesired movements
- high precision and high accuracy
- high speed
- heavy actuators can be centrally mounted on a single platform
- errors do not cumulate when the number of links increase

On the other hand the drawbacks of parallel manipulators are as follows;

- limited workspace
- link geometries are limited to avoid collisions

Figure 1.7. Stewart platforms
(Source: Wikipedia 2015)

1.3. Joint Structures in Industrial Robots

That the mechanism of a robot manipulator comprises links and joints. There are several types of joints used for industrial robots. Most common joint types are shown in Figure 1.8.

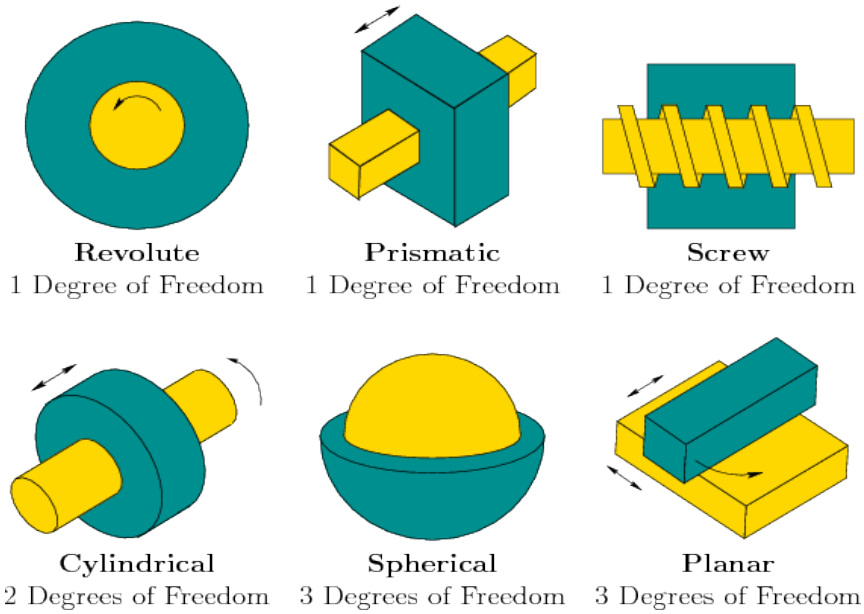

Figure 1.8.Joint types
(Source: Planning Algorithms 2006)

The revolute joints enable the two links connected to each other to rotate about a direction with respect to each other. Revolute joints have single DoF.

The prismatic joints admit only translation along a direction between the two connected links. This joint is also called sliding joint. Prismatic joints have also single DoF.

The screw joints let helical motion between the connected bodies. This helical motion comprises both sliding and rotational motions. Both of these motions depend on the helix angle of the thread. If the helix angle is zero, the screw will rotate. On the other hand, if the helix angle is 90°, the screw will slide. Helical joints have one DoF.

The cylindrical joints allow rotation about one direction and translation along the same direction. Cylindrical joints have two DoF.

The spherical joints, also called ball joints, allow rotation about any direction between the connected links. Spherical joints have three DoF.

The flat joint is also called planar joint. It has three DoF. Two of the DoF provide translation, and the other one provides rotation.

Each of these joints are of great importance for the performance of the robot. Two important measures for the performance of robot manipulators are accuracy and repeatability (Ammattikorkeakoulu 2011).

1.4. Accuracy and Repeatability

All robots are programmed to complete their tasks. However in the applications, most of the time, the results differ from the expected behavior. One of these errors is the positioning errors of the end-effector. There are several reasons for these positioning errors. Backlash problems, sensor sensitivity, rigidity and noise are some of sources of errors. Due to these errors, accuracy and repeatability errors appear. The positioning accuracy of a robot manipulator is concerned with the proximity about the position of the end effector and the desired location. Computational errors, machining accuracy in the construction of the manipulator, flexibility effects such as the bending of the links under gravitational and other loads, joint backlash and other static and dynamic effects affect the accuracy. On the other hand, the repeatability of a robot manipulator is related with the success in repeating the task. Controller resolution is one of the most affective

factors on the repeatability. In Figure 1.9 the accuracy and the repeatability concepts are demonstrated (Pandilov and Dukovski 2014).

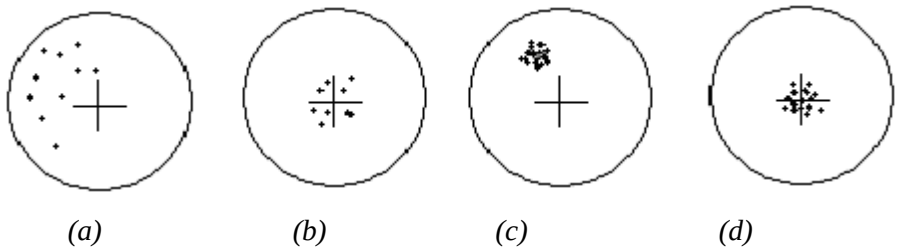

Figure 1.9.Accuracy and repeatability
(Source: Pandilov and Dukovski 2014)

In Figure 1.9 (a) there is a distance between the desired point and the end-effector position. The end-effector position changes in different attempts. For these reasons, attempt (a) is called as low accuracy and repeatability. In Figure 1.9 (b) the difference between the desired point and the end-effector position is acceptable but the repeatability cannot meet the expectations. In these circumstances it is called as high accuracy but low repeatability. In Figure 1.9 (c) the exact opposite situation occurs. Even though the repeatability is good, the accuracy is bad. This situation is called high repeatability but low accuracy. In Figure 1.9 (d) all the conditions are provided perfectly. It is called high accuracy and repeatability, which is the desired behavior for all robots. The most significant factor generating these errors is joint errors.

1.5. Accuracy and Repeatability Errors

The flexibility of joints and kinematic errors in the transmission systems result in positioning errors. Accuracy and repeatability errors may be due to manufacturing tolerances, joint axis misalignments, backlash in joints, flexibility of links and joints, thermal effects, resolution of encoders and control commands.

Most geometric errors of a robot result from manufacturing imperfections, misalignments and joint wear. Thermal effects arise from thermal distortion and expansions of robot components owing to both internal and external heat sources such as motors, friction and ambient temperature change.

The accuracy of robot manipulators can be enhanced by calibration. Calibration is the procedure for analyzing and reforming the positional accuracy. Calibration has four stages: modeling, measurement, identification and compensation. The identification stage provides estimates of the parameters of the model. Kinematic construction parameters such as manufactured link lengths, steady state errors in joint positions and payload carried by the manipulators are some of the factors which affect the mathematical model of the system. In compensation, various techniques such as model based method and sensor based method are used. When two methods are compared with respect to accuracy, sensor based method is more effective than the model based method.

An electric motor is a force or torque generator. The motor power changes with the amplitude of the both angular velocity and torque. If the input power in the electric motor is constant then torque is inversely related to the angular speed. When high torque values are required, speed reducers, i.e. torque amplifiers are used to increase the output torque. There are different types of torque amplifiers such as gearboxes, pulley and timing belt mechanisms, harmonic drive and capstan drive used in industrial robots.

In the long term usage of a gearbox, wear occurs. Because of the wear in the gearbox, backlash problem grows in time.

In a pulley and timing belt mechanisms, the timing belt is enveloped by a flex spline with teeth. In this torque amplifier, the contact happens between the timing belt and the two pulleys. Thus the contact is soft and backlash problem does not affect the system. On the other hand, backdrivability is a significant problem in pulley and timing belt mechanisms. A pulley and timing belt mechanism is shown in Figure 1.10.

Figure 1.10.Pulley and timing belt mechanism
(Source: Ming 2003)

Harmonic drives comprise three parts: elliptical wave generator, flex spline and rigid circular spline. The elliptical wave generator is an elliptical bearing coupled to the motor drive shaft. The flex spline is a non-rigid cup whose inner surface clutches the wave generator at the open end of the cup. The edge of flex spline fits to the wave generator elliptical shape as the generator rotates. The outer surface of the flex spline has teeth which contact the internal teeth of the rigid circular spline. According to the rigid circular spline, the flex spline has two less teeth. For this reason, a relative motion which occurs between the rigid circular spline and the flex spline is generated by rotation of the wave generation.

Capstan drive mechanisms are particularly used in haptic devices to increase the torque value. A capstan drive includes smooth cables to envelope pulleys of differing diameter to provide a reduction ratio. Various envelopes of cable supplies high friction contact between pulleys without slide. Though, the reduction ratio of the capstan drive is limited.

1.5.1. Gearbox Backlashes

Gears are the commonly used transmission elements in industry. The movement of robot manipulators depends on the transmission in joints. Despite this, transmission in joints is not ideal for some situations especially with high gear ratios.

Backlash is a clearance in mechanisms caused by gaps between the parts especially between the teeth of the meshing gears as shown in Figure 1.11. Backlash is also described as the maximum distance through which any part of a mechanical system can be moved in one direction without implementing any remarkable force or motion to the next part (Jawale and Thorat 2013).

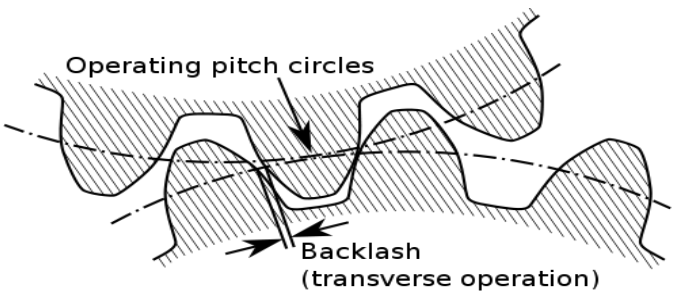

Figure 1.11.Backlash
(Source: Wikipedia 2014)

In precision positioning applications backlash directly affects the positioning accuracy. Thus backlash has an important role for robot manipulators. There are two main methods used for reducing the backlash. The first method, which is called static method, is related to the assembling of the gears. On the other hand, the second method, which is called dynamic method, is based on external forces which continuously remove all backlashes without considering rotational position.

Precision planetary servo gearheads are often significant components of a servo system, not only providing a mechanical advantage but also being able to control large loads quickly. Also servo gearheads supply speed and inertia reduction and torque manipulation. In planetary gears, backlash may be about 1°-2°.

1.5.2. Joint Clearances

Joints are crucial elements of robot manipulator systems and are either rigid or flexible. The dynamic response of the system depends on different factors about joints. Joint clearance, lubrication, friction and impact forces are some of the important factors which affect dynamic response of the system.

For revolute joints, joint clearance occurs as a difference between the diameter of the pin and the housing of the mechanical joint as shown in Figure 1.12 (Ting et al. 2000).

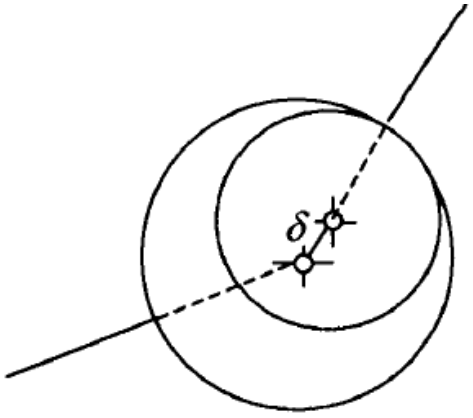

Figure 1.12.Joint clearances
(Source: Ting et al. 2000)

The manufacturing errors, part tolerance mismatches, wears, part deformations and imperfections result in joint clearance. Because of these unavoidable errors joint clearance is inevitable.

Since joint clearances are inevitable, compensating the effects of joint clearances is of significant importance for the robot manipulators. Joint clearance has crucial role on dynamic stability and performance of robot manipulators (Schwab et al. 2002). Some of the negative effects due to joint clearances are;

- Increase of residual vibration and noise
- Decrease of parts life
- Loss of positioning accuracy

Joint clearances cause uncertainty in the end-effector position and direction because of the unpredictable effects (Erkaya and Uzmay 2010).

Each joint clearance acts like a small link and adds an extra DoF to the linkage (Figure 1.13). For this reason, there is a redundant freedom created, and it affects uncertainty of the positioning of the robot manipulator. In serial manipulators because of the geometrical design, the effects of joint clearances cumulate at each link. Even if the magnitude of joint clearance is small, it might have a crucial role on the end effector's position.

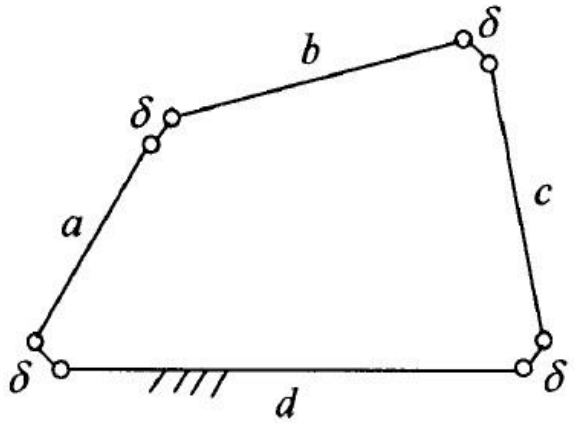

Figure 1.13.Four-bar mechanisms with clearance
(Source: Ting et al. 2000)

1.6. Input Shaping

Input shaping is a feed-forward method of reducing the residual vibrations in computer controlled systems. This method works by varying the shape of the input commands and is mostly combined with feedback controller such as proportional-integrator-derivative (PID) control, variable structure control, positive position feedback (PPF) control and auto disturbance rejection control (ADRC). Input shaping is generally used in space-based antenna, cranes, pendulums, bridges, flexible manipulators and flexible spacecrafts. The advantages of the input shaping are;

- Reduce residual vibrations effectively
- Precision to frequency uncertainty
- Increase settling time
- Develop positioning accuracy
- Simple design
- Available used for a multimode system

On the other hand, the main drawback of this method is system uncertainties which result from both model errors and changes in the system parameters (Luo et al. 2013).

The input shaping studies started based on linear systems. Simple schematic of this technique is shown in Figure 1.14. This figure shows that input shaping is applied by convolving a sequence of impulses by an input shaper, with a desired system command. Then the convolved signal is used to generate the system (Luo et al. 2013).

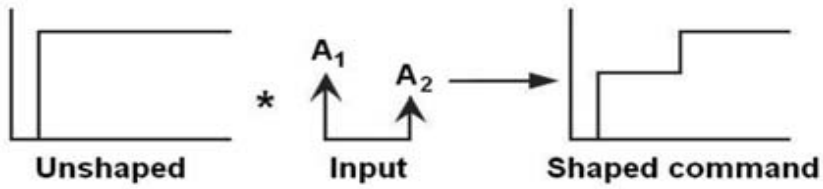

Figure 1.14.Input shaping method
(Source: Luo et al. 2013)

The input shaping process is demonstrated in Figure 1.15 with a two-impulse shaper. The duration of the shaped input originates from addition of the duration of the unshaped input to the duration of the shaper. Generally a shaper has the ability to involve in any number of impulses and in any duration. However, the difficult part of

input shaping is to create an input shaper to succeed the performance level. A shaper is created by producing a set of dynamical constraint equations which limit the residual vibrations and ensure some level of robustness to modelling errors (Singhose et al. 1996).

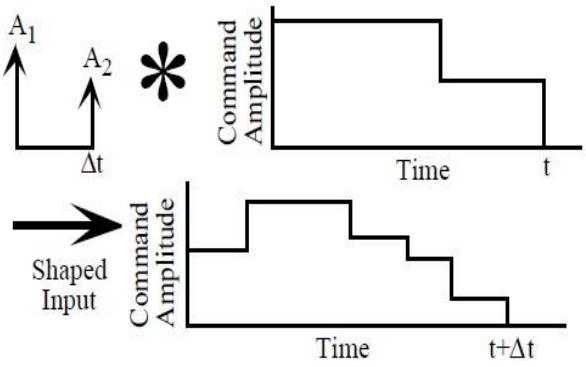

Figure 1.15.Input shaping process
(Source: Singhose et al. 2013)

1.7. Aim of the Study

The aim of this study is to adapt input shaping method to the controller of a single DoF mechanism to compensate for the negative effects of joint clearance such as residual vibrations.

1.8. Outline

In Chapter 2, literature review on previous studies about joint clearance and input shaping are given. In the second part, the different models are investigated for joint clearance and input shaping.

Chapter 3, the methodology part, involves information related to data collection and data analysis. In this part, simulations and experimental test setups are described. Moreover the joint clearance and control models are shown in this part.

System identification studies are presented in Chapter 4. The parameters necessary for the transfer function representing the mechanical system are determined based on measurements on the experiment set-up.

Simulation and experimental tests are presented in Chapter 5. The results of the simulation and experimental tests are compared with respect to their effects on reduction of joint clearance. Input shaping method is implemented and the results of without input shaping and input shaping are compared.

The last chapter is for the conclusions. In this part, a brief review of the study, implications of the results and suggestions for the future works are stated.

CHAPTER 2

LITERATURE SURVEY

Joint clearance is widely investigated in the literature regarding its affects and modelling techniques. It is not possible to fully eliminate joint clearances in mechanical systems. This leads to the investigation of reasons, affects and mathematical modelling of joint clearance. The aim of this chapter is to present a survey on modelling of joint clearance and input shaping, as a possible solution for reducing joint clearance's affect.

2.1. Survey on Joint Clearance

A kinematic model to understand the effects of joint clearance is introduced by Ting et al. (2000), in which direction deviation is investigated for both single DoF mechanisms and multi-dof mechanisms. This study presents a novel and simple approach to describe the worst position and direction errors due to the joint clearance of linkages and robot manipulators. Ting et al. show that the magnitude and direction of the errors created by joint clearance changes by DoF.

Bauchau and Rodriguez (2002) created a model of joint clearance for flexible multibody systems which are generally used in aerospace applications. In their study, the negative effects of joint clearance are investigated and results are presented numerically for both revolute and spherical joints of a slider-crank mechanism. The formulation used to create a joint clearance model is adapted within the framework of energy preserving and decaying time integration schemes methods. As a result it is stated that to calculate the effects of joint clearance one needs appropriate conditions such as not only a suitable model of the elasticity of the system but also a proper simulation of the drive system.

In (Zhu and Ting 2000), general probability density functions of the end-effector for both planar and spatial robots are presented. By generating a probability density function for the end effector position distributions, the repeatability of robot manipulator is calculated and uncertainties are reduced.

In literature, researchers adapt dynamic models to identify the joint clearance and predict their behaviors in mechanical systems. First, the joint clearance's impact on dynamics of revolute joint is investigated by Schwab et al. (2002). Various continuous force contact models and impact models are compared with respect to their dynamic effects on both rigid and elastic bodies. Hertzian contact model, hydrodynamic bearing model and discontinuous contact force model are illustrated for a slider-crank mechanism with a revolute joint clearance. As a result of experimentation, it is deduced that in lubricated models, dynamic response of the system is improved compared to the unlubricated models. In another study, Ravn (1998) implements continuous contact force models which include Kelvin-Voigt, Hertzian and line contact force on a slider-crank mechanism and a double pendulum with revolute joints and compared simulation results. The main purpose of this paper is to measure the reduction in the performance caused by joint clearance by different modelling techniques. As the result of these tests, continuous contact force model gave the best result for predicting dynamic behavior of joint clearance. Zhang et al. (2014) implemented a joint clearance model on a 3-RRR planar parallel mechanism, which has six defective joints with different loads, and discussed the result for various end-effector trajectories. Newton-Euler equations, Lankarani-Nikravesh contact force model and Coulomb friction force model are used in this study. Also Baumgarte stabilization approach is used to develop the stability. In conclusion, it is claimed that heavy loads create high impact forces and deeper penetration depth and cause dynamic response of the system become more instable. In addition, velocity directly affects efficiency of the system.

In (Tsai and Lai 2004) joint clearance is modelled as a virtual link to analyze the transmission performance of links. Joint clearances are added to the model as equivalent kinematic pairs. Not only link-length equations but also reciprocal relationships between joint twist screw and joint transmission wrench screw are used to solve the position level kinematics of a single loop linkage.

In a more recent study, Tsai and Lai (2008) have developed a generalized method for error analysis of multi-loop mechanisms with joint clearances by utilizing virtual links. In additions to the previous study, the tests are implemented on six-bar linkages with various specified input links. As a result they have proved that joint clearance errors can be properly modeled by using this generalized method in planar multi-loop mechanisms.

In (Liu et al. 2012), Absolute Coordinate Based method, which consists of the Natural Coordinate Formulation for rigid bodies and Absolute Nodal Coordinate Formulation for flexible bodies is used to control a multibody system with multiple cylindrical clearance joints. In addition, joint trajectories are followed by means of a PID controller with feed forward torque.

In (Xu et al. 2012) Hertzian continuous contact force model is implemented for a slider-crank mechanism which has a deep groove ball bearing joint to develop a generalized method for dynamic modeling and analysis of planar multibody systems.

In (Parenti-Castelli and Venanzi 2005) kinematic modeling and specifying a configuration of mechanism are investigated to determine the effects of the clearance. This study proposes a new procedure for the calculation of the position error on the links by using a local kineostatic model. This new method is suitable for investigating the effects of clearance for both static and dynamical systems.

Nonlinear equivalent spring-damper model and Coulomb friction model are used in (Zhao and Bai 2011) to obtain a practical method for the analysis of the dynamic characteristics of a space robot manipulator with joint clearances. The effect of joint clearance on angular velocity and acceleration is examined.

The vibrations and noises caused by joint clearances are investigated with experiments in (Erkaya and Uzmay 2010). As a model, planar slider-crank mechanism with two joint clearances is used and joint clearances are modelled as massless virtual links. As a result of these tests it is proved that joint clearances cause degradation in vibration characteristics, thus it increases both vibration and noise level compared to the mechanism without joint clearance. In addition to that, high contact force values affect dynamic performance of the mechanism negatively.

Types of planar revolute joint clearances are described in (Flores and Ambrosio 2004). Moreover the differences between continuous and discontinuous contact force models are specified clearly. Furthermore the methodologies are tested and proved for a slider-crank mechanism with revolute joint clearance.

In (Flores et al. 2010), multibody clearance joint models are discussed and investigated not only numerically but also experimentally by using a slider-crank mechanism. The main target of this paper is to provide an experimental confirmation of the predictive abilities of the clearance joint models.

All these studies about joint clearances are summarized in Table 2.1.

Table 2.1 Comparisons of joint clearances studies

	Joint Clearances							
		Modeling Joint Clearances						
		Kinematic Model			Force Model			
	Joint Clearances Effect	Virtual Link	Revolute Joint	Spherical Joint	Continuous Force Model	Discontinuous Force Model	Simulation Tests	Experiment Tests
Ting et al. 2000		+					+	
Bauchau and Rodriguez 2002	+		+	+			+	
Zhu and Ting 2000	+		+				+	
Schwab et al. 2002	+		+		+	+		
Ravn 1998	+		+		+	+	+	+
Zhang et al. 2014	+		+				+	
Tsai and Lai 2004		+					+	
Tsai and Lai 2008		+					+	
Liu et al. 2012				+	+		+	
Xu et al. 2012			+		+		+	
Parenti-Castelli and Venanzi 2005	+			+			+	
Zhao and Bai 2011			+		+		+	
Erkaya and Uzmay 2010	+	+			+			+
Flores and Ambrosio 2004			+		+		+	
Flores et al. 2010			+		+		+	+

2.2. Survey on Input Shaping

In (Luo et al. 2013), vibration control strategy which combines the input shaping technique and auto disturbance rejection controller is described and implemented by simulation and experiments with a flexible manipulator.

In (Singhose and Singer 1996), the effects on input shaping on following circular and square trajectory is investigated for simulating the response of a fourth-order system. In the experimental part, input shaping method is implemented and the result of these experiment compared to the without input shaping methods. According to this comparison, following the trajectory is improved by using input shaping method.

Procedures for precisely specifying the degree of robustness for several input shaping methods are discussed in (Singhose et al. 1996). Also, characteristics of the input shaper and constraint equations are described and presented.

Pre-shaping command inputs are implemented on the Draper Laboratory's Space Shuttle Remote Manipulator System Simulator. (Singer and Seering 1990) applied input shaping for a closed loop system. Moreover, a new approach is proposed in terms of the content of the system input and output. As oppose to most researchers, Singer and Seering (1990) identified transient residual vibration as a function of its transient input.

Hyde and Seering (1991) developed the multiple mode input shaper method. The main goal of this study is is not only applying the new method easily on the real system, but also decrease time delays. However, the results failed to satisfy the requirements because of linear system equations for a non-linear system.

Magee and Book (1992) worked on the robustness criterion for input shapers. Moreover they used frequency response analysis for reducing the vibrations. Experiments are conducted on a two dof flexible manipulator. The main advantage of the proposed robustness constraint over the robustness criterion for the original input shaping method of (Singer and Seering 1990) is providing high insight on reducing residual vibrations.

In (Crain et al. 1996), shaper design techniques for multi-mode systems are examined in detail. Shapers can be determined separately and then convolved, or they can be determined simultaneously for using constraint equations. In thieir study, these two methods are compared with respect to function of the mode ratio with simulations and experiments.

In (Shan et al. 2005), input shaping method is modified for robustness and multimode vibration reduction. Modified input shaping with a PD feedback controller is implemented on a rotating single link flexible manipulator and tested both with simulations and experiments. It is proved that this new method can be used to reduce residual vibrations.

In (Chen et al. 2013), for the first time input uncertainties and joint clearance are thought together for accuracy performance. The planar 3-RRR parallel manipulator is used for numerical examples.

All these studies about joint clearances are summarized in Table 2.2.

Table 2.2 Comparisons of input shaping studies

	Input Shaping							
	Constraint Equations	Control System Design			Manipulator Type		Simulation Tests	Experiment Tests
		ZV Shaper	ZVD Shaper	ZVDD Shaper	Rigid Manipulator	Flexible Manipulator		
Luo et al. 2013		+	+	+		+	+	+
Singhose and Singer 1996			+			+	+	
Singhose et al. 1996	+	+	+			+	+	
Singer and Seering 1990	+	+	+	+			+	+
Hyde and Seering 1991	+					+		+
Magee and Book 1992	+	+				+		+
Crain et al. 1996	+	+	+				+	+
Shan et al. 2005		+	+	+		+	+	+

2.3. Joint Clearance Modeling

Because of unavoidability of joint clearance, modeling of joint clearance is important in order to compensate the effects of joint clearance. The modeling of joint clearance consists of two phases: kinematic part and force contact condition.

2.3.1 Joint Clearance Kinematics

For an ideal revolute joint, the joint axes of the two bodies are coincident. However in practice, a revolute joint clearance results in free translation of the journal inside the bearing. Accordingly, revolute joint clearance adds two extra DoF. For this reason, the journal moves inside the bearing boundaries easily. When the journal reaches the boundary, an impact occurs and contact forces occur, affecting the dynamics of the system.

Generally, main modeling strategies for mechanical systems with revolute joint clearance are divided into three approaches:

- Massless link approach
- Spring-damper approach
- Momentum exchange approach

In the massless link approach, the revolute joint clearance is modeled by adding a link of zero mass that has a constant length equal to the radial clearance, as shown in Figure 2.1. Thus, mechanism gets an extra degree of freedom.

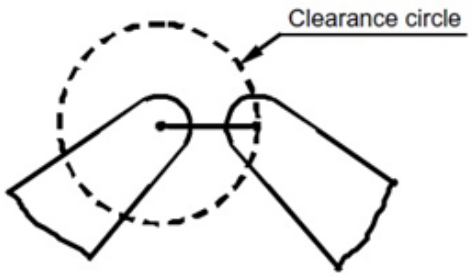

Figure 2.1 Massless link approaches in revolute joint clearance
(Source: Flores and Ambrosio 2004)

In the spring-damper approach, the clearance is modeled by adding a spring-damper element to simulate the flexibility of the contact. On the other hand this approach is inadequate to represent the physical nature of energy transfer during the impact process. In addition to this, identifying the parameters of the spring and damper elements may be hard and this is another disadvantage of the spring-damper approach. In Figure 2.2 spring-damper approach is illustrated.

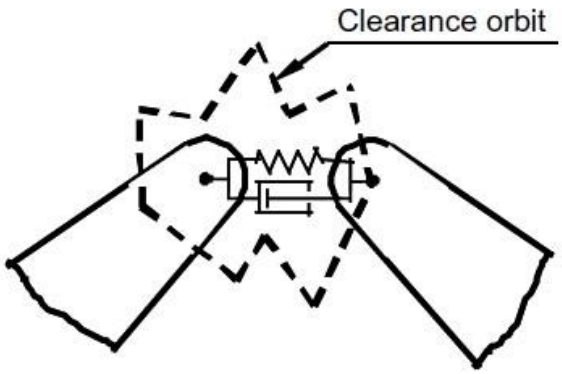

Figure 2.2 Spring-damper approach in revolute joint clearance
(Source: Flores and Ambrosio 2004)

In momentum exchange approach, the journal and bearing parts are taken into consideration as two contacting bodies and thus contact forces arises and controls the dynamics of the joint clearance.

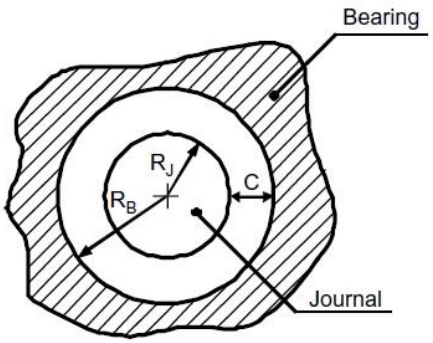

Figure 2.3 Momentum exchange approach in revolute joint clearance
(Source: Flores and Ambrosio 2004)

The presence of impacts in the joints causes high level of contact forces during dynamic analysis. Radial clearance is strictly relevant to the model of contact forces. In both of massless link approach and spring-damper approach, joint clearance is simulated with a constant or variable distance. However in momentum exchange approach, the contact force models are constructed as a function of the elasticity properties of contacting surfaces. Thus the dissipation of energy during the impact is considered.

In the most general form, for a revolute joint, joint clearance is mostly modeled by the horizontal and vertical displacements of the journal center related to the sleeve center as depicted in Figure 2.4.

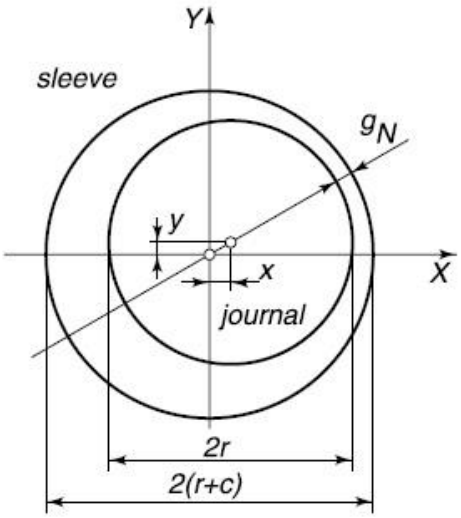

Figure 2.4 Planar revolute joint clearances
(Source: Schwab et al. 2002)

In this figure r represents radius of journal, c represents the radial clearance and g_n is the kinematic contact condition. g_n is calculated as;

$$g_n = c - \sqrt{x^2 + y^2} \tag{2.1}$$

There is no contact if $g_n > 0$. Contact with local deformation near the contact zone, i.e. penetration, is specified by a negative value of g_n.

2.3.2. Force Contact Models

One of the key points of modeling of joint clearance is the simulation of force contact models. These force contact models are categorized in two parts according to duration of contact: continuous and discontinuous force contact model.

2.3.2.1. Continuous Force Contact Models

In the continuous force contact approach, duration of contact is finite. The time history of the forces acting between the contacting bodies which can be either rigid or deformable is clearly calculated during the simulation. In the continuous contact force model, the forces resulting from the collisions are assumed to be a continuous function of deformation. Thus velocities in this force contacts are continuous.

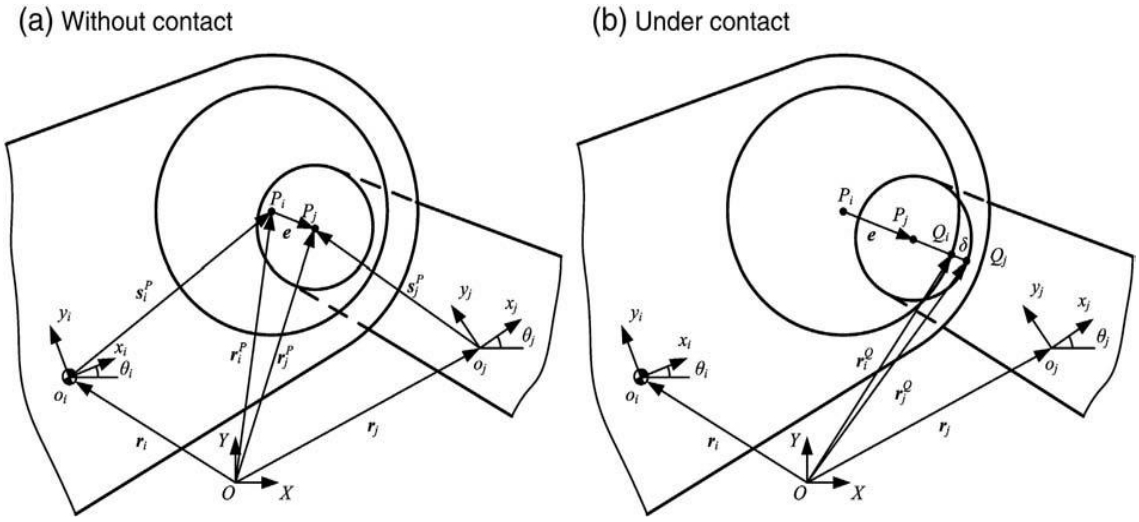

Figure 2.5 Continuous force contact model in planar revolute joint clearances (Source: Xuchong et al. 2014)

No contact and contact modes are demonstrated in Figure 2.5. When contact is detected, a kinematic constraint is implemented. During the contact, force is a continuous function of deformation. When contact is detected, the force is applied normal to the contact. The best known models of these continuous contact models are Kelvin-Voigt contact model which is used for linear systems such as a spring/dash-pot and Hertzian contact model which is used for nonlinear systems.

Kelvin-Voigt continuous contact force model is the simplest and it is a viscoelastic contact force model. In this contact model, there has a linear correlation between the impact force and penetration depth. Energy losses are elementarily accounted for multiplying the rebound force by the coefficient of restitution, e. In Kelvin-Voigt contact model the force is determined as;

$$F_N = \delta c \; ; \nu_N > 0 \tag{2.2}$$

$$F_N = e\delta c \; ; \nu_N < 0 \tag{2.3}$$

where δ describes penetration depth, c is a spring constant and ν_N is the normal relative speed. Despite the simplest contact model, the main drawback of Kelvin-Voigt model is determining the spring constant. This spring constant changes with the geometry and material properties of the bodies in contact. For this reason it is very difficult to correlate the impact force with the penetration depth.

On the other hand, Hertzian continuous contact force model involves a nonlinear correlation between impact forces and penetration depth. Hertzian contact force model is usually preferred in situations where there is insufficient information about the contact area, especially for unlubricated joints. In modified Hertzian contact force model (Lankarani and Nikravesh 1994), contact force is describes as;

$$F_N = \begin{cases} K\delta^n + D\dot{\delta}; \; \delta > 0 \\ 0 \quad ; \delta \le 0 \end{cases} \tag{2.4}$$

In the formulation, n= 3/2, K represents stiffness coefficient, D is hysteretic damping coefficient and δ is the penetration depth. The stiffness coefficient is also calculated as

$$K = \frac{4}{3\pi\left(h_1 + h_2\right)}\sqrt{\bar{R}} \tag{2.5}$$

$$\bar{R} = \frac{R_1 R_2}{R_1 + R_2} \; ; h_i = \frac{1-\nu^2{}_i}{\pi E_i} \; ; i = 1, 2, \ldots \tag{2.6}$$

where R_1 and R_2 are radii of the spheres, ν is the Poisson's ratio and E_i is the Young's modulus of the each sphere. In addition to that, the damping coefficient is calculated as;

$$D = H\delta^n \; ; where \, H = \frac{3K\left(1-e^2\right)}{4\dot{\delta}^-} \tag{2.7}$$

where H is the hysteretic damping factor, e is the coefficient of restitution and $\dot{\delta}^{-}$ is the penetration speed before impact.

One of the main disadvantages of Hertzian contact model is the involvement of the impact velocity $\dot{\delta}^{-}$. In some situations, due to this impact velocity the Hertzian contact model does not work properly. Additionally since the dissipated energy is ignored, high velocity values occur after the impact.

Hertzian continuous contact model can also be used for line contact force model. Thus this contact model can also be used for cylinders. A rectangular contact area is modelled between two cylinders with parallel axes. Line contact force model assumes exact parallel alignment of the colliding cylinders. Moreover, other limitations of this contact model is that uniform force distribution is assumed over the length of the cylinders and some outer effects such boundary effects are neglected. With all these conditions, the penetration depth is determined as

$$\delta = \left(\frac{h_1 + h_2}{2a}\right)\left[ln\left(\frac{8a^3}{F_N \bar{R}\left(h_1 + h_2\right)}\right) + 1\right]F_N \tag{2.8}$$

where a a is the half length of cylinder. h_1, h_2 and $\bar{R}$ are same as in Equation 2.6.

Moreover the friction is also taken into consideration when the impact velocity has a tangential component. The dynamic friction force is modeled as Coulomb friction. The tangential force is determined as

$$F_T = -\frac{\vartheta_T}{|\vartheta_T|}\mu F_N \tag{2.9}$$

where ϑ_T is the tangential velocity, μ is the friction coefficient and F_N is the normal contact force. Friction model is expected to manage to detect sliding and sticking during the impact, so the friction forces play critical role in discontinuous contact force models. On the other hand, hydrodynamic contact model is the simplest type of fluid film bearing model for revolute joints. In this contact model contact force is calculated as;

$$\begin{bmatrix} F_x \\ F_y \end{bmatrix} = 2\upsilon l\left(\frac{r}{c}\right)^3 v_s \begin{bmatrix} \cos\varphi & -sin\varphi \\ \sin\varphi & \cos\varphi \end{bmatrix}\begin{bmatrix} W_x \\ W_y \end{bmatrix} \tag{2.10}$$

where r is the radius of the journal, c is the radial clearance, l is the bearing length, υ is the lubricant dynamic viscosity, v_s is the pure-squeeze velocity and W_x and W_y are the components of dimensionless damping coefficients.

In a revolute clearance joint, three modes of motion, called continuous contact mode, free-flight mode and impact mode exist between the journal and the bearing. In the continuous contact mode, the journal and the bearing come into contact and sliding motion occurs. The penetration depth changes along the boundary of the journal. When the journal and the bearing is separated, continuous contact mode is finalized and free-flight mode starts. In free-flight mode, journal is self-contained to motion along the boundary. At the end of the free-flight mode the journal goes into the impact mode. In impact mode there are impact forces. These forces are applied instantaneously. For this reason, the momentum between the two bodies changes significantly and these changes cause discontinuity in the kinematic and dynamic characteristics. All these modes are shown schematically in Figure 2.6.

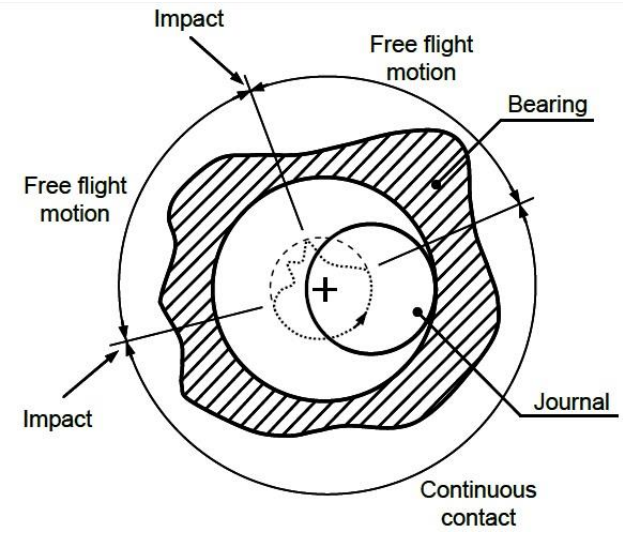

Figure 2.6 Different types of journal motion
(Source: Flores et. al 2010)

2.3.2.2. Discontinuous Force Contact Models

In discontinuous force contact approach, there is no continuous contact between two parts. Thus the duration of contact is assumed to be zero. Under these circumstances, velocity change is instantaneous, and therefore impact occurs. The

velocity rise is constrained by a high value of the contact force acting only during a small time of interval of contact. The integral of the force over the duration of the impact, i.e. the impulse, has a finite value due to the velocity rise. The impact is generally separated into two parts: compression phase and expansion phase. The relative speed between these parts depends on the coefficient of restitution. The direction of motion after impact is the opposite to the direction before impact. If impact is fully elastic, e = 1, however, if impact is inelastic, e = 0 (Schwab et al. 2002). On the other hand, energy balance is inadequate when the principle of impulse and momentum is applied. Furthermore, the accuracy of this approach is limited because of the zero duration of contact (Bauchau and Rodriguez 2002).

The equation of motion for an unconstrained system is calculated as

$$M\ddot{q} = f \tag{2.11}$$

where M is a mass matrix, f is generalized force and $\ddot{q}$ is the acceleration of the generalized coordinates. On the other hand, when system is constrained then this equation becomes

$$M\ddot{q} + g_N'^{\,T}\,\lambda_N = f \tag{2.12}$$

where g_N represents the constraint equations, g_N' is vector of the derivatives of g_N with respect to q and λ_N the vector of Lagrange multipliers. Accordingly, equation of momentum for the system is calculated as

$$M\dot{q}^{+} + g_N'^{\,T} s_N = M\dot{q}^{-} \tag{2.13}$$

where $\dot{q}^{-}, \dot{q}^{+}$ are the generalized velocities before and after impact, respectively and s_N represents the contact impulses which are determined as

$$\dot{q}^{+} = -e\dot{q}^{-};\; s_N = \lim_{t^{-} \uparrow t^{+}} \int_{t^{-}}^{t^{+}} \lambda_N dt \tag{2.14}$$

Considering the equation of motion and momentum equation together, the following matrix equation is obtained:

$$\begin{bmatrix} M & g_N'^{T} \\ g_N' & 0 \end{bmatrix} \begin{bmatrix} \dot{q}^{+} \\ s_N \end{bmatrix} = \begin{bmatrix} M\dot{q}^{-} \\ -eg_N'\dot{q}^{-} \end{bmatrix} \tag{2.15}$$

When the dissipation effects are neglected in the contact force model, the maximum contact force is determined as;

$$F_{N\,max} = \left(\frac{n+1}{2} \frac{\sqrt[n]{K}}{m_e} s_N^{\,2} \right)^{n/n+1} \tag{2.16}$$

where m_e is the effective mass, n = 3/2 in Hertzian contact force model; n = 1 for a linear spring, K represents stiffness coefficient..

Up to this point, joint clearance and the negative effects of joint clearance are discussed. In the following sections, a solution of this problem is discussed.

2.4. Vibration Reducing Methods

There are different methods used to reduce the residual vibrations. While some of these are passive, the others are active. Waiting for residual vibrations to stop, implementing a thin layer of visco-elastic material and using piezo-resistive films are examples of passive methods to reduce vibrations.

Using a bang-bang controller is a way generally utilized in pendulums. Bang-bang controllers are designed to implement constant output torque on the system periodically. Bang-bang control depends on the principle of playing swing. In this type of control, both external torques and friction is assumed to be zero. A constant torque is first implemented through a limited angular motion of the two links starting from the equilibrium position. The output torque of the upswing bang-bang controller is a constant. Moreover the direction of this output is same as the angular velocity of the grounded actuated joint. However, the bang-bang controller works only when the total energy is less than the energy of instable equilibrium position where both of the links

are in upright position. Therefore, this bang-bang controller is implemented around the low position due to the low potential energy (Zhao and Yi 2003).

Another method is to apply a Gaussian shaped torque input which is the first derivative of the Gaussian distribution function (Azad et al. 2008). The input is applied as an acceleration profile. The Gaussian distribution function is identified as

$$P(x) = \frac{1}{\sqrt{2\pi}\sigma} e^{\left[-(x-\mu)^2/2\sigma^2\right]} \tag{2.17}$$

where; σ and μ are the standard deviation and mean of the variable x. Taking the derivative of Equation 2.17, the system input torque is determined as

$$\tau(t) = \frac{(t-\mu)}{\sqrt{2\pi}\sigma^3} e^{\left[-(t-\mu)^2/2\sigma^2\right]} \tag{2.18}$$

The Gaussian shaped torque input is demonstrated in Figure 2.7.

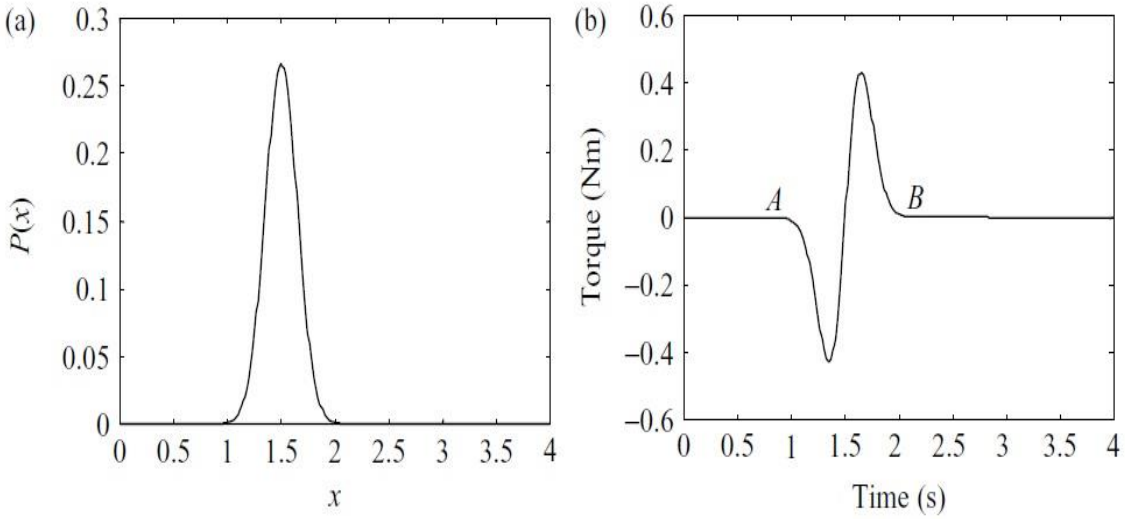

Figure 2.7 Gaussian shaped torque input
(Source: Azad et al. 2008)

Another method to reduce the residual vibration is called input shaping. Input shaping has not been applied on joint clearance up to now. In this study, input shaping is implemented to compensate the negative effects on joint clearances.

2.5. Input Shaping

Input shaping is a method that reduces residual vibrations by converting original input to a sequence of inputs. Thus, input shaping provides positioning accuracy when applied correctly. There are three types of input shaping methods. Shapers are not characterized by amplitudes, but time constants (Singhose et al. 1996).

To apply input shaping method, a procedure should be followed by an order. First of all the vibration amplitude of the system can be formulated according to the response of the impulses (Magee and Book 1992):

$$V(\omega,\xi) = e^{-\xi\omega t_m}\left\{\left(\sum_{i=1}^{m} A_i e^{\xi\omega t_i}\cos(\omega_d t_i)\right)^2 + \left(\sum_{i=1}^{m} A_i e^{\xi\omega t_i}\sin(\omega_d t_i)\right)^2\right\}^{1/2} \tag{2.19}$$

where ω is the natural frequency, ξ is the damping ratio, ω_d is the damped vibration frequency and A_i and t_i represent the magnitude and duration of the impulses. To neutralize the vibration amplitude, the required constraints are

$$\sum_{i=1}^{m} A_i e^{\zeta\omega t_i}\cos(\omega_d t_i) = 0 \quad \text{and} \quad \sum_{i=1}^{m} A_i e^{\zeta\omega t_i}\sin(\omega_d t_i) = 0 \tag{2.20}$$

To achieve the input shaping correctly, two more constraints which include the first time impulse and the total amplitude impulse should be added to the two constraints given by (2.20):

$$t_1 = 0\ , \sum A_i = 1 \tag{2.21}$$

The first added constraint in Equation 2.21 simplifies the system. On the other hand, the second added constraint in Equation 2.21 ensures that the total amount of the input remains the same.

After the constraints are described, input shaping impulses can be calculated. The first shaper which is called zero vibration (ZV) shaper is the simplest shaper and contains two impulses.

$$A_1 = \frac{1}{1+K}, t_1 = 0 \tag{2.22}$$

$$A_2 = \frac{K}{1+K}, t_2 = \frac{\pi}{\omega_d} \tag{2.23}$$

where A_i is the amplitude and t_i is the time instant while K and ω_d are determined as

$$K = exp\left(-\frac{\pi\xi}{\sqrt{1-\xi^2}}\right), \ \omega_d = \omega_n\sqrt{1-\xi^2} \tag{2.24}$$

However despite the simplicity of this shaper, usage of ZV shaper depends on natural frequency and damping ratio. If one of them is unknown then this shaper cannot be used. Additionally because of the sensitivity on any error in the parameters of the model, ZV shaper cannot be used on most systems. Further limitations can be inserted to create a more robust shaper such as zero vibration derivative (ZVD) shaper. The main disadvantage of ZVD shaper is the time delay. ZVD shaper requires partial derivative of the vibration amplitude with respect to frequency and includes three impulses (Magee and Book 1992):

$$A_1 = \frac{1}{1+2K+K^2}, t_1 = 0$$

$$A_2 = \frac{2K}{1+2K+K^2}, t_2 = \frac{\pi}{\omega_d} \tag{2.25}$$

$$A_3 = \frac{K^2}{1+2K+K^2}, t_3 = \frac{2\pi}{\omega_d}$$

Zero vibration derivative derivative (ZVDD) shaper includes four impulses.

$$A_1 = \frac{1}{1+3K+3K^2+K^3},\ t_1 = 0$$

$$A_2 = \frac{3K}{1+3K+3K^2+K^3},\ t_2 = \frac{\pi}{\omega_d}$$

$$A_3 = \frac{3K^2}{1+3K+3K^2+K^3},\ t_3 = \frac{2\pi}{\omega_d} \tag{2.26}$$

$$A_4 = \frac{K^3}{1+3K+3K^2+K^3},\ t_4 = \frac{3\pi}{\omega_d}$$

ZVDD shaper is the most accurate shaper. On the other hand, the delay becomes more than the other shapers.

CHAPTER 3

METHODOLOGY

This section presents the testing methodology in both simulation tests and experimental tests to clearly reveal the procedure of how input shaping is applied on a physical test system. The procedure is devised such that, first the model of the real system is constructed by empirical data and the input shaping methodologies are tested on simulation model to evaluate the performance of input shaping method. Next the method is implemented on the experimental system and re-evaluated through tests with different inputs to verify the simulation results. Experimental and simulation test procedures are explained with the sequence followed through the overall procedure in test procedure sub-section. The overall procedure is implemented in the given order: system identification, modeled system verification, input shaping method evaluation and application of the input shaping to the real system. The methodology has two sections: simulation and experimental and they are illustrated in Figure 3.1.

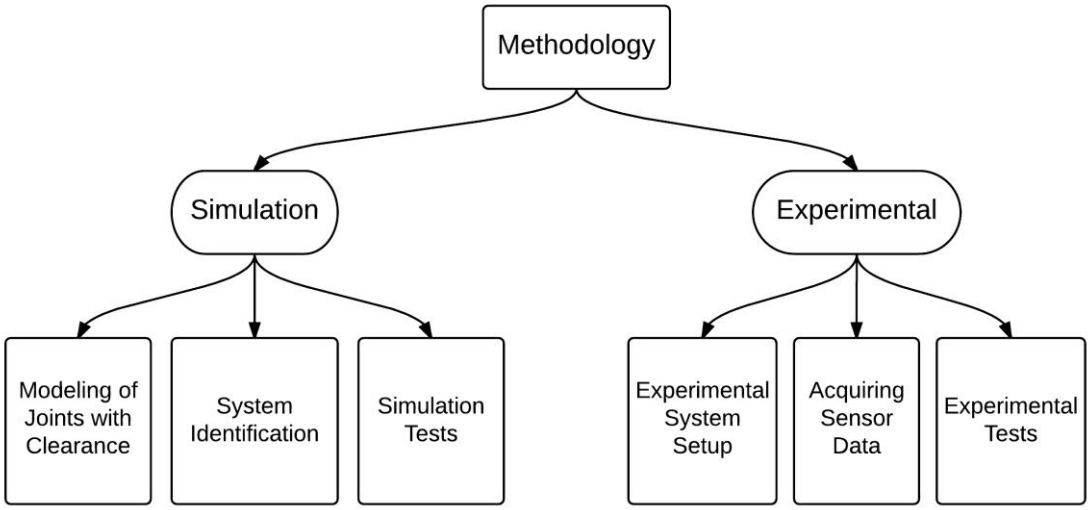

Figure 3.1.Methodology chart

This study is carried out in Iztech Robotics Laboratory (IRL). The information about hardware and software used in this study is provided in next sub-sections. In this

study, a revolute type mechanical joint is controlled by MATLAB Simulink environment algorithms over Humusoft DAQ card by compiling the real-time codes via Real-Time Windows Target™. Furthermore, for acquiring digital gyroscope data, an Arduino Mega 2560 is used as a DAQ card and connected to the same Simulink environment that is running in real time under Real Time Windows Target™. Details of the experimental system's set-up are explained in the next sub-section.

3.1. System Set-up

The mechanical part of the system is a mechanical link attached to the rotor of a servomotor. As the servomotor is run, the residual vibrations are observed at the tip of this mechanical link. The rest of the hardware and software is required to run the system and collect the necessary data from this mechanical part of the system. The hardware and software used to construct the experimental test set-up are listed as follows:

Software

- Matlab Simulink Real-Time Windows Target
- Arduino 1.05

Hardware

- Revolute type mechanical joint components:
  - LS Mecapion VS04G4N-P1 driver and Power Supply
  - LS Mecapion AC Servo Motor with Li-Ming planetary gear reduction
  - 3000 p/r Incremental Encoder
- Sensors and Data acquisitions peripherals:
  - ITG 3200 Digital Gyroscope
  - Proximity Sensor / Limit Switch
  - Humusoft MF 614 I/O Card
  - Arduino Mega 2560
  - Power Supply 36V 10A

The information flow between the system components is demonstrated by flow chart in Figure 3.2. In this figure, black lines represent the commands sent from Matlab to the servomotor. Blue lines represent the angular position feedback received from the

encoder and the red lines represent the angular velocity feedback from the gyroscope. At first, demands are created in the Matlab Simulink environment. From Matlab Simulink environment analog, digital and frequency outputs (different forms of demands) are transmitted over Humusoft I/O card to the servomotor driver. At that point driver takes the demand and provides the necessary energy to run the servomotor. While motor is running, positional feedback collected from the incremental encoder is sent from the servomotor to the driver. The positional feedback is then received by the Humusoft DAQ card and sent into the Matlab hardware-in-the-loop (HIL) environment running in real-time. Meanwhile, angular velocity of the mechanical link connected to the servomotor's rotor is acquired through the gyroscope and Arduino Mega 2560 DAQ card. The acquired angular velocity information is fed back into the Matlab HIL environment. The necessary codes embedded in the Arduino Mega 2560 DAQ card to acquire gyroscope date and send it into the Matlab HIL environment is provided in APPENDIX B.

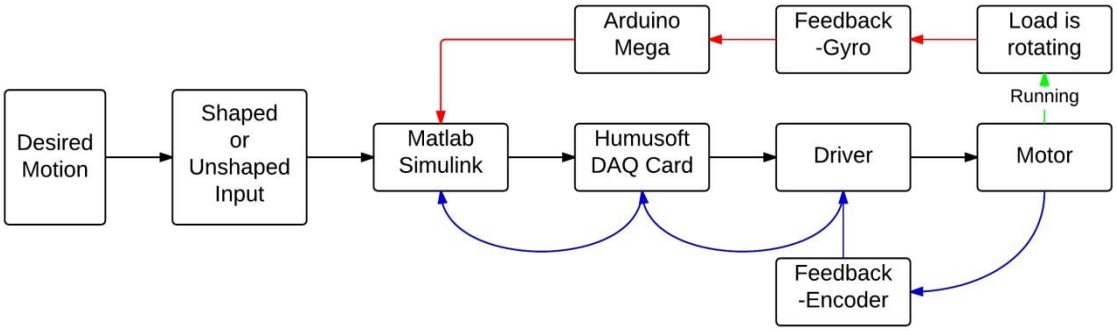

Figure 3.2.Flowchart

Input shaping method is constructed in Matlab Simulink software to shape the inputs for both the simulation tests and experimental tests. The Real Time Windows Target is used to construct the HIL environment for information exchange between the computer environment and real-time devices. Using this methodology, system identification and verification of the mathematical model of the system are carried out.

3.2. Components of the revolute-type mechanical joint

The revolute-type mechanical joint is composed of the base, the servomotor and the mechanical link which are shown in Figure 3.3. The servomotor system consists of a planetary gear reduction system, AC motor and encoder. The servomotor is connected to the base from its stator and connected to the mechanical link from its rotor.

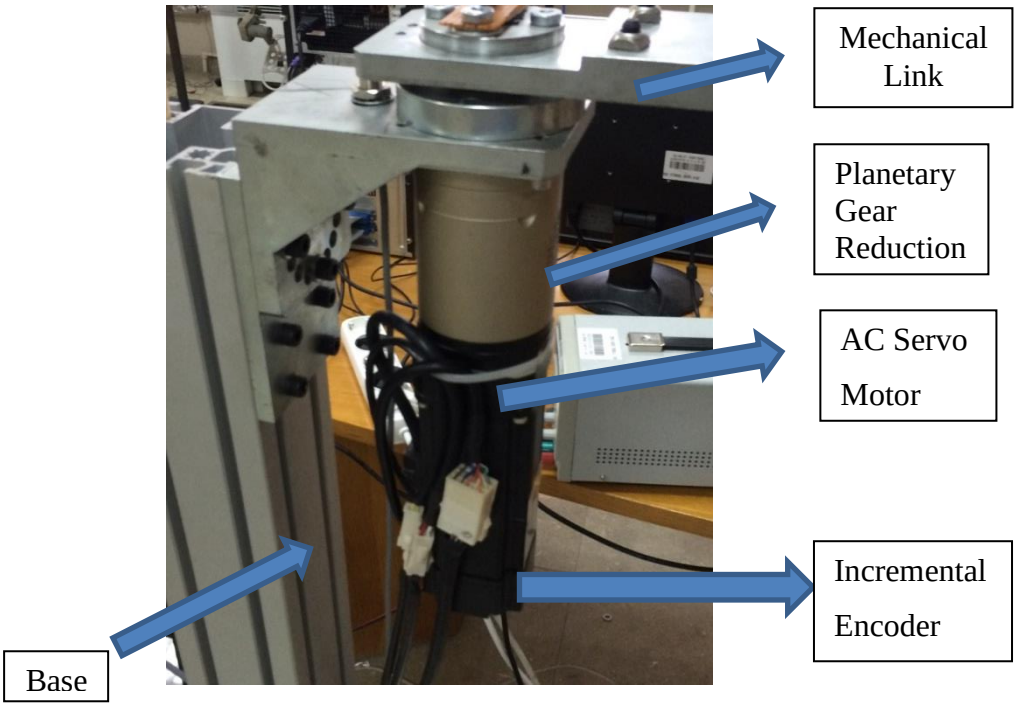

Figure 3.3.Planetary gear reduction - servo motor – encoder

The servomotor used in this system is an AC servo motor, APM-SB04AEK2 produced by LS Mecapion. The specifications of the AC servomotor are listed in Table 3.1. Motor has an electromechanical brake to be released before operations and an incremental quadrature encoder with 3000 pulse per revolution (P/R) attached on the rear end of it.

Table 3.1. AC Servomotor specifications

Motor Shape Type	Solid Shaft
Flange Size	60 Flange
Motor Capacity	400 W
Rated Speed	3000 rpm
Encoder Type	Inc. 3000 [P/R]
Shape of Shaft	One Side Round (Standard)
Brake type	Electromechanical brake

The servomotor driver used in this system is VS04G4N-P1 driver from LS Mecapion. These drivers are capable of providing 400 W power and can be variously used according to the upper controller command which is sent from the Matlab Simulink Environment through the DAQ card. Specification documents of the driver indicate that three different control commands can be received by the driver: position, speed and torque. The information flows for each command type are given in Figure 3.4.

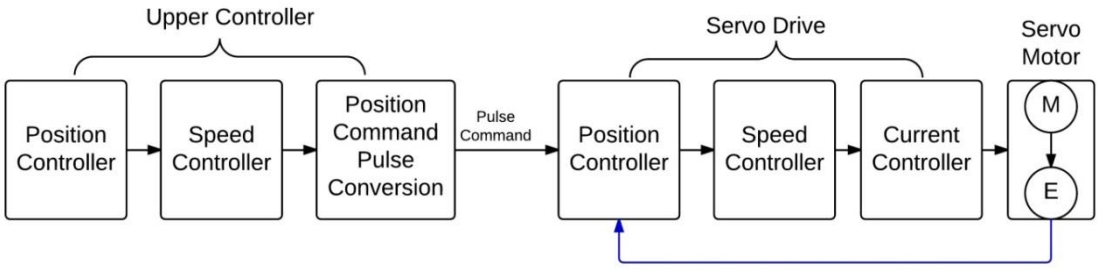

(a)

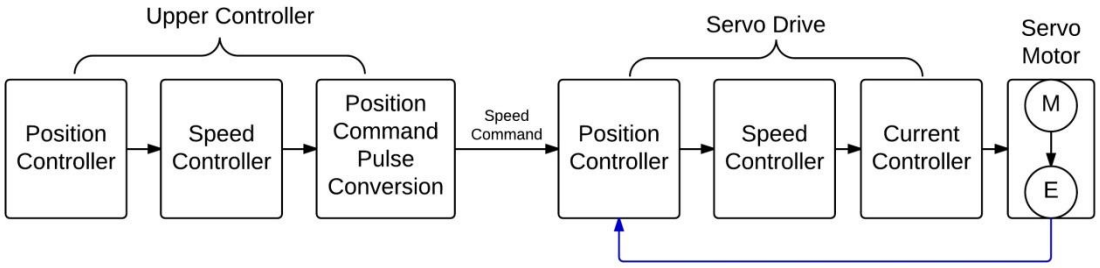

(b)

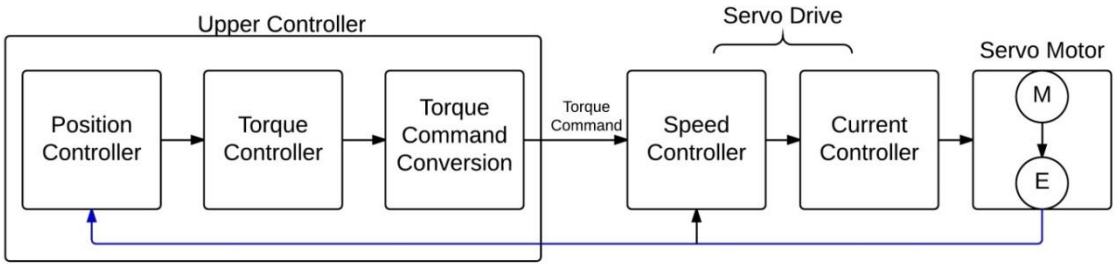

(c)

Figure 3.4 Information flow with the servomotor driver: a) Position operation mode b) Speed operation mode c) Torque operation mode

For transmitting pulse commands from the upper controller to the driver, a trajectory is first generated by the operator. After this trajectory is generated as a position level input, its derivative is taken to find the velocity profile for the trajectory. Finally, this velocity profile is converted to pulse commands to be sent to the driver. The algorithm changes the frequency of the pulses generated in Simulink Real Time Windows Target™ to be sent to the driver for converting the velocity profile to pulse commands.

The pulse commands should be in the same configuration with the encoder, which is a quadrature encoder. In quadrature encoders, A and B channels follow each other with some delay (Figure 3.5). The input pulse configurations are is shown in Figure 3.6. Among these the input pulse logic identified with “0” is selected to be the

velocity input shape to be sent from the upper controller in Matlab. The direction of the velocity is determined with the phase difference and magnitude of the velocity is set by changing the frequency of the pulses. It was later experimentally tested that the frequency change is detected by the driver at 30 Hz. Therefore, the change in velocity is sampled at 30 Hz.

Figure 3.5 Encoder pulse commands

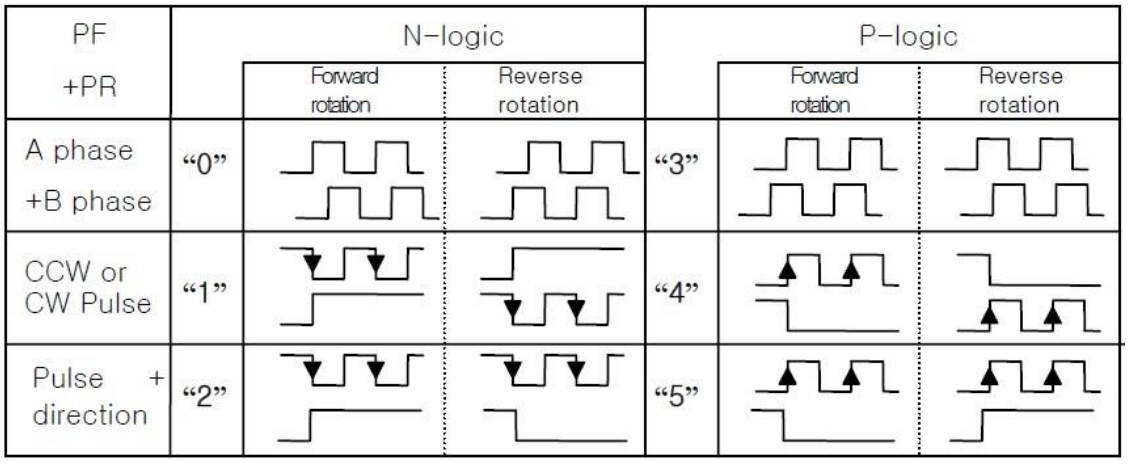

Figure 3.6 Input pulse logic
(Source: LS Mecapion user manual 2010)

These pulses are then sent to the driver which includes position, velocity and current controller within respectively. In position operation mode, as the command pulses are received and compared to the pulses coming from the encoder, a velocity demand is fed in the velocity and current controllers of the driver. The strength of

position operation mode is that the input signal is immune to the noise from the environment. However, the change in the velocity is limited at only 30 Hz.

In Figure 3.4.b, the velocity commands are generated from the velocity profile generated for the motor in Matlab (upper controller) and fed to the driver as analog signal. This signal is then received by the driver's speed controller and compared to the speed of the motor. The output of this controller is then feed to the motor through current controller. Fast response time is the strength of this type of control. However, noise in the speed command is the weakness of this type of control.

The last option for the operation mode is the torque operation mode as identified in Figure 3.4.(c). After performing experimentation with this mode, it was found out that this mode is not any different from the speed operation mode. Therefore, it is not possible to send in torque commands to this driver.

Additionally, the servo drivers are capable of receiving input pulses in 500 KHz. Therefore, any signal provided to the driver should be smaller than this value to be perceived by the driver. The other properties of the driver are explained in Appendix A.

A digital gyroscope is used to collect the angular velocity of the mechanical link attached to the motor to reveal the effects of the joint clearance in in terms of residual vibrations. The gyroscope attached to the system is ITG 3205 digital 3 axes gyroscope. The specifications of the gyroscope are provided below.

- 14.375 LSB per° sensitivity
- ±2000 °/sec full-scale range
- Low pass filter which is programmable digitally
- 6,5 mA operating current
- Not necessary to apply high pass filter
- 50ms turn on time
- I^2C serial interface

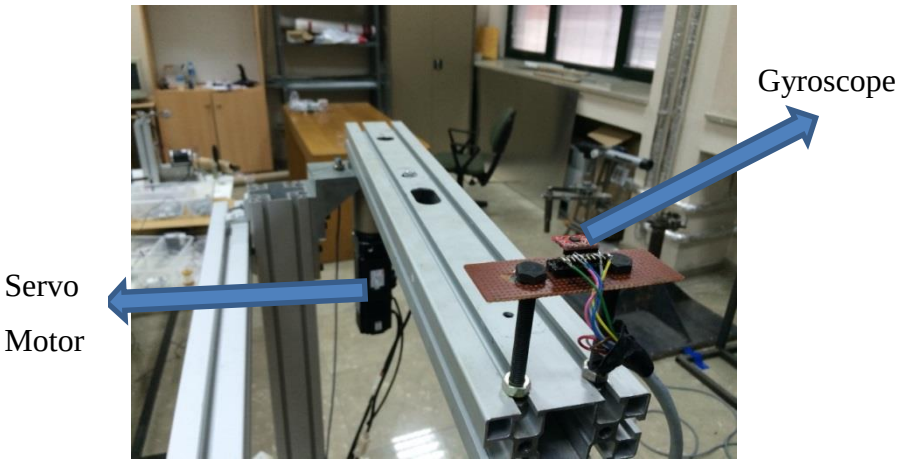

Figure 3.7 Location of the digital gyroscope on the mechanical link

Arduino Mega 2560 microcontroller board is used to collect the digital data transmitted from the ITG 3205 gyroscope via I^2C communication protocol. The microcontroller is also used to transmit the collected data to the computer where the Matlab Simulink Real Time Windows Target^{TM} is running. By this way Arduino Mega 2560 is used as a DAQ card, which enables data acquisition from the gyroscope.

A data acquisition card, Humusoft MF-614 DAQ card, is used for acquiring real world analog/digital signals that are transmitted from the driver (encoder and speed output) and sending control commands to the driver. This card is a multifunction I/O card designed to provide A/D and D/A converters having 12 bit resolution, other digital I/O options, counters and timers. The ports of the DAQ card used in this study are listed in Table 3.2.

Table.3.2.DAQ card ports used in the study

Signal Name	**I/O used in DAQ**
Speed Limit	Analog Output (-10 V to +10V)
Torque Limit	Analog Ouput (-10 V to +10V)
Measured Speed	Analog Input (-10 V to +10V)
Velocity Command (for velocity control)	Analog Output (-10 V to +10V)
Pulse Command (for position control)	Digital/Pulse Train Signal (A phase/B phase)
Servo On	Digital Output (+5V or 0V)
Proximity Sensor	Digital Input (+5V or 0V)
Encoder Feedback	Digital/Pulse Train Signal (A/B phase)

The CTS 9513 counter/timer chip provided in Humusoft MF-614 has a 20 MHz input clock offering a wide range of pulse frequencies, which covers the full range velocity control required by the LS Mecapion driver. This counter/timer chip is used to generate pulses in position control.

3.3. Test Procedure

In this study among the three input modes position and speed operation modes are used since the torque operation mode works in the same way as the speed operation mode. A test procedure is devised for both modes and repeated for both. For each operation mode, the procedure followed is shown in Figure 3.8.

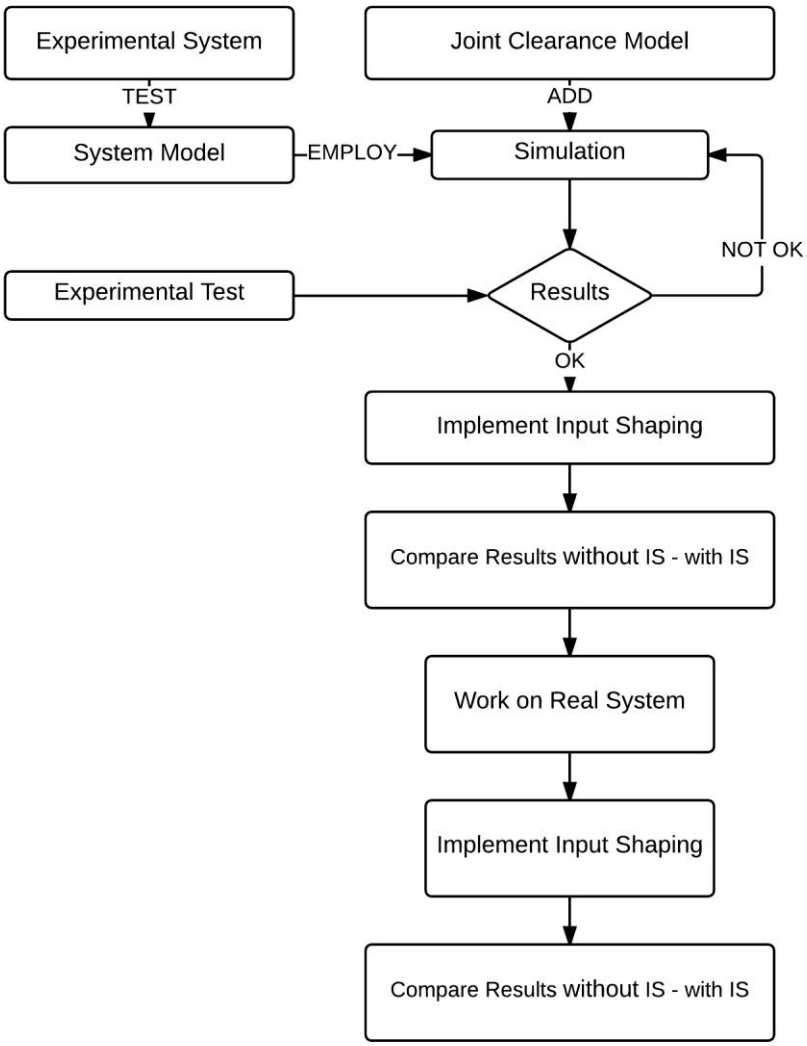

Figure 3.8. Test procedure

In the test procedure, first, selected input types (step, ramp, sinusoidal, pseudo-random-binary-signal) are used. The outputs of the system in both control and position operation modes are collected through the encoder as angular position and processed in Matlab to represent the output in degrees. However, in speed operation mode, data collected from encoder are differentiated with respect to time to calculate the angular speed of the motor shaft in degrees per second. In addition, the calculated angular speed data is filtered by a 4th order Low-Pass Butterworth filter with passband edge frequency of 30 rad/s.

Inputs and outputs of the system are used in system identification process. In this stage of the test procedure, the transfer function of the system is estimated by using Matlab System Identification Toolbox. System identification is executed for different input types by trying different possible mathematical models of the system (i.e. third order system with a transport delay). A detailed explanation of the system identification procedure is given in the next Chapter.

After a transfer function is identified for a specific input type, it is tested in simulation for the other types of input. The results from the simulation tests are then compared with the experimental results for each input signal. By this way, estimated transfer functions are evaluated and the best fit among the others is implemented to construct the simulation model for following stages. The estimated transfer functions are evaluated against each other by their transient state response (speed of the response and the overshoot values) and steady-state response (tracking performance).

After the most suitable transfer function representing the system dynamics is selected, joint clearance model is added onto this model. The parameters of the joint clearance model is verified though experimental tests. In these experimental tests the motion data in terms of angular velocities are collected from the gyroscope, which is attached to the other end of the mechanical link. The joint clearance between the rotor of the servomotor and the mechanical link is increased for better observation of the residual vibrations. The test results for all the system identification procedures are presented in the next Chapter.

Since the input shaping method is a model-based approach, the damping ratio, ξ, and the natural frequency, ω_n, of the system are of crucial importance. These critical values are calculated from the transfer function which was selected after the system identification procedure. To be able to calculate these values, the transfer function is compared to the general form of the 3rd order single-input single-output transfer

function. By using these calculated values, the amplitude of the input shapers and the implementation times are determined.

Then, three types of input shaping methods are tested in simulations. In these tests, decrease in the levels of the residual vibrations when using input shaping is compared for different inputs. As a result of the evaluation of the input shaping methods, the most appropriate one is selected to be implemented for the experimental tests. Finally, experimental tests are carried out by implementing the selected input shaping method. The results in terms of residual vibration levels are compared between the ones in which the input shaping was implemented and not implemented.

The next chapter is reserved for explaining the system identification procedure used in this thesis. After explaining the procedure, the work carried out for system identification of the system without the joint clearance and with joint clearance is described. Finally, the parameters of the identified system model are given.

CHAPTER 4

SYSTEM IDENTIFICATION

According to the test procedure, first of all, the system is run for the specified inputs and the experimental data are collected. In experimentation, two kinds of operation modes are used: speed operation mode and position operation mode. The procedure for identifying the system model with and without joint clearance is explained in section 4.2. However, in order to apply the procedure experimental data should be acquired. The next sub-section explained the data acquisition procedure in experimental tests for two modes of operation.

4.1. Acquiring Experimental Test Data

It was explained in the previous Chapter that two operation modes are used in experimental tests. These modes are speed and position operation modes. Data acquisition protocols in both operation modes are explained in the next sub-sections.

4.1.1. Speed Operation Mode

Velocity commands are generated from designated inputs (step, ramp, etc.) are fed to the driver as analog signals in this operation mode. Then these signals are received by the driver operating in speed operation mode and compared to the speed of the motor. The output of this operation mode is fed to the motor through current controller. The main advantage of this operation mode is the fast response time of the system. The commands are implemented very fast. On the other hand, due to the use of analog signals, effects of the noise on the analog signals are observed in the output of the system.

As determined in the test procedure, first experimental system is run and the encoder output is acquired. The acquired encoder data is processed to convert the counts to degrees and then differentiated with respect to time to calculate the angular velocity.

The differentiation process results in spikes and therefore, a low-pass filter mentioned in the previous Chapter is used. In the speed operation mode, the inputs used are listed in Figure 4.1 as:

- Step Input
- Ramp Input
- Sinusoidal Input
- PRBS Input (Pseudo Random Binary Signal)

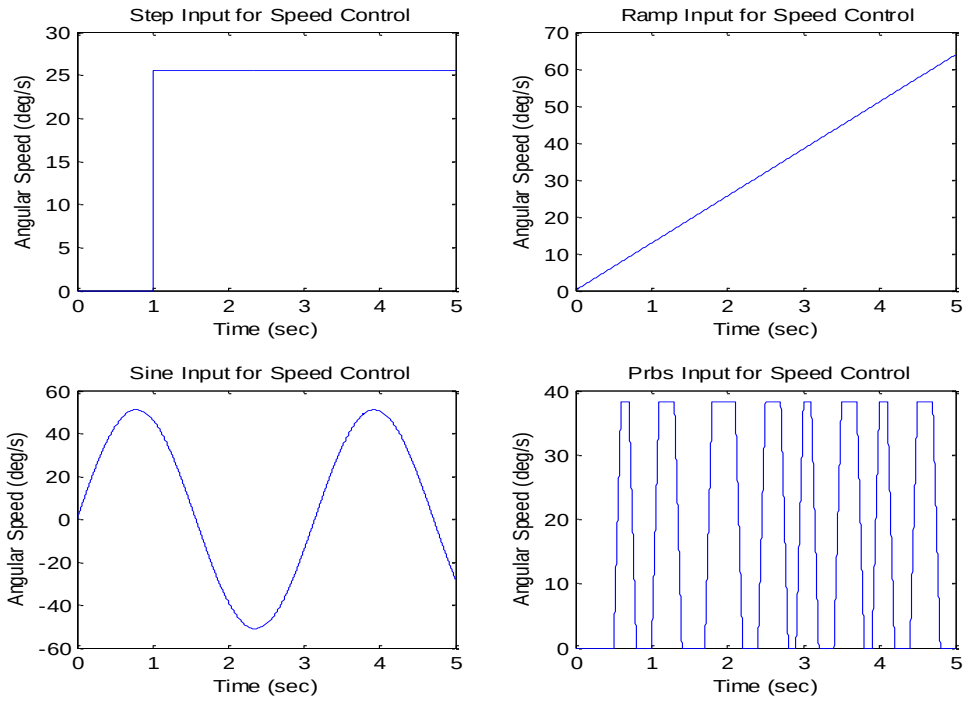

Figure.4.1. Angular velocity inputs

For each type of input, experimental tests are conducted for 10 times. The main purpose of 10 tests is to show the consistency of the system response. The responses of the system with respect to a step, ramp, sinusoidal and PRBS inputs are illustrated in Figures 4.2, 4.3, 4.4 and 4.5 respectively.

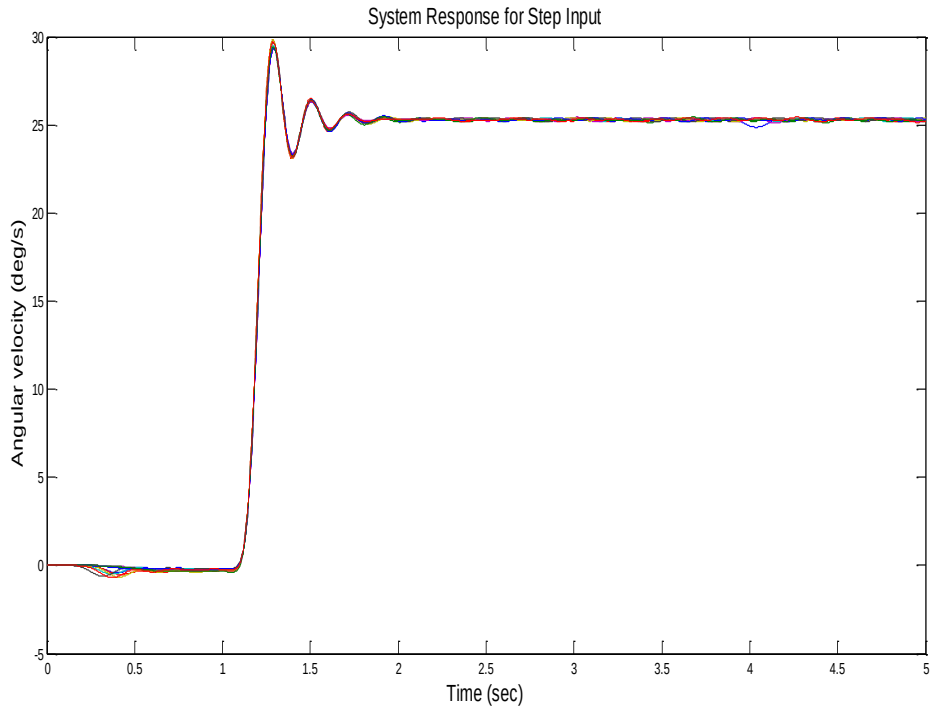

Figure.4.2. Response of the system without joint clearance to a step input in velocity domain for 10 successive of experiment (speed operation mode)

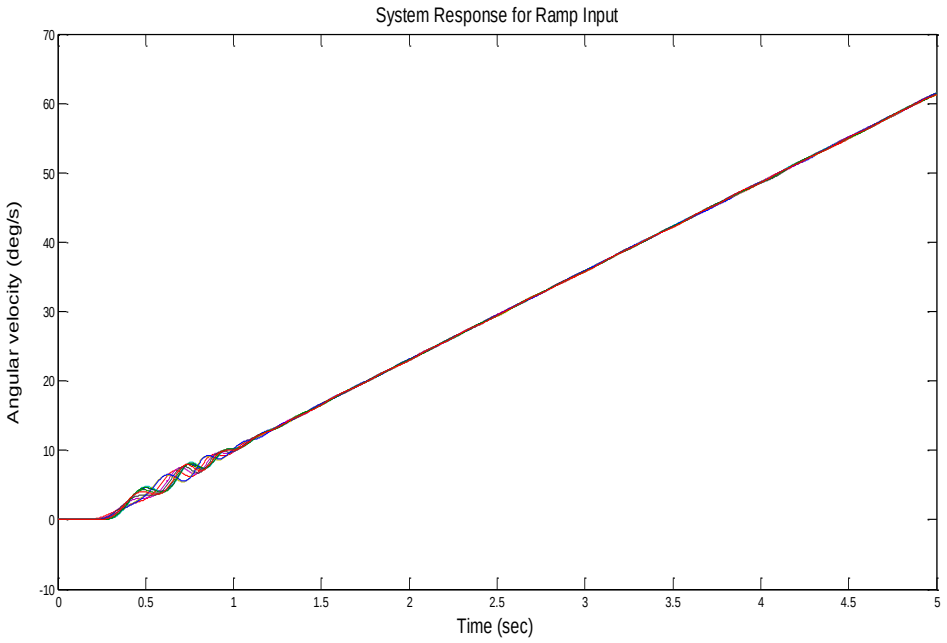

Figure.4.3. Response of the system without joint clearance to a ramp input in velocity domain for 10 successive of experiment (speed operation mode)

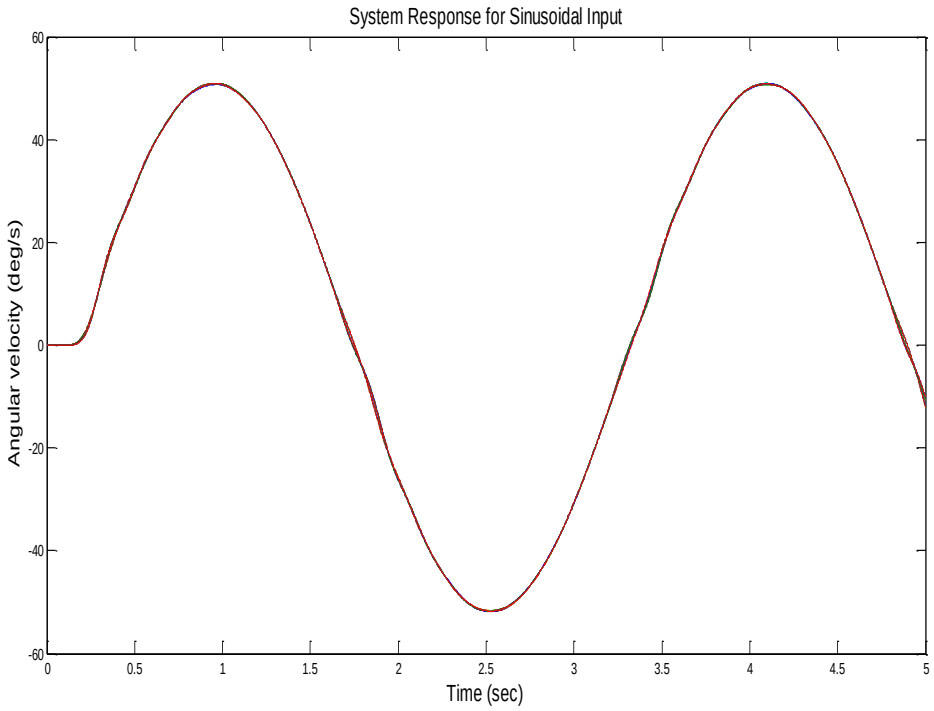

Figure.4.4. Response of the system without joint clearance to a sinusoidal input in velocity domain for 10 successive of experiment (speed operation mode)

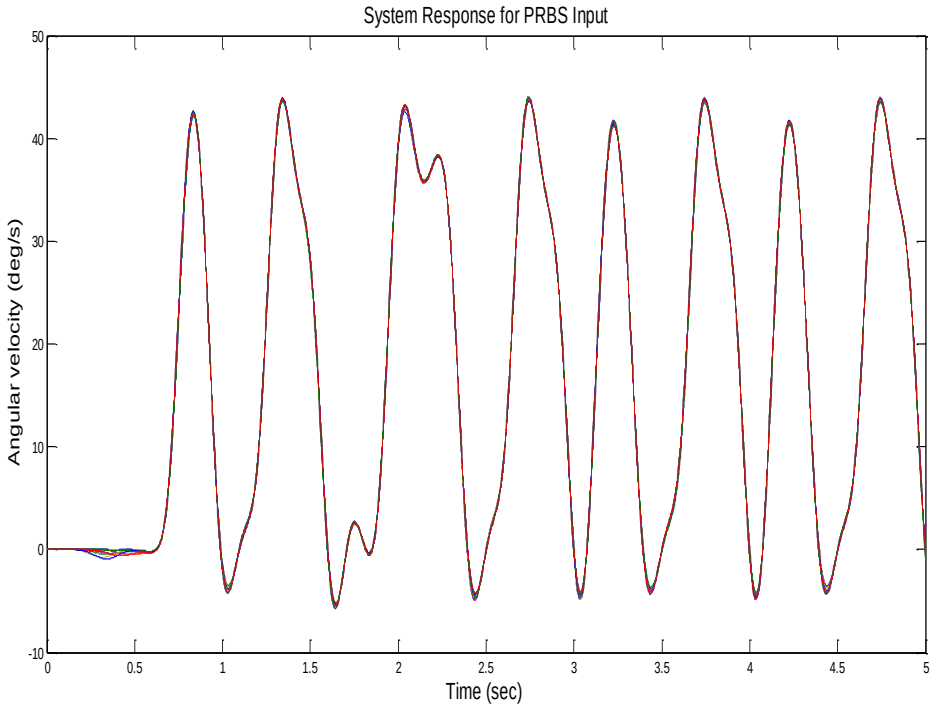

Figure.4.5. Response of the system without joint clearance to a PRBS input in velocity domain for 10 successive of experiment (speed operation mode)

The results of these measurements are evaluated by calculating the mean value for the 10 successive measurements and finding the error of each signal from the mean. The result of this evaluation provides us the information about the consistency of the measurements. The error value, E_i, for each measurement is calculated as shown in Equation 4.1.

$$E_i = \frac{\left(\sqrt{\sum_{j=1}^{n} \left(m_j - t_{ij} \right)^2 \Big/ n} \right)}{r} \quad ; \qquad i = 1, 2, \ldots 10 \tag{4.1}$$

In equation 4.1, m_j is the mean value of the output signals for the specific input function at the jth interval, t_{ij} is the value of the ith output signal at the jth interval, n is the number of interval (i.e. 5000 for 5 seconds of data at 1 kHz) and finally r is the total range of the mean value of the output signals. The error value for each measurement conducted for each input signal is given in Table 4.1.

Table.4.1. Error values for each measurement

Test Number	Step Input	Ramp Input	Sine Input	PRBS Input
1	0.0021	0.0018	0.0012	0.0035
2	0.0024	0.0015	0.0013	0.0039
3	0.0022	0.0022	0.0013	0.0029
4	0.0018	0.0019	0.0009	0.0028
5	0.0021	0.0016	0.0007	0.0038
6	0.0016	0.0023	0.0006	0.0041
7	0.0024	0.0015	0.0007	0.0039
8	0.0021	0.0023	0.0010	0.0038
9	0.0023	0.0018	0.0008	0.0038
10	0.0023	0.0014	0.0011	0.0032
mean	0.0021	0.0018	0.0010	0.0035

It is observed from Table 4.1 that the difference between the measurements is considerably small and therefore, there is a consistency in the system response for each input signal.

4.1.2. Position Operation Mode

The velocity commands are converted the pulse train with varying frequency and constant duty cycle. Driver counts the pulses and calculates the requested angular position for the system. Since the encoder is rated at 3000 pulse per revolution, 3000 pulses are required to achieve a full rotation of the motor shaft. The main advantage of this operation mode is using digital signals which result in noise free inputs for the system. On the other hand, there is a limitation on the change of the input pulse frequency, which is at 30 Hz. This fact limits the response time of the system with respect to the speed operation mode.

As determined in the test procedure, first experimental system is run and the encoder output is acquired. In position operation mode, the inputs used are listed in Figure 4.6 as:

- Step Input
- Double Step Input

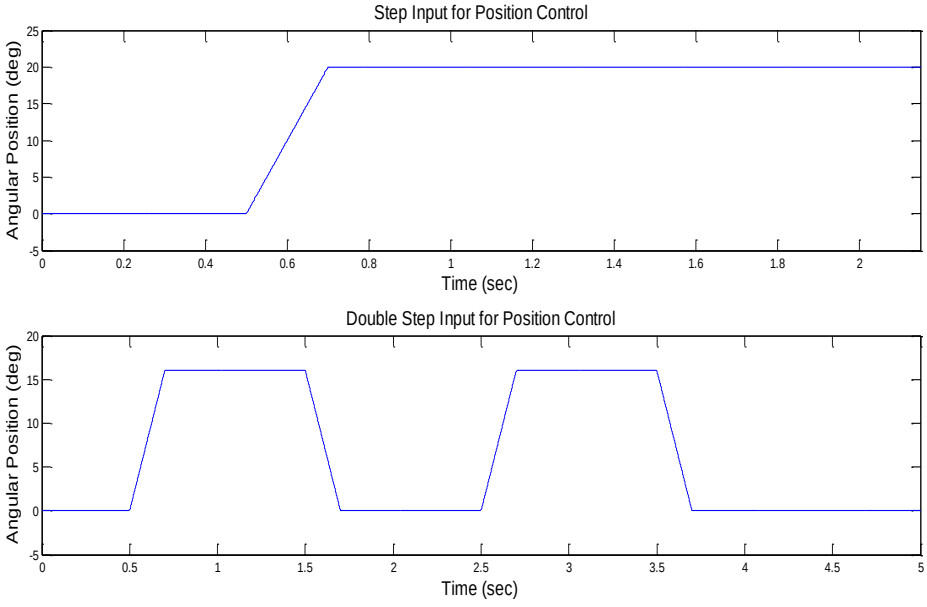

Figure.4.6. Angular position inputs

For each type of input, experimental tests are conducted for 10 times. The main purpose of 10 tests is to show the consistency of the system response. The responses of the system with respect to a step, and double step inputs are illustrated in Figures 4.7, and 4.8 respectively. Although the inputs are specified as step, since the change in velocity is limited in 30 Hz by the system set-up, the input is actually a higher sloped ramp input until it reaches the desired step value.

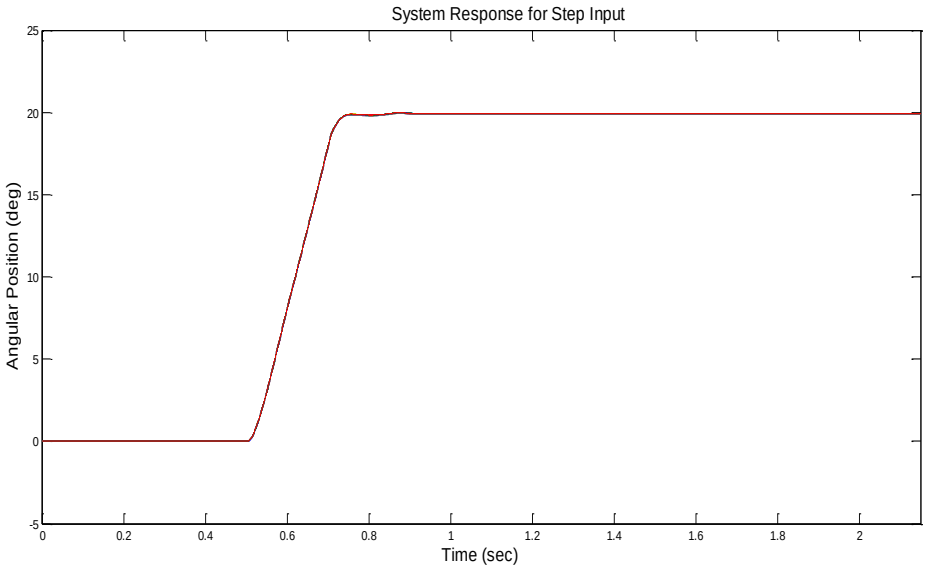

Figure.4.7. Response of the system without joint clearance to a step input in position domain for 10 successive of experiment (position operation mode)

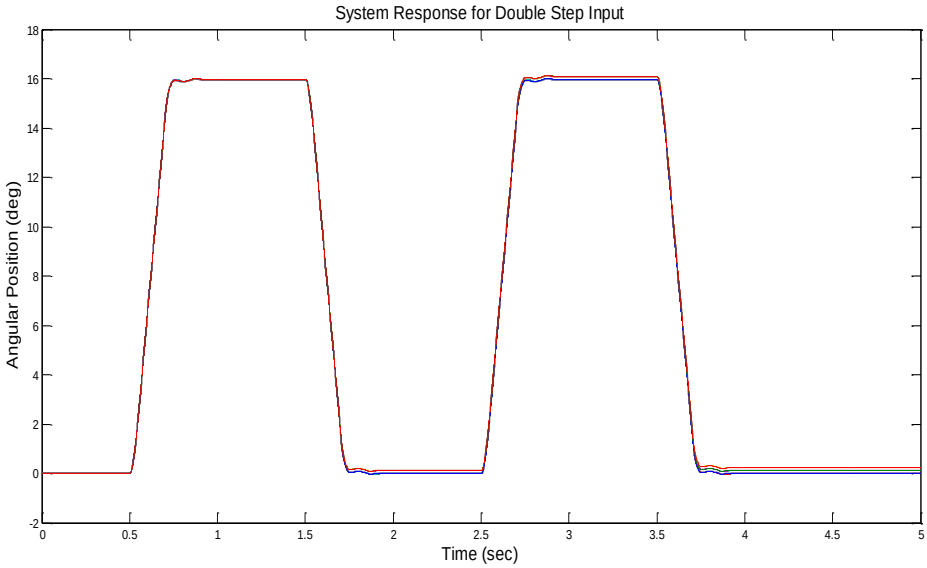

Figure.4.8. Response of the system without joint clearance to a double step input in position domain for 10 successive of experiment (position operation mode

The error value for each measurement conducted for each input signal is calculated by using Equation 4.1 and the results are given in Table 4.2.

Table.4.2. Error values for each measurement with position operation mode

Test Number	Step Input	Double Step Input
1	$1.56x10^{-4}$	0.0027
2	$1.39x10^{-4}$	0.0026
3	$1.05x10^{-4}$	0.0026
4	$1.22x10^{-4}$	0.0018
5	$2x10^{-4}$	0.0024
6	$1.24x10^{-4}$	0.0045
7	$1.72x10^{-4}$	0.0026
8	$0.98x10^{-4}$	0.0026
9	$1.39x10^{-4}$	0.0024
10	$1.15x10^{-4}$	0.0044
mean	$1.37x10^{-4}$	0.0028

It is observed from Table 4.2 that the difference between the measurements is considerably small and therefore, there is a consistency in the system response for each input signal.

After the system is confirmed to have a consistent response for the provided inputs, the collected data from encoder is used to identify the transfer function of the total system without joint clearance. The system model consists of the transfer functions of the motor, mechanical link, gear, encoder and the controller. System identification procedure is explained in the next section.

4.2. System Identification Procedure

System identification is used to construct mathematical models of control system. Then mathematical model in terms of the transfer function is required to implement the input shaping method since the method is a model-based approach.

System identification is applied by using the system input and the system response data acquired from the experimental tests. System identification procedure is outlined in Figure 4.9. First the data is collected through experimental tests for certain inputs. These tests are explained in the previous section. Then the system identification toolbox in Matlab is used to identify the parameter of the estimated system transfer function. The system model is then run in simulation and tested for specified inputs. The results are compared with the experimental results to verify the system model. At this stage the system model does not have joint clearance. In the next subsection the system identification for the system without joint clearance is explained. After the verification procedure, the selected joint clearance model is added to the identified system and once again verified by experimental results.

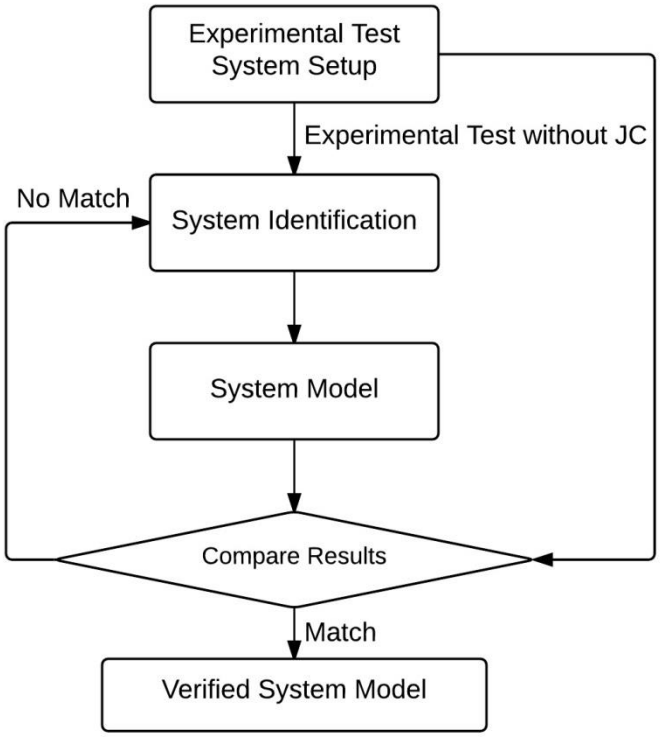

Figure.4.9. System identification

System identification is applied with both speed operation mode and position operation mode. In this section, first, system identification in speed operation mode and then in position operation mode are described.

Speed operation mode: Encoder data is used to identify the transfer function of the total system composed of the motor, mechanical link, gear, encoder and the

controller. The total system's block diagram is shown in Figure 4.10. The components belonging to the identified system and the Matlab environment are identified in this figure.

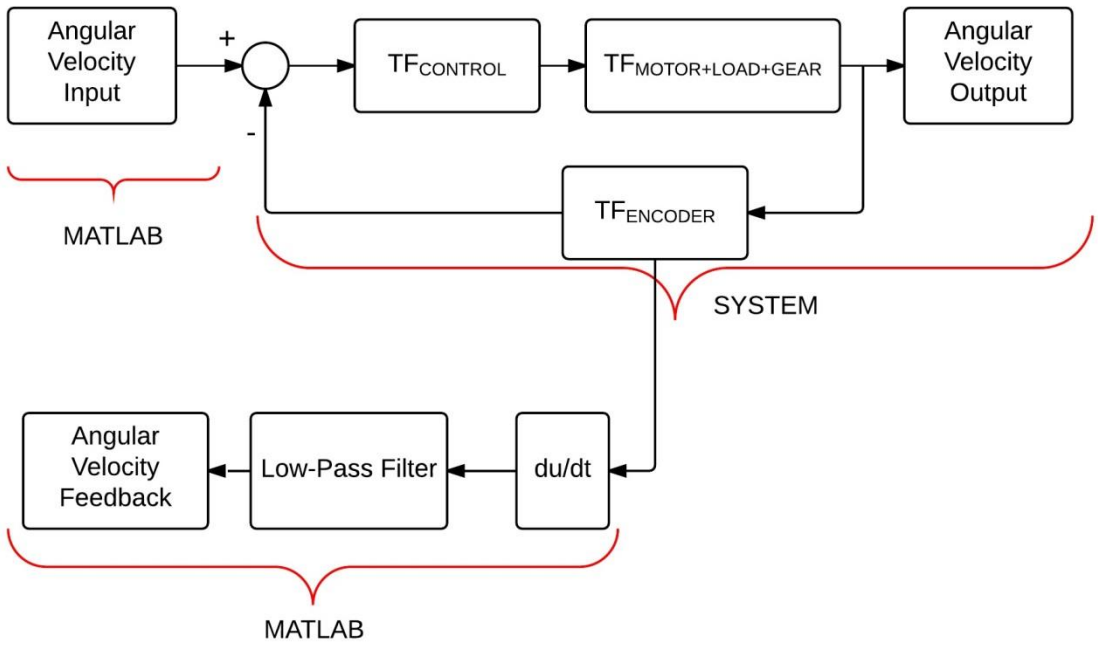

Figure.4.10. System's block diagram in speed operation mode

In speed operation mode, system identification is applied by acquiring angular velocity input and output data in time domain to estimate transfer function coefficients. However, the output is received from encoder in position level and therefore; angular velocity of the system is obtained by deriving of the encoder data. A second option to receive the angular velocity of the system is by using the angular velocity monitor signals received from the driver as analog signals. This option is not selected since the analog signals captured much noise in their path to the data acquisition system. Derivation of the encoder data also results in a noisy signal. To solve this problem, a low pass filter is applied on the differentiated encoder data and finally acceptable output data is obtained. However, in this case the system identification procedure does not only identify the system components but also the transfer function of the low-pass filter is included in the obtained transfer function.

Position operation mode: System identification is applied by using the angular position input and angular position output. Since the encoder data is used directly without any post-processing, the system that is to be identified is shown in Figure 4.11.

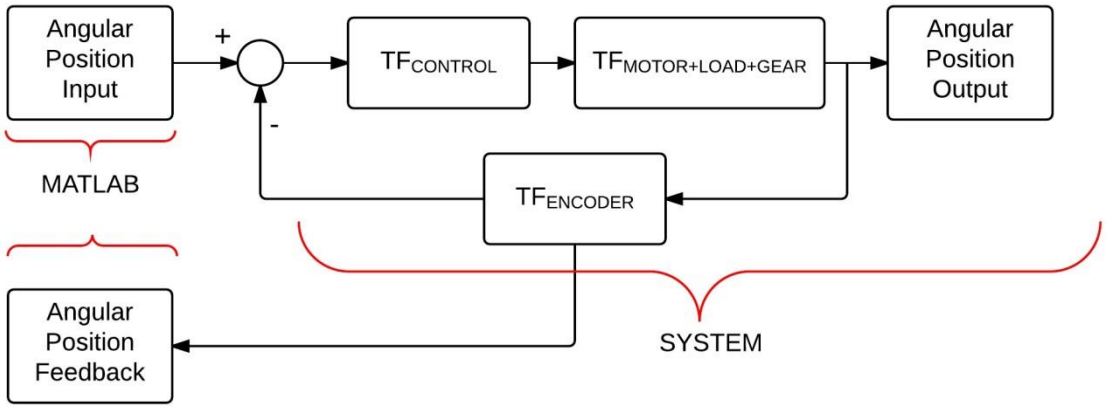

Figure.4.11. Block diagram representation of the system in position operation mode

To identify the transfer function of the system for both operation modes, Matlab System Identification Toolbox is used. Input-output data can be imported to the toolbox in two different domains: time domain data and frequency domain. In this toolbox, input signals can be edited and also the model of the system can be estimated by using different models. In Figure 4.12, a menu list is opened to show the possible models to select from.

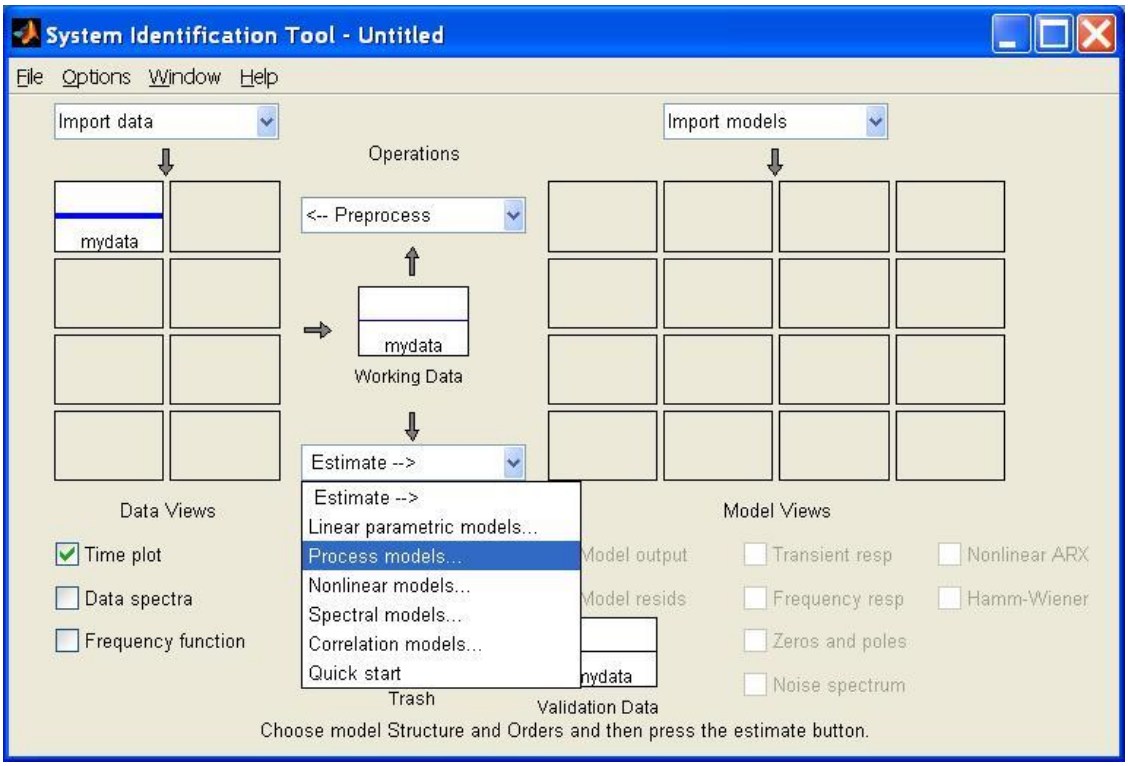

Figure.4.12. System identification toolbox

Since the real system is nonlinear, two types of models are possible candidates to represent the system model. One of the estimation methods is nonlinear model and the other is process model by assuming that the system is linear in the vicinity of its operation range. If the nonlinear model is chosen, Grey box and Hammerstein-Wiener nonlinear models can be used. The results obtained by using these models can only be used in Matlab Simulink environment by using their specific blocks. A representation of the use of the model fitted to the Hammerstein-Wiener nonlinear model is shown in Figure 4.13.

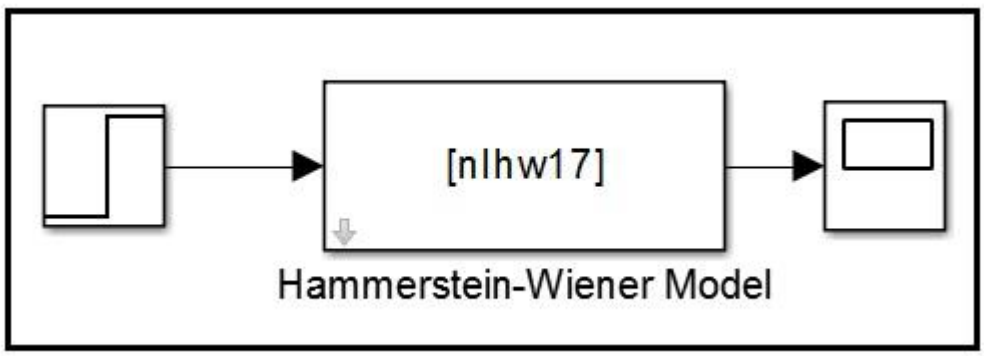

Figure.4.13. Hammerstein-Wiener model

Input shaping method is a model-based approach which requires the knowledge of the exact transfer function. Thus, despite the successful results obtained by using Hammerstein-Wiener model, this model cannot be used for this study.

Process model can also be used for the nonlinear system identification assuming that the system representation is linearized in the vicinity of the operation condition. The tool to identify the system model as a process model allows approximating the system model as a second or a third order transfer function with a zero, a transport delay and an integrator by using given input and output time domain data. The user interface for the mentioned choices for the system model is shown in Figure 4.14. The approximated system parameters can be retrieved from the right side of the interface window. This allows the user to access the required parameters to be used in input shaping method.

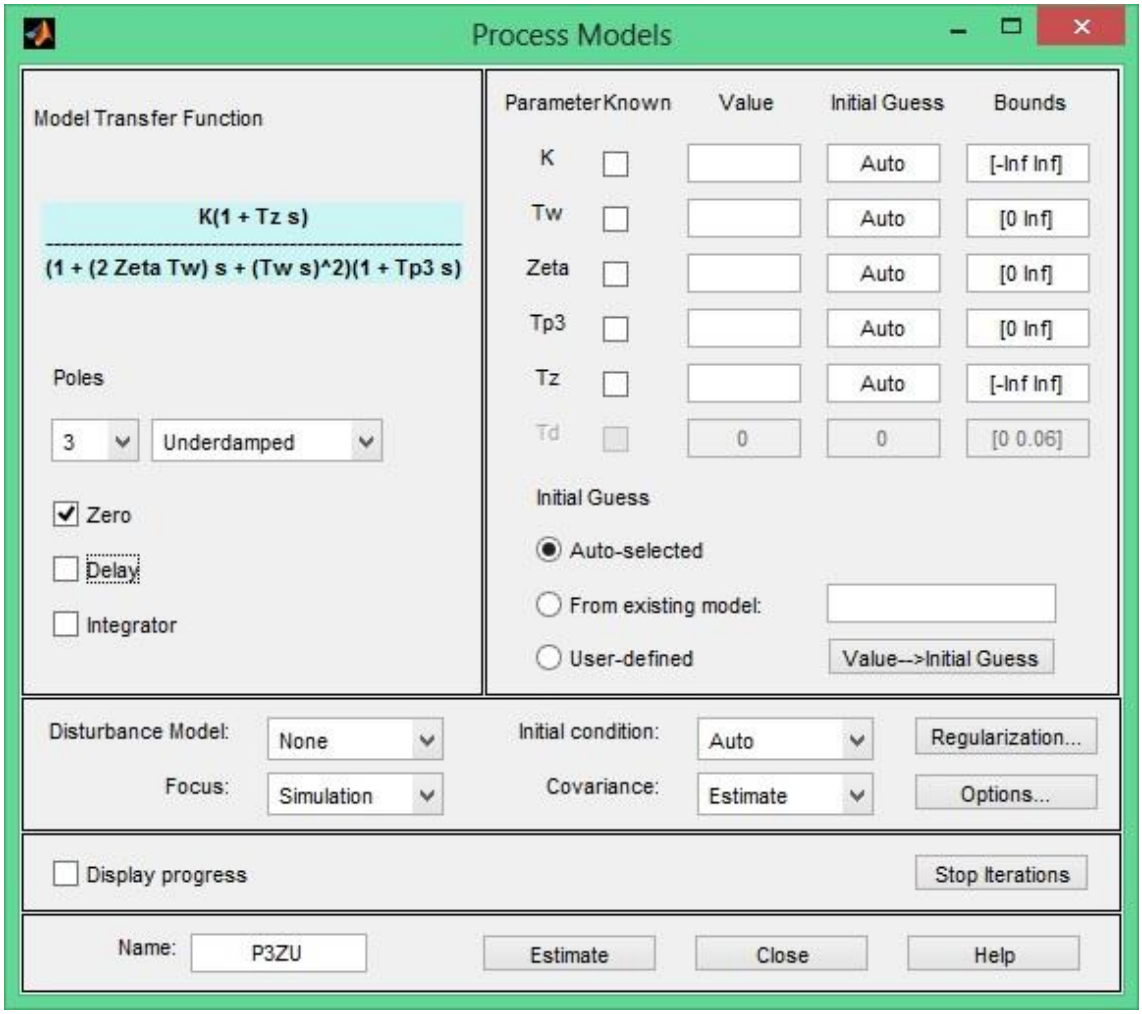

Figure.4.14. Process model user interface

After system identification is done by using process model, the transfer function is determined in the form given in the user interface window. The block diagram of the identified system is illustrated in Figure 4.15.

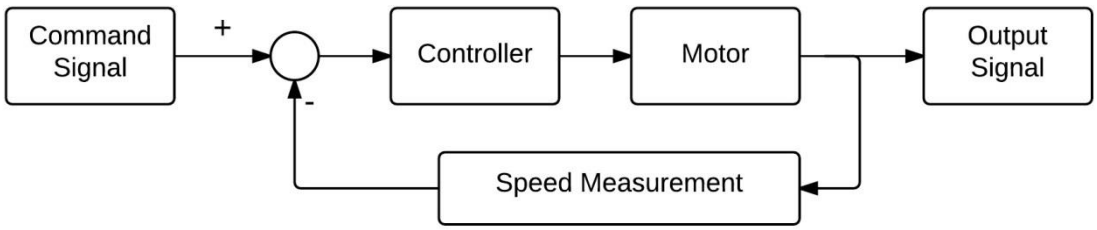

Figure.4.15.Identified system model

There is no information for the built-in controller inside the driver. Therefore, it is impossible to exactly identify the control type used for this system. For a better approximation second-order system model and third-order models are examined during system identification. The results indicated that the under-damped third-order system model with a zero represents the system response relatively better.

Transfer function of the system is identified for each input type separately and all these identified transfer functions are tested for each input type to find out the best suitable transfer function. After transfer functions results are compared, the transfer function which is identified by step input is evaluated to be the best fit among the other inputs. The transfer function of the model is given in Equation 4.2. From the identified model parameters the natural frequency and damping ratio, which are required for implementing input shaping, are calculated as $\omega_n = 1/Tw$ and $\xi = Zeta$.

$$\frac{K\left(1+T_Z s\right)}{\left(1+\left(2\,Zeta\,T_w\right)s+\left(T_W s\right)^2\right)\left(1+T_{P3}s\right)} \tag{4.2}$$

System identification results with speed operation mode: The parameter values for the best fit are found out to be: K=25.47; T_Z =-0.0398; Zeta=0.2880; T_W =0.0479; T_{P3}=0.0857. The simulation test result of the identified transfer function for step input is compared with the experimental test results as presented in Figure 4.16.

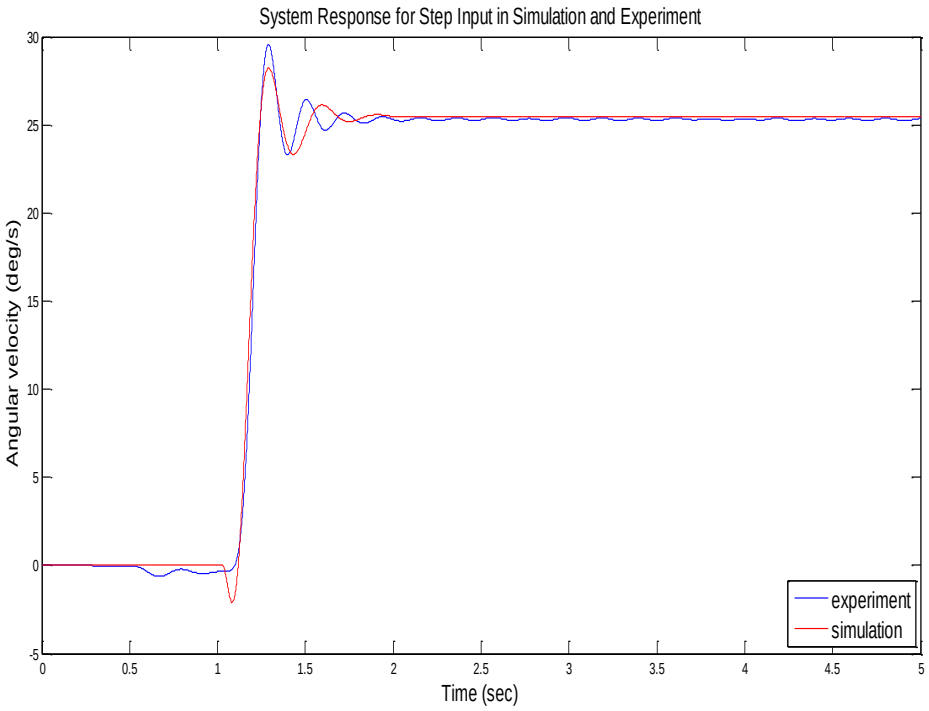

Figure.4.16. Response of the system without joint clearance for step input in simulation and experimental tests (speed operation mode)

System identification results with position operation mode: The same process is repeated for the identification of the system in position operation mode. The identified transfer functions are compared and the transfer function of step input is selected because it provides better results with respect to the other in terms of consistency of simulation and experimental results. The parameters of the identified transfer function of the system are: K=0.9959; T_Z =0.0042; Zeta=0.9968; T_W =0.0102; T_{P3} =0.0034. The simulation test result of the identified transfer function for step input is compared with the experimental test results as presented in Figure 4.17.

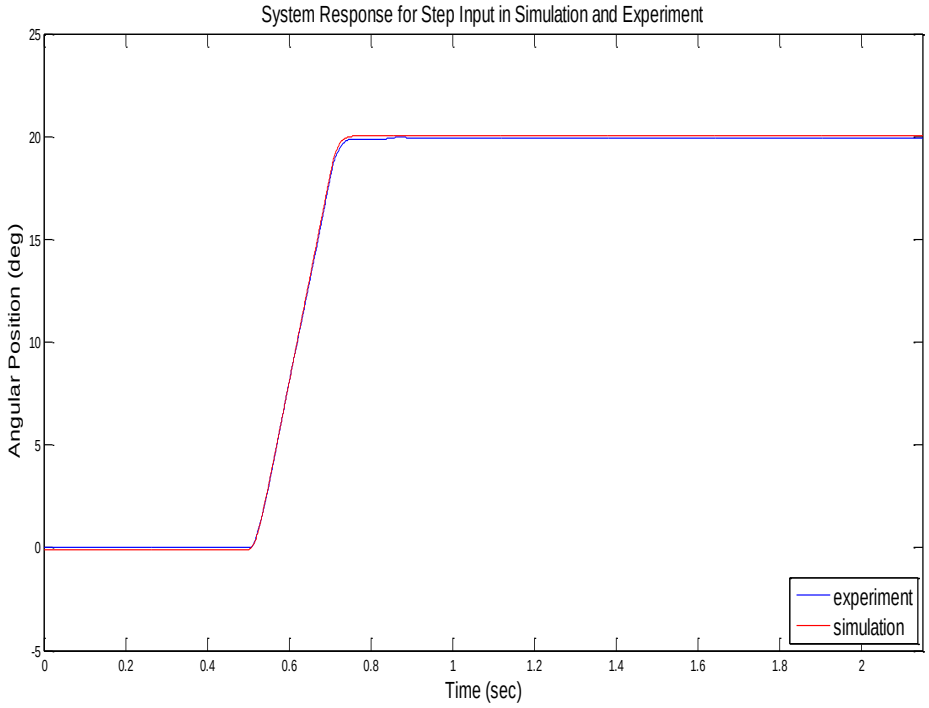

Figure.4.17. Response of the system without joint clearance for step input in simulation and experimental tests (position operation mode)

After system transfer function is verified, joint clearance model is added to the system and the system is run with joint clearance in simulation. The angular velocity measured from the tip of the mechanical link in the simulation model, is compared to the output of the gyroscope attached to the tip of the mechanical link in experimental tests. If the results of the simulation and the experimental tests indicate consistency, the joint clearance model is verified. Otherwise, the joint clearance model parameters are updated. The procedure followed to verify the system model with joint clearance is shown in Figure 4.18.

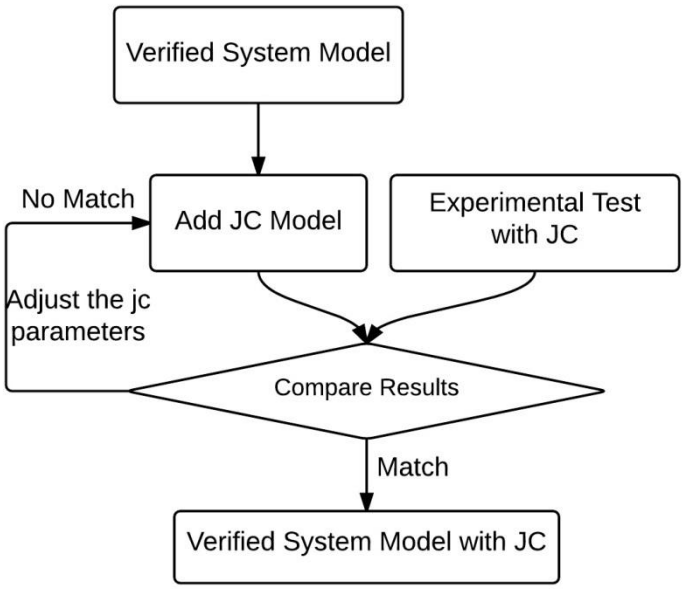

Figure.4.18. System model verification

Hertzian force contact model is selected as the joint clearance modelling method. This method was explained in detail in Chapter 2. The force equation of the Hertzian force contact model is described in Equation 4.3.

$$F_N = K\delta^n + D\delta \tag{4.3}$$

The stiffness, *K*, and the damping ratio, *D*, are the parameters of the Hertzian model to be calibrated by the joint clearance verification procedure. The parameter *n* is selected as 1.5 because it has to be larger than 1 and in the previous studies it was selected as 1.5. After some iteration for these parameter values to fit the experimental test results, the parameters are determined as K=5 and D=350 in speed operation mode and K=10000 and D=300 in position operation mode. After adjusting the joint clearance parameters, the simulation and experimental test results for step inputs are plotted in both speed and position operation modes. The plots are given in Figures 4.19 and 4.20.

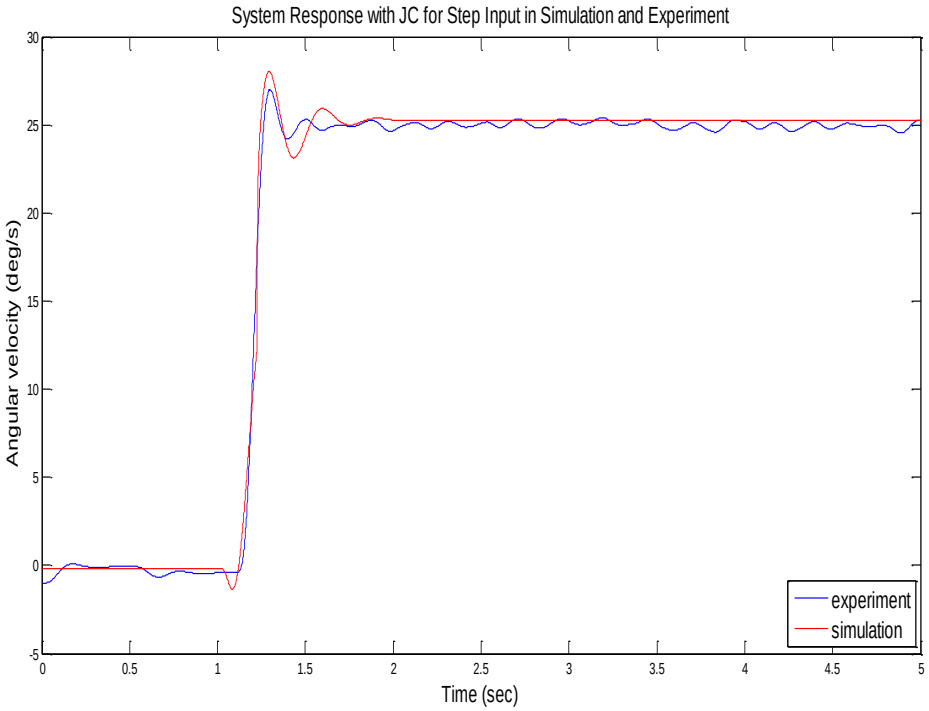

Figure.4.19. Response of the system with joint clearance for a step input in simulation and experimental tests (speed operation mode)

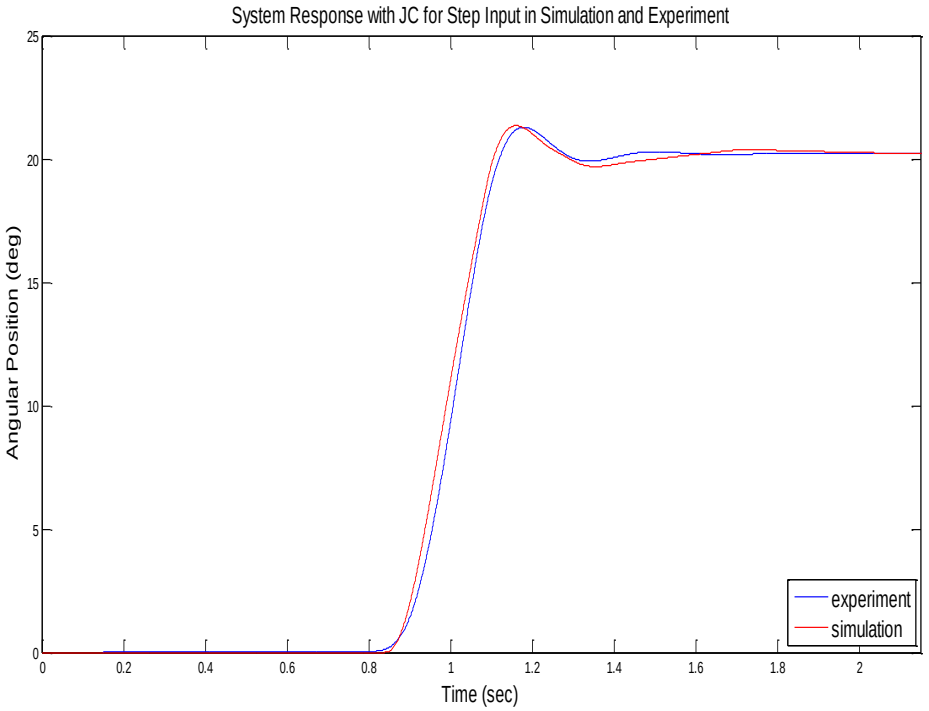

Figure.4.20. Response of the system with joint clearance for a step input in simulation and experimental tests (position operation mode)

The consistency of the test results in simulation and experimentation is evaluated by using the same calculation method presented in Equation 4.1. The results came out to be 0.0067 for speed operation mode and 0.0042 for position operation mode. The results indicate that the system model with joint clearance was developed with a relative precision. After system model with joint clearance is verified, the input shaping method is used in the simulation environment and later in experimental tests. In the next section, input shaping test results are provided.

CHAPTER 5

TEST RESULTS

Simulation and experimental tests are carried out to assess the performance of the input shaping method applied to a mechanical joint with joint clearance. Initially, simulation tests are conducted on the identified model of the system with joint clearance. In simulation tests, the same model is tested for the same input signals when the input shaping method is applied and when it is not applied. In addition, three types of input shaping methods are examined in the simulation tests.

After the simulation tests are completed and the results are acquired, for verification of the tests results, experimental tests are carried out. In experimental tests, the input shaping method which provided better results in terms of residual vibration is chosen to be implemented. The experimental tests results are then compared with the simulation test results for verification. Simulation and experimental test results for the system working in speed operation mode is given in the next section followed by the results obtained with the position operation mode tests.

5.1. Speed Operation Mode Tests

After the system model with joint clearance is approximated by using system identification procedure explained in the previous Chapter, input shaping method is implemented on the system. Initially, the simulation tests are carried out in speed operation mode. After the response of the system is obtained from simulations, for verification of the results, the input shaping is implemented on the experimental system. The next sub-section defines the simulation tests and provides the results for speed operation mode. Later, the experimental results for the speed operation mode are given.

5.1.1. Simulation Test Results in Speed Operation Mode

The same inputs that were used in the system identification in speed operation mode are used in simulation tests. The response of the system with joint clearance measured from the servomotor's rotor is shown in Figure 5.1 and measured from the gyroscope at the end of the mechanical link is shown in Figure 5.2. It should be noted that these measurements are done in simulation environment through the encoder and gyroscope models. The results shown in Figure 5.1 and 5.2 are acquired when the input shaping method is not implemented.

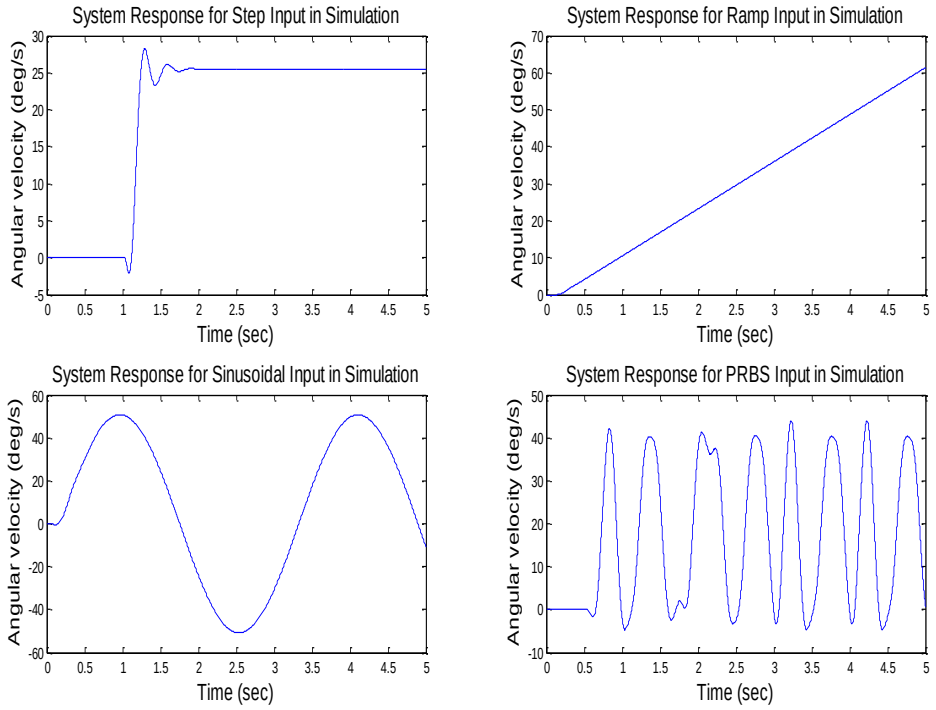

Figure.5.1. Response of the system with joint clearance to inputs in velocity domain measured from the encoder in simulation (speed operation mode – not shaped inputs)

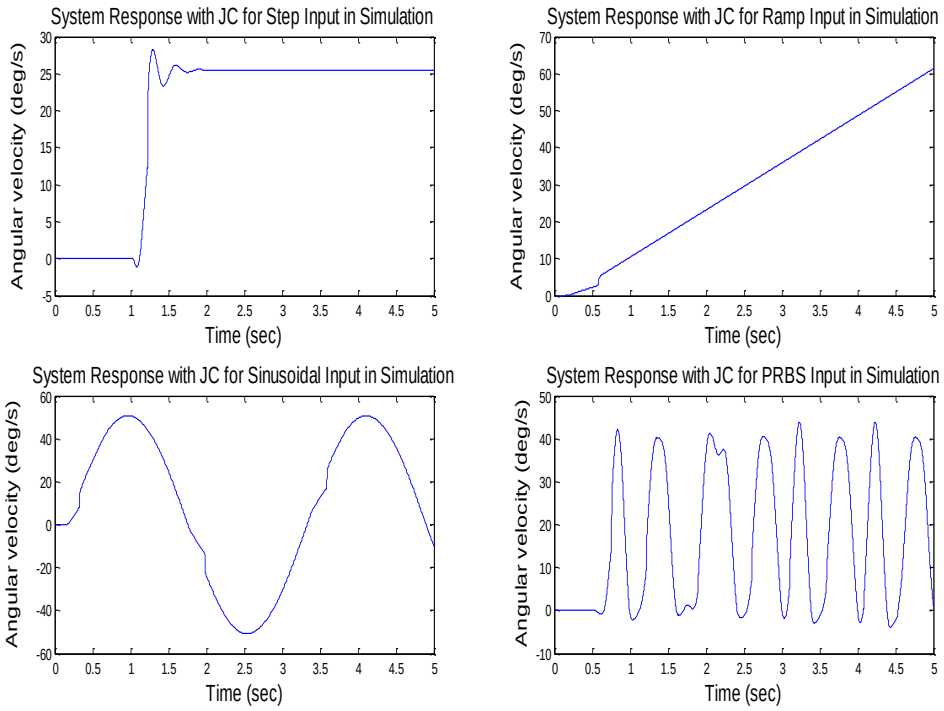

Figure.5.2. Response of the system with joint clearance to inputs in velocity domain measured from the gyroscope in simulation (speed operation mode – not shaped inputs)

After acquiring the response of the system when inputs shaping is not implemented, three kinds of input shaping methods, which were explained in Chapter 2, are implemented to observe the effect of these methods. Shaping of a step input is shown in Figure 5.3 for the three kinds of input shaping methods.

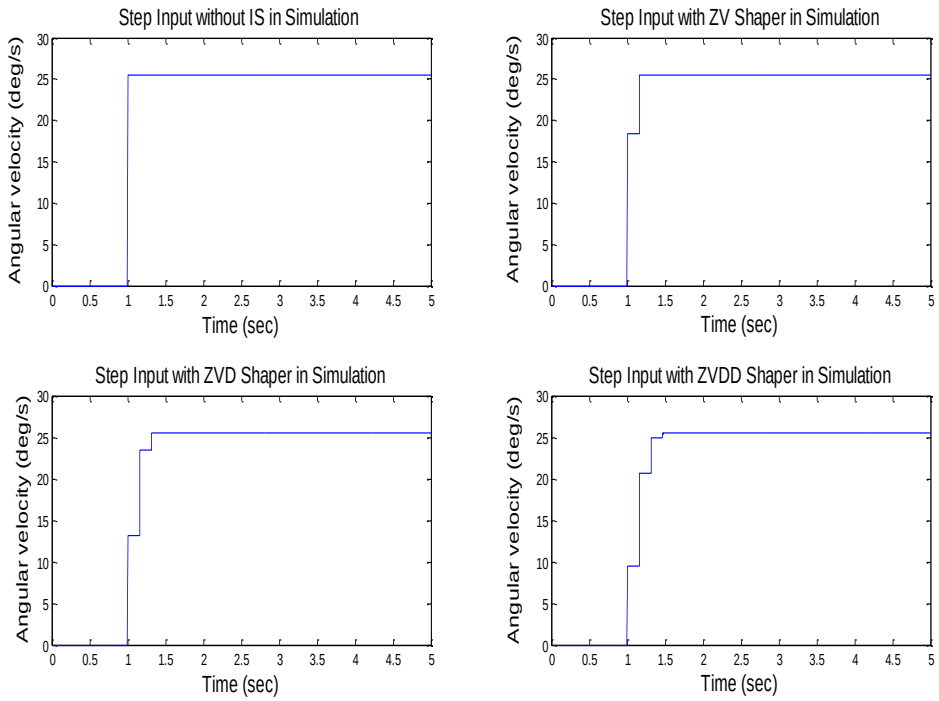

Figure.5.3. A step angular velocity input shaped with different input shaping methods

These input shaping methods are implemented for all the other inputs selected for this study. However, expect the PRBS signal, all the other input signals have finite jerk profiles and as a result of this, the effect of the input shaping methods in shaping the inputs are not observed clearly with respect to the effects of input shaping for a step input.

In Figure 5.4, responses of the system for step inputs, which are shaped with three different input shaping methods, are given along with the response of the system for an unshaped step input. The overshoot and oscillations in the system response for the unshaped input, which is identified with red color in the figure, are reduced by using input shaping methods.

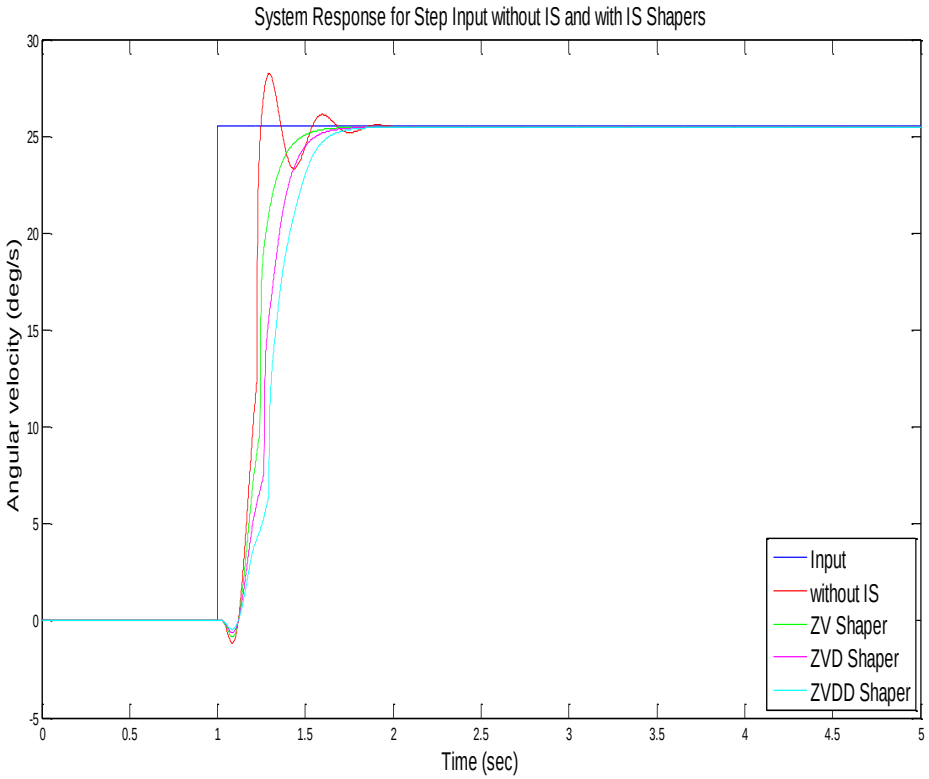

Figure.5.4. Responses of the system with joint clearance for step inputs in velocity domain in simulation measured from the gyroscope (speed operation mode)

The system responses for the ramp and sinusoidal inputs are shown in Figures 5.5 and 5.6 respectively. It can be observed that the system does not have residual vibrations in its response for the shaped and unshaped inputs of these kinds. The main reason for this is that the jerk of the system is limited. The only effect of the shaped inputs on the system response is that they made the system response slower with respect to the unshaped input. For the ramp input, inputs shaping increased the time to reach the steady state and increased the steady state error and for the sinusoidal input, input shaping increased the phase difference with respect to the input signal decreased the amplitude of the resultant sinusoidal motion.

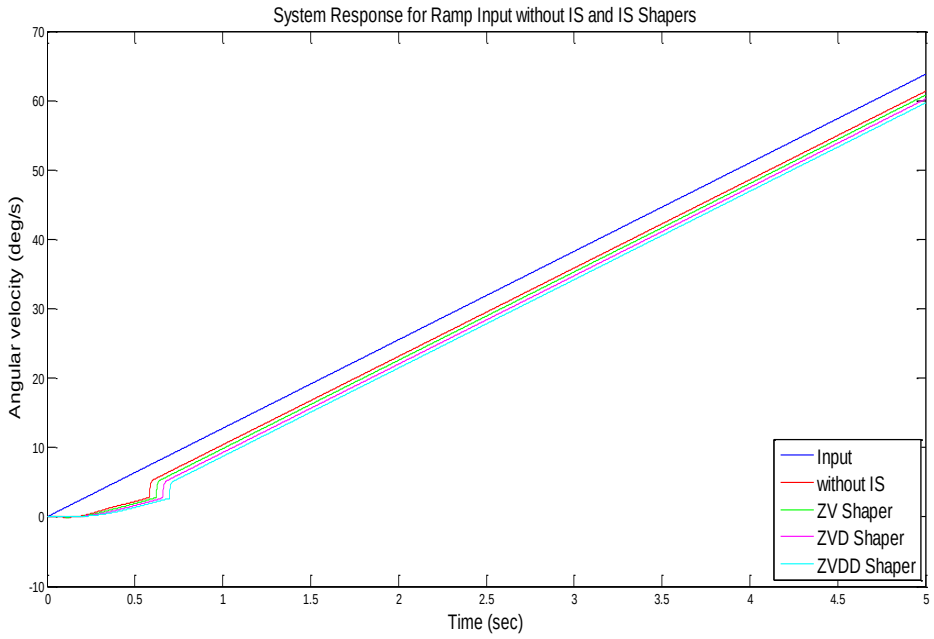

Figure.5.5. Responses of the system with joint clearance for ramp inputs in velocity domain in simulation measured from the gyroscope (speed operation mode)

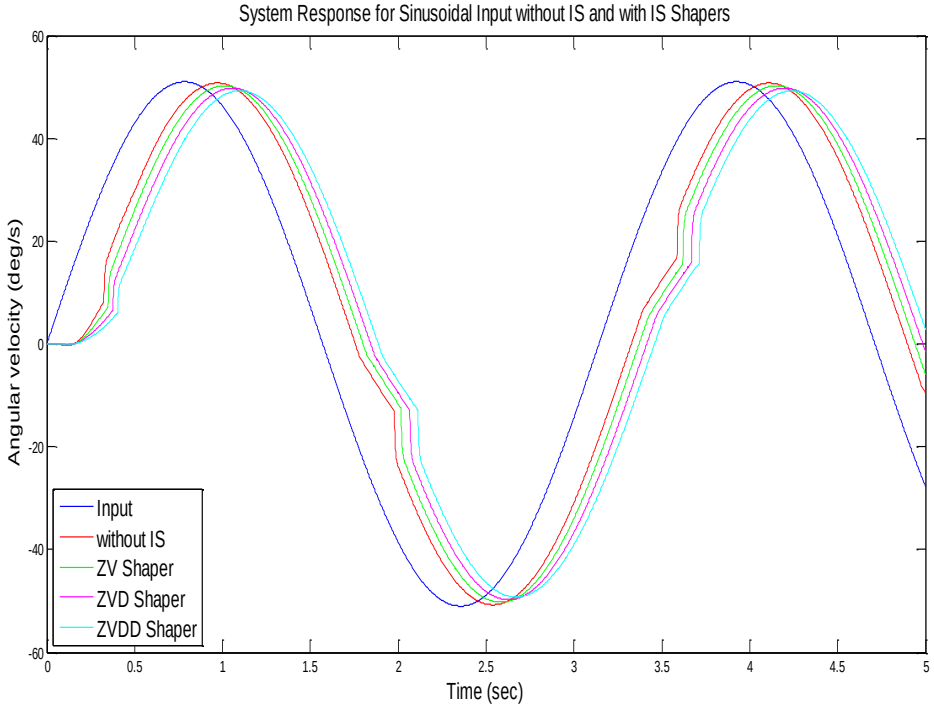

Figure.5.6. Responses of the system with joint clearance for sinusoidal inputs in velocity domain in simulation measured from the gyroscope (speed operation mode)

The last type of input used in the tests was the PRBS input. The responses of the system to the unshaped and shaped inputs designed for PRBS input is provided in Figure 5.7. The range of the signal was selected large with respect to the frequency of the inputs pulses for this electromechanical system dynamics. Therefore, the system was not able to reach the desired input values especially when the width of the pulse is relatively small. However, it can be observed that the response of the system for the unshaped input pulse between 1.5 and 2.5 seconds has an oscillatory behavior. These oscillations are canceled by implementing input shape methods.

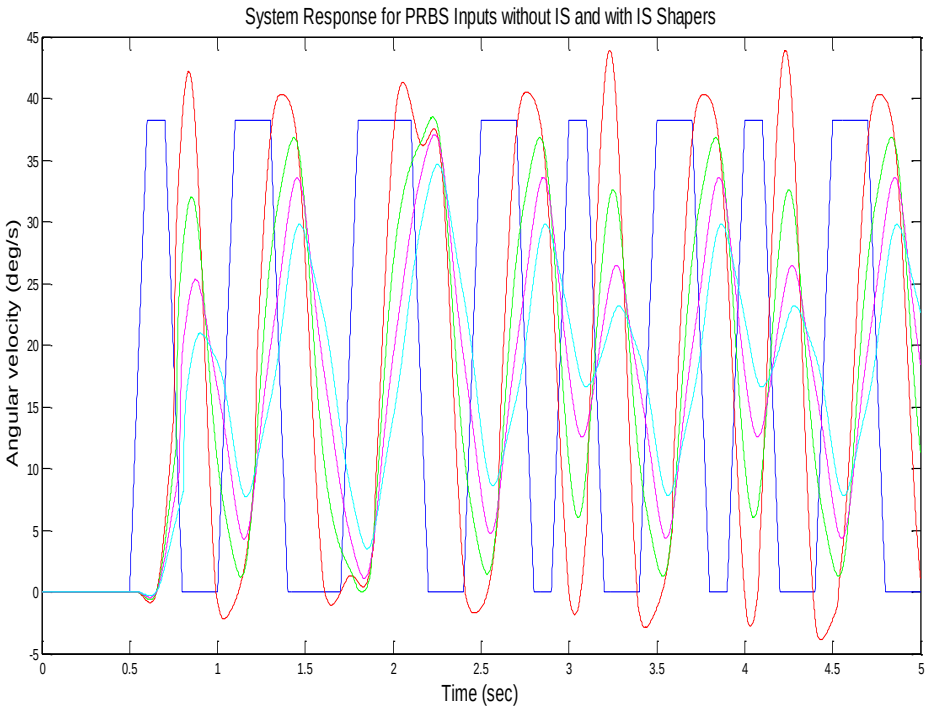

Figure.5.7. Responses of the system with joint clearance for PRBS inputs in velocity domain in simulation measured from the gyroscope (speed operation mode)

In all the presented test results, it can be observed that the largest delay in the system response is induced by the ZVDD input shaping method.

5.1.2. Experimental Test Results in Speed Operation Mode

After input shaping is implemented and verified in the simulation tests in speed operation mode, this sub- section describes the implementation of the input shaping on experimental tests in speed operation mode. It was previously observed from the

simulation test results that the input shaping provides better results in terms of cancelling residual vibrations for the inputs that have higher jerk values such as the step input and the PRBS input. Therefore, in the experimental tests, the system is tested against a higher jerk input profile, which is the same step input used in the simulation tests. The response of the system measured from the gyroscope attached to the end of the mechanical link in the experimental set-up is shown in Figure 5.8.

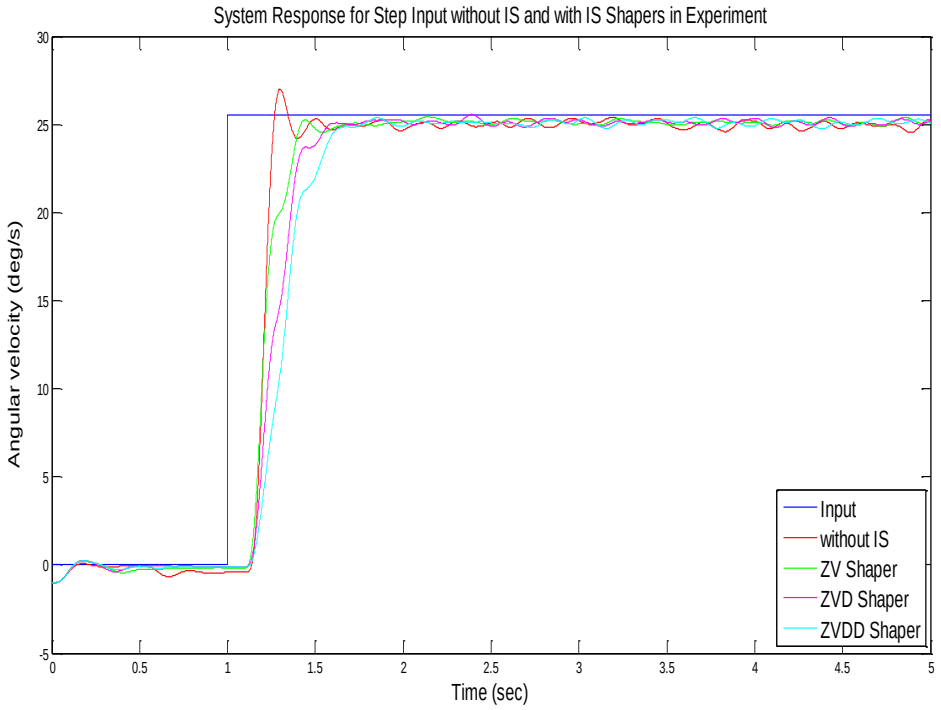

Figure.5.8. Responses of the system with joint clearance for step inputs in velocity domain in experimentation measured from the gyroscope (speed operation mode)

In order to compare the effectiveness of the input shaping methods with respect to each other an error calculation method is derived. In this method, first the mean value in of the system response after it reaches the steady-state is calculated and named as *M*. Then the deviation of the system response from this mean value is calculated to observe the effect of residual vibrations.

The calculation of the level of residual vibrations is given in Equation 5.1. In this equation, depending on the sampling time, the mean deviation for the system response, *MD*, is calculated in *n* number of intervals. The value of the system response signal at the i^{th} interval is denoted as s_i.

$$MD = \sqrt{\frac{\sum_{i=1}^{n} (M - s_i)^2}{n}} \tag{5.1}$$

To use Equation 5.1, mean of the system response is determined. The first coincide point of the system response and the mean data is taken as a start point to calculate the mean deviation of the steady-state response of the system. In Figure 5.9 mean deviation procedure is illustrated.

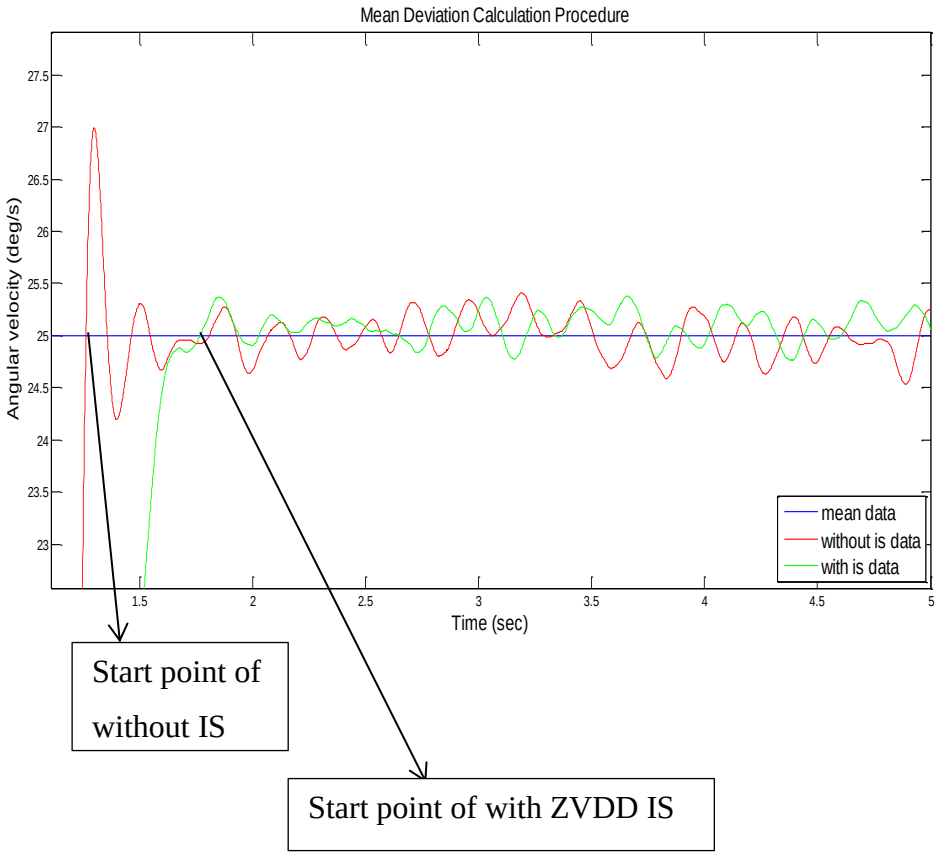

Figure 5.9. Mean Deviation

After 10 successive tests with input shaping methods and without input shaping are conducted, the mean deviations of the system response are calculated and tabulated in Table 5.1. The average mean deviation of the tests indicate that residual vibration effects are lower for all input shaping methods with respect to the unshaped input results. Among the input shaping methods, ZVDD resulted in better performance in cancelling the effects of residual vibrations. However, it can be clearly observed from Figure 5.8 that the ZVDD input shaping method results in a slower system response

with respect to the other input shaping methods. The improvement in the cancelling the effects of residual vibrations can be calculated by the difference between the mean deviations of the ZVDD input shaping method and the unshaped input. The improvement is percentage comes out to be at (0.392-0,191)/ 0.392=52.1%.

Table.5.1. Mean deviations of the steady-state responses of the system

Test Number	Without is	ZV Shaper	ZVD Shaper	ZVDD Shaper
1	0.303	0.172	0.166	0.146
2	0.364	0.232	0.264	0.220
3	0.385	0.195	0.124	0.123
4	0.317	0.262	0.240	0.259
5	0.409	0.156	0.127	0.145
6	0.402	0.276	0.254	0.231
7	0.431	0.181	0.159	0.159
8	0.420	0.294	0.268	0.250
9	0.463	0.244	0.154	0.149
10	0.421	0.273	0.241	0.230
mean	0.392	0.229	0.198	0.191

5.2. Position Operation Mode Tests

The same procedure as it was for the speed operation mode is followed for the position operation mode tests. Initially, the simulation tests are carried out in position operation mode. After the response of the system is obtained from simulations, for verification of the results, the input shaping is implemented on the experimental system. The next sub-section defines the simulation tests and provides the results for position operation mode. Later, the experimental results for the position operation mode are given.

5.2.1. Simulation Test Results in Position Operation Mode

In simulation tests, because of the limitations of the motion input method in position operation mode, as it was explained in the previous Chapter, different inputs with respect to the speed operation inputs are used. These inputs are selected to have larger and smaller jerk values. The selected inputs are step input (with a finite jerk value), ramp input, two step inputs on top of each other (with finite jerk value), two step inputs one after the other (with finite jerk value), parabolic input and a pulse input (with finite jerk value). The response of the system with joint clearance measured from the servomotor's rotor is shown in Figure 5.10 and the gyroscope at the end of the mechanical link is shown in Figure 5.11. It should be noted again that these measurements are done in simulation environment through the encoder and gyroscope models. The results shown in Figure 5.10 and 5.11 are acquired when the input shaping method is not implemented.

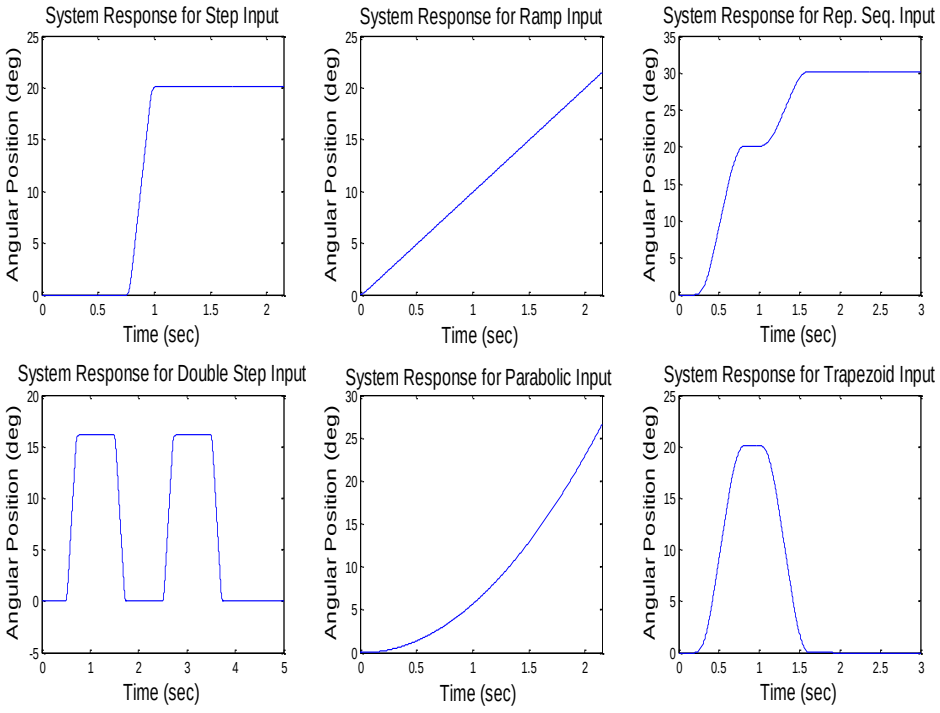

Figure.5.10. Response of the system with joint clearance to inputs in position domain measured from the encoder in simulation (position operation mode – not shaped inputs)

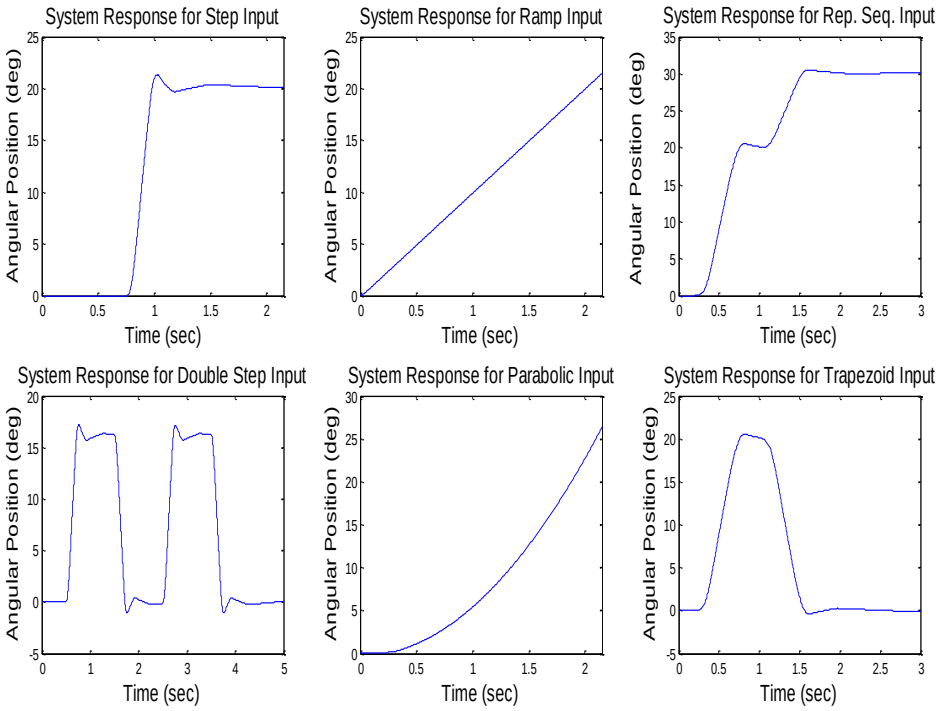

Figure.5.11. Response of the system with joint clearance to inputs in position domain measured from the gyroscope in simulation (position operation mode – not shaped inputs)

In simulation tests with in the position operation mode, only ZVDD type of input shaping is used since in the speed operation mode, ZVDD type of input shaping was found to be providing the best solution for cancelling the effects of joint clearance in terms of residual vibrations. In Figure 5.12, system responses for the step input without input shaping and with ZVDD input shaping method are compared. The overshoot and oscillations of the unshaped input, which is printed in red color in the figure, are reduced by using ZVDD input shaping method. The system response with the input shaping is denoted with green color in Figure 5.12.

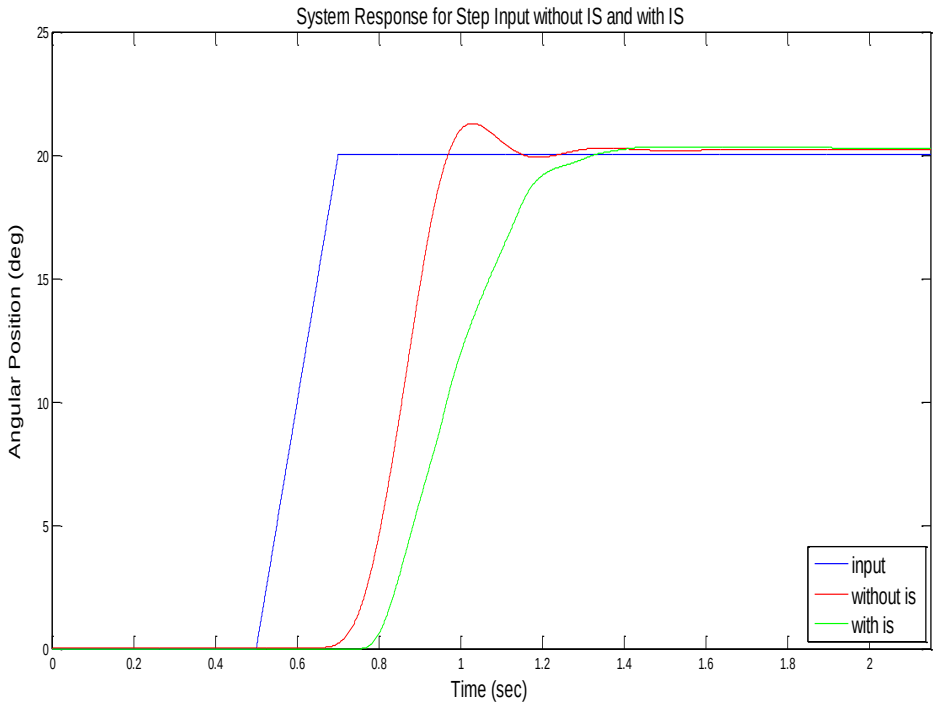

Figure.5.12. Response of the system with joint clearance for step input in position domain in simulation (position operation mode)

In ramp input and two step inputs on top of each other (with relatively low jerk values), the jerk values are very low. The joint clearance in the system does not induce observable residual vibrations to the system for these inputs. Therefore, the input shaping method only makes the system response slower. System responses for the ramp input and two step inputs on top of each other are shown in Figure 5.13 and 5.14 respectively.

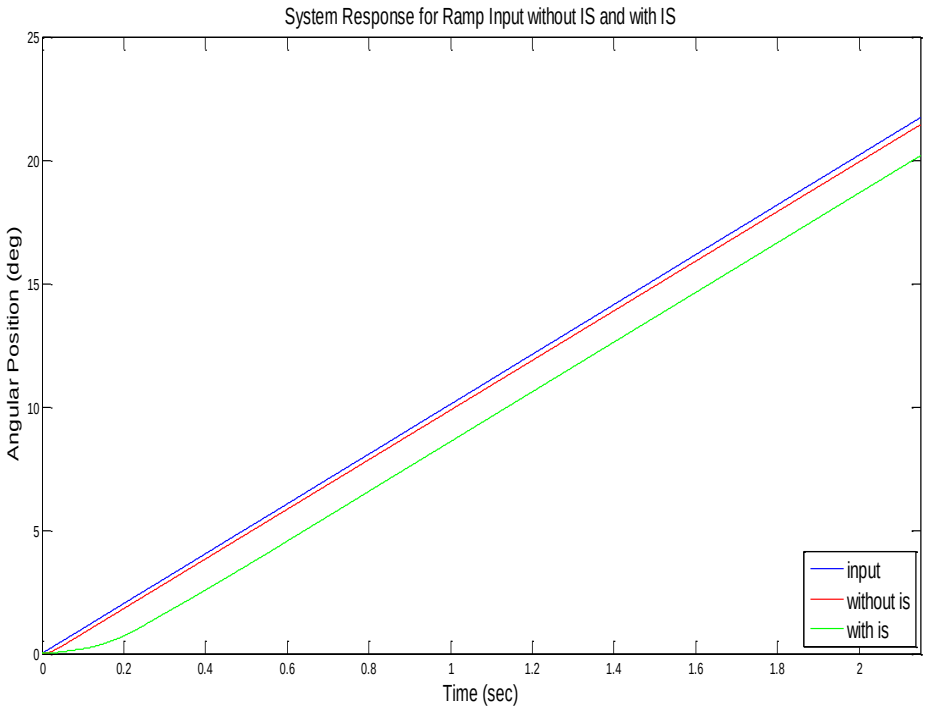

Figure.5.13. Response of the system with joint clearance for ramp input in position domain in simulation (position operation mode)

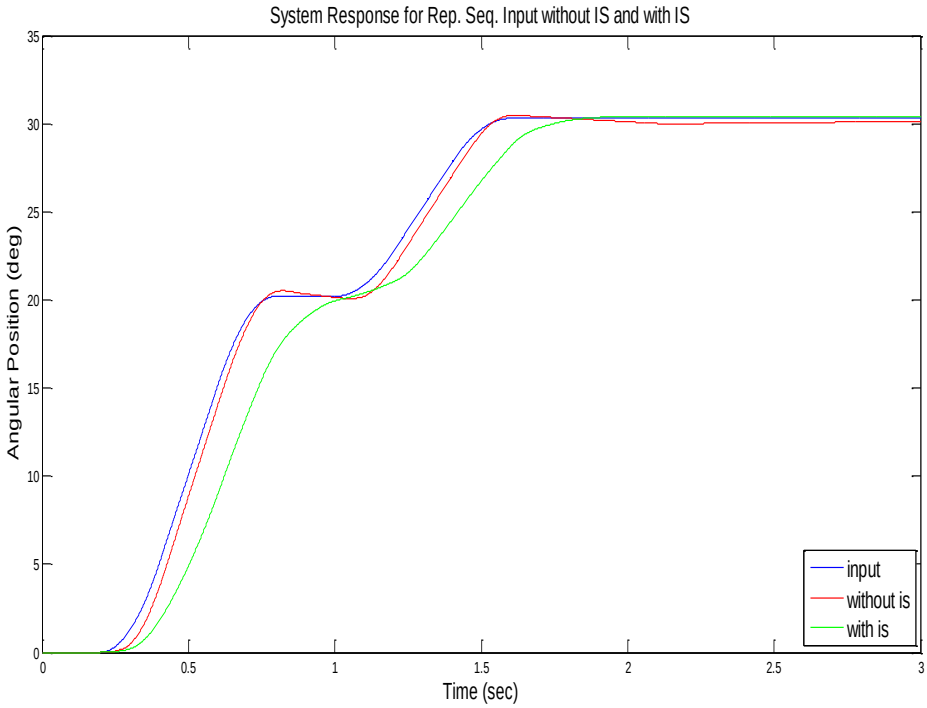

Figure.5.14. Response of the system with joint clearance for repeating sequence input in position domain in simulation (position operation mode)

The next input type tested is the double step input one coming after the other one. In this case the jerk values are selected to be relatively high and as a result of this, the joint clearance results in residual vibrations. The response of the system for the unshaped input is denoted with red color in Figure 5.15. The overshoot which is clearly observed in this figure is cancelled by implementing the ZVDD type input shaping method. The response of the system for the shaped input is shown in green color in this figure.

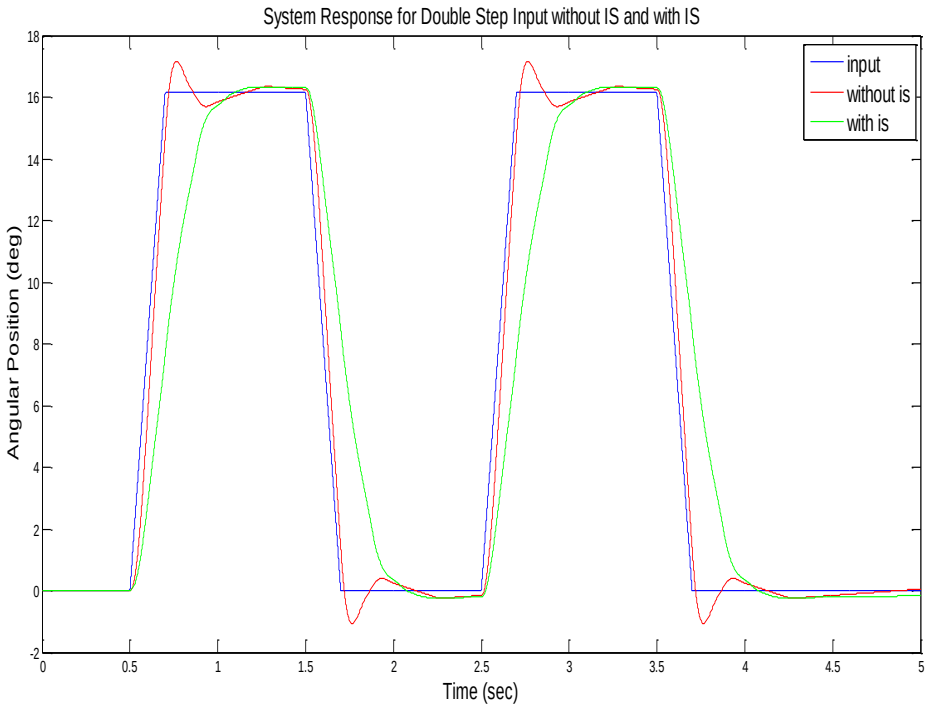

Figure.5.15. Response of the system with joint clearance for double step input in position domain in simulation (position operation mode)

Parabolic input in position is representing a constant acceleration profile where initially (at time 0), the jerk is infinite and then (at time 0^{+}) it is equal to zero. As a result of this, there are no residual vibrations present in the system response for the unshaped input, which can be observed from Figure 5.16. The effect of the ZVDD type input shaping method for this input is that is slows down the system response.

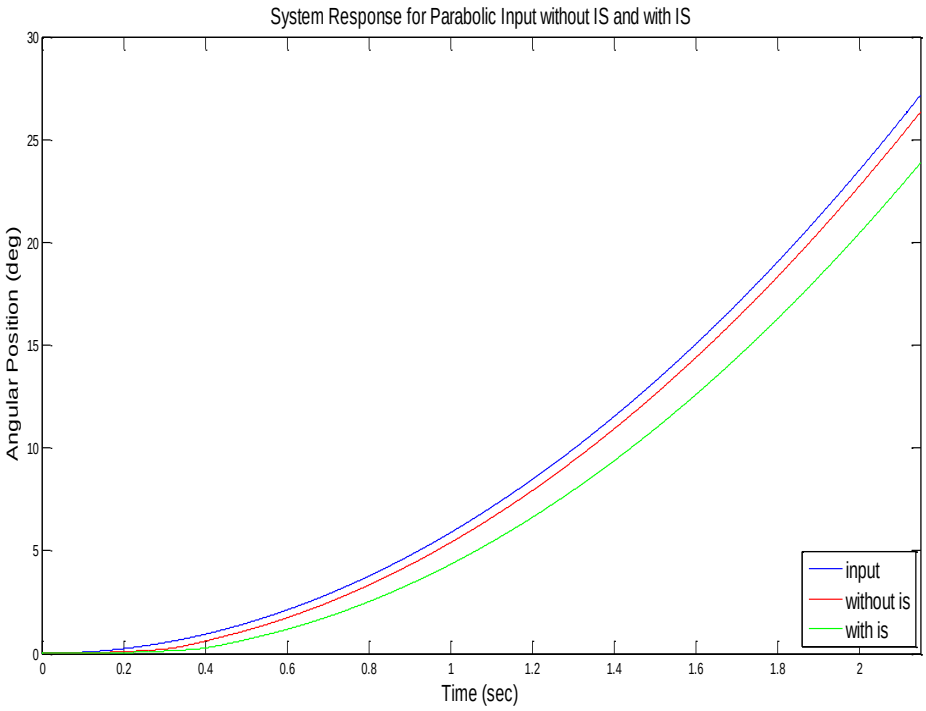

Figure.5.16. Response of the system with joint clearance for parabolic input in position domain in simulation (position operation mode)

The last input type examined in simulation tests with position operation mode is the pulse input with relatively low jerk values. In this case, residual vibration can be observed from the system response for unshaped input, which is denoted with red color in Figure 5.17. The ZVDD method cancels out the residual vibrations as it was expected and the system response for the shaped input is shown in green color in this figure.

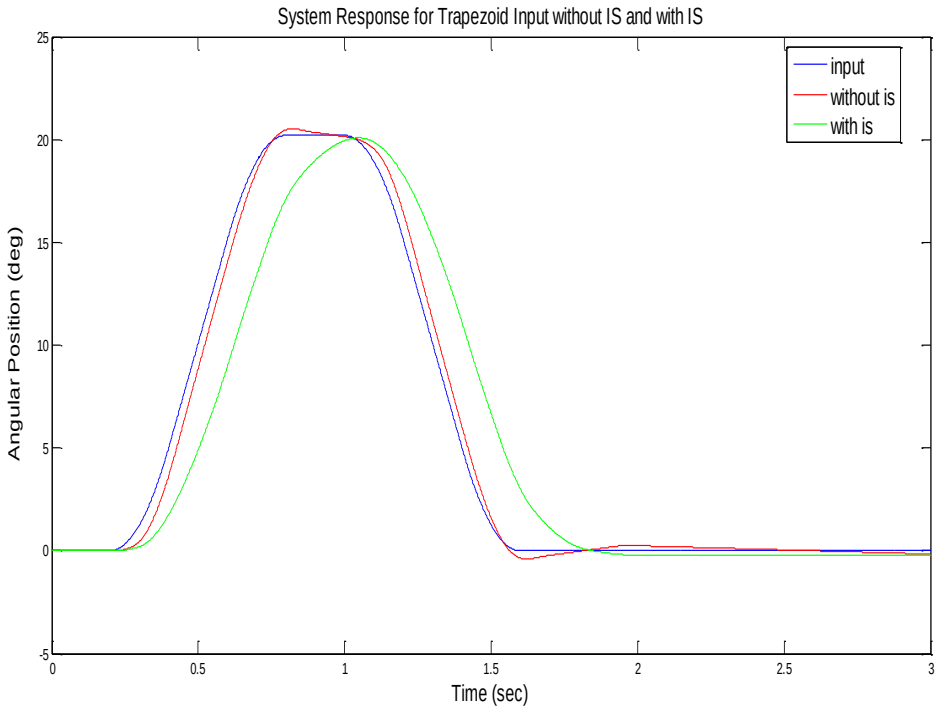

Figure.5.17. Response of the system with joint clearance for trapezoid input in position domain in simulation (position operation mode)

After input shaping is implemented and proved to reduce the residual vibrations in simulation tests, input shaping is applied on the experimental tests.

5.2.2. Experimental Test Results in Position Operation Mode

After input shaping is implemented and verified in the simulation tests, this sub-section describes the implementation of the input shaping on experimental tests. It was previously observed from the simulation test results that the ZVDD type input shaping provides better results in terms of cancelling residual vibrations for the inputs that have higher jerk values such as the step input and the double step input. Therefore, in the experimental tests, the response of the system to parabolic, ramp and two step inputs on top of each other and pulse input with low jerk values inputs are not examined. The original input for the selected input types and the shaped version of these inputs with ZVDD input shaping method are presented in Figure 5.18. The original inputs are shown with blue color and the shaped inputs are shown with the red color.

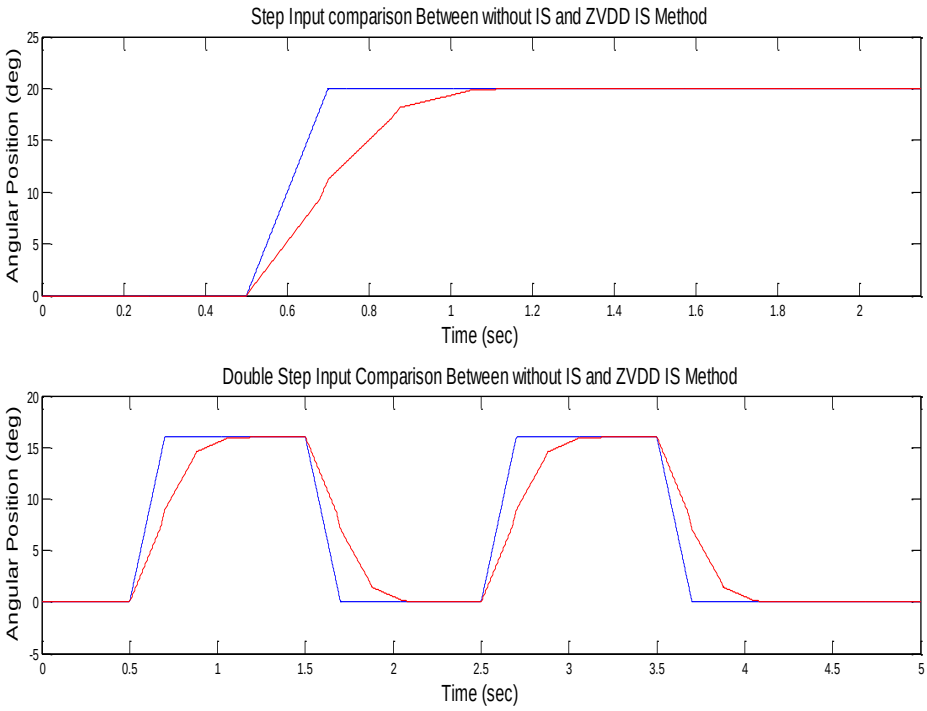

Figure.5.18. Unshaped and shaped inputs in position domain to be used in the experimental tests (position operation mode)

The response of the system to a step input measured from the gyroscope attached to the end of the mechanical link in the experimental set-up is shown in Figure 5.19. In figure 5.19, blue line represents step input, red line represent system response to unshaped input and green line represents system response to shaped input.

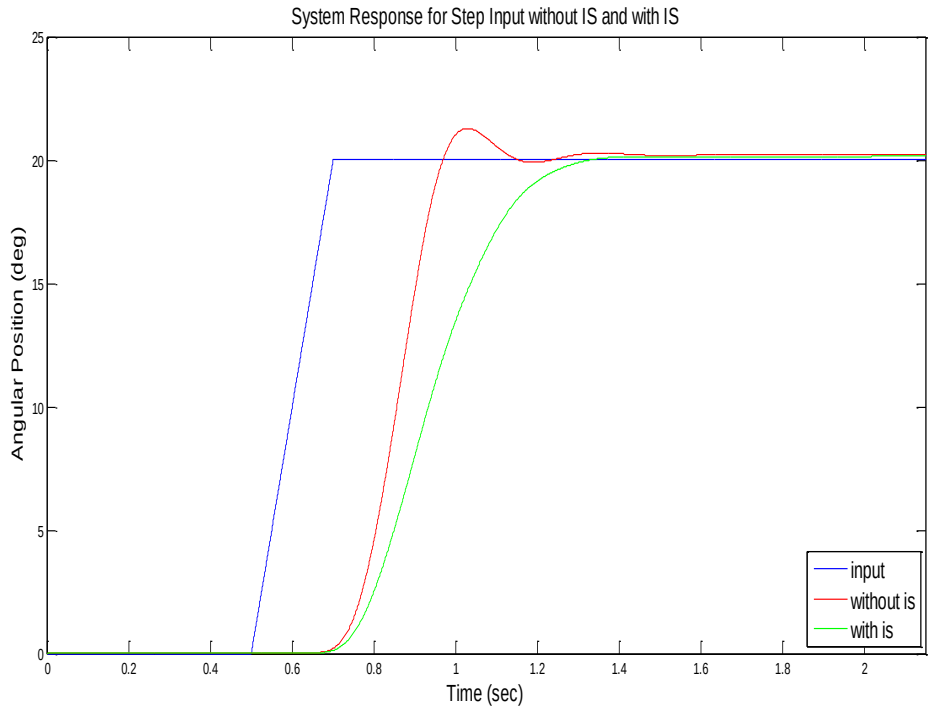

Figure.5.19. Angular position of the link attached to the joint with joint clearance for step output comparison between without is and zvdd method in experiment

It is observed that the overshoot present for the unshaped input response is lost for the shaped input response of the system in Figure 5.19. The system is then subjected to the double step input and the system response to the unshaped and shaped double step input is shown in Figure 5.20. Also, from this figure it is clearly observed that the overshoot present in the unshaped input response is lost and there are no residual vibrations in the shaped input response of the system.

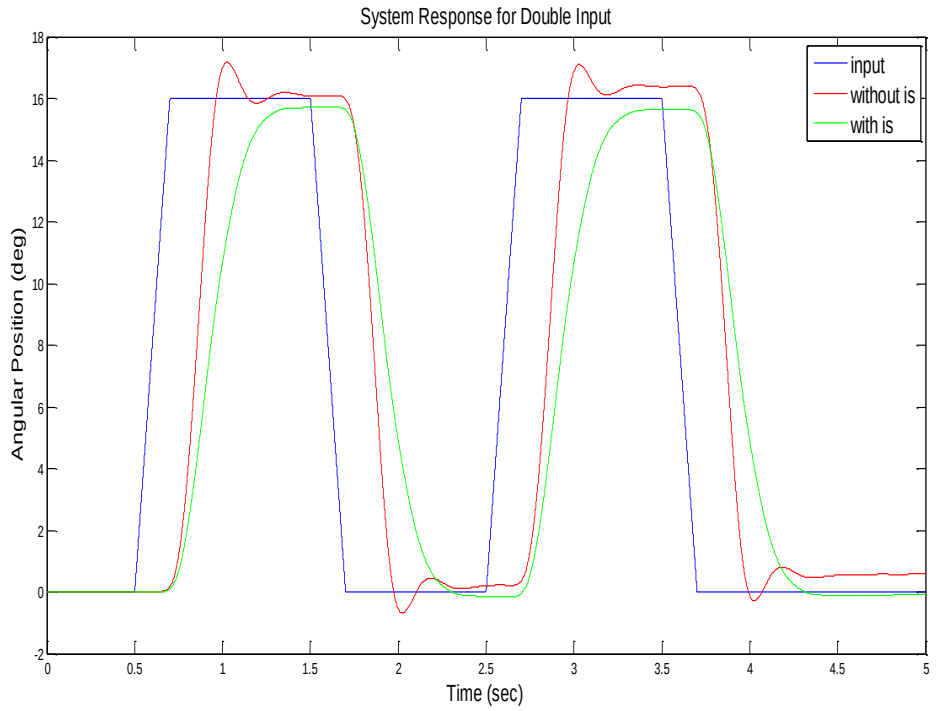

Figure.5.20. Response of the system with joint clearance for different inputs in position domain in experiment (position operation mode)

The effects of the inputs shaping for these inputs are quantified using the Equation 5.1 by finding the mean deviation of the system response from the calculated mean value. The results for both input types are tabulated in Table 5.2.

Table.5.2. Mean deviations of the steady-state responses of the system for step input

	Step Input		Double Step Input	
	Without IS	With IS	Without IS	With IS
1	0.270	0.014	0.273	0.027
2	0.307	0.007	0.266	0.019
3	0.307	0.011	0.288	0.018
4	0.308	0.015	0.265	0.026
5	0.318	0.016	0.288	0.020
6	0.334	0.014	0.286	0.020
7	0.271	0.010	0.277	0.025
8	0.302	0.013	0.284	0.022
9	0.283	0.011	0.263	0.023
10	0.332	0.018	0.281	0.023
Mean	0.303	0.013	0.277	0.022

The improvement is percentage comes out to be at (0.303-0.013)/ 0.303=95.7% for step input and the improvement is percentage comes out to be at (0.277-0.022)/ 0.277=92.1% for the double step input.

CHAPTER 6

CONCLUSIONS

In this study, for the first time, input shaping method is applied to reduce the joint clearance effects in terms of residual vibrations. A mechanical joint with joint clearance is used for both simulations and experimental tests. First, a transfer function for the mechanical system is determined via system identification. Two different transfer functions are set for position and speed operation modes. In the simulation part, the mechanical system and the joint clearance are modelled and the effects of joint clearance are determined using the model constructed in Matlab Simulink environment. After that, input shaping is added to the system for reducing the residual vibrations. Simulation tests are used for checking the results with the experimental results. Both speed operation mode and position operation mode are used to drive the system. For each operation mode, several inputs are given. Input shaping is implemented and it is revealed that input shaping method is capable of reducing the residual vibrations. After simulation and experimental tests, this study pointed the issues described below.

Speed operation mode, which is available for the test set-up used in this study, provides fast response although analog velocity commands are noisy. Moreover, adding a low-pass filter to eliminate noises in encoder signals affects quality of the information obtained during the system identification to determine the transfer function parameters. Despite the inaccurate transfer function, when input shaping is applied to step input, an improvement is observed as 52.1% improvement of mean deviation values in speed operation mode.

Position operation mode is almost noise free; however the system response is slower than the speed operation mode. The main reason for this is that he change in the input velocity can be realized for almost in 30 Hz. For this reason the step input is not exactly a step input, but modified version of it with a finite jerk value. Since slower response creates low oscillations, the rotating mass is increased to observe vibrations with greater amplitude. Using a digital gyroscope instead of an analog measurement device increased the consistency and hence reliability of feedback. As the transfer

function of the rotating system is estimated successfully, outputs of the simulation and outputs of the experiments results were close to each other for the same inputs.

The success of input shaping depends on jerk profile of the input function. For the input types with relatively lower jerk values, input shaping does not have significant effect. However, significant improvement is more observed when input shaping is applied inputs with relatively higher jerk profiles. Deviation of the response of the system in its steady state from the mean value of the response at steady state is accepted as a quantification method for calculating the improvement in terms of cancelling residual vibrations for this system. The improvement is observed in between 92.1% to 95.7% for different inputs in position operation mode, which proves that the implementation of input shaping results in a successful cancellation of residual vibrations.

In position operation mode several angular displacements are tested for the same type of input and the results presented in the APPENDIX B of this thesis show that input shaping is more effective for the larger angular displacements.

As a future work input shaping method can be implemented on multi DoF robot manipulators. Also, the motion profile of a system with joint clearances can be pre-processed to cancel the residual vibration when relatively larger jerk profiles are required.

REFERENCES

Alıcı, G., Jagielski, R., Şekercioğlu, Y.A., Shirinzadeh, B. 2006. "*Prediction of Geometric Errors of Robot Manipulators with Particle Swarm Optimization Method*", Robotics and Autonomous Systems, v 54, pp. 956-966.

Ammattikorkeakoulu, L. 2011. "*The Basics of Robotics*", Mechatronics Thesis.

Angeles, J. 2003. "*Fundamentals of Robotic Mechanical Systems: Theory, Methods, and Algorithms*", Second Edition.

Azad, A.K.M., Shaheed, M.H., Mohamed, Z., Tokhi, M.O., Poerwanto, H. 2008. "*Open Loop Control of Flexible Manipulators Using Command-Generation Techniques*", in: Tokhi, M.O., Azad, A.K.M. (Eds.) Flexible Robot Manipulators – Modelling, Simulation and Control, The Institution of Engineering and Technology.

Bauchau, O.A., Rodriguez, J. 2002. "*Modeling of Joints with Clearance in Flexible Multibody Systems*", International Journal of Solids and Structures, v 39, pp. 41-63.

Chen, G., Wang, H., Lin, Z. 2013. "*A Unified Approach to the Accuracy Analysis of Planar Parallel Manipulators Both with Input Uncertainties and Joint Clearance*", Mechanism and Machine Theory, v 64, pp 1-17.

Chen, J., Chao, L. 1987. "*Positioning Error Analysis for Robot Manipulators with All Rotary Joints*", Robotics and Automation, v Ra-3, No 6, pp. 539-545.

Craig, J.J. 2005. "*Introduction to Robotics*", Third Edition.

Crain, E.A., Singhose, W.E., Seering, W.P. 1996. "*Derivation and Properties of Convolved and Simultaneous Two-Mode Input Shapers*", IFAC World Congress.

Erkaya, S., Uzmay, İ. 2010. "*Experimental Investigation of Joint Clearance Effects on the Dynamics of a Slider-Crank Mechanism*", Multibody System Dynamics, v 24, pp. 81-102.

Flores, P. and Ambrosio, J. 2004. "*Revolute Joints with Clearance in Multibody Systems*", Computers and Structures, v 82, pp. 1359-1369.

Flores, P., Koshy, C.S., Lankarani, H.M., Ambrosio, J., Claro, J.C.P. "*Numerical and Experimental Investigation on Multibody Systems with Revolute Clearance Joints*", Nonlinear Dynamics, v 65, pp. 383-398.

Gong, C., Yuan, J., Ni, J. 2000. "*Nongeometric Error Identification and Compensation for Robotic System by Inverse Calibration*", Machine Tools & Manufacture, v 40, pp. 2119-2137.

Hyde, J.M., Seering, W.P. 1991. "*Using Input Command Pre-Shaping to Suppress Multiple Mode Vibration*", IEEE, International Conference on Robotics and Automation, Sacremento, California, pp 2604-2609.

Innova WEB Site. http://www.innova.no/ (accessed February, 2015)

Jawale, H.P., Thorat, H.T. 2013. "*Positional Error Estimation in Serial Link Manipulator Under Joint Clearances and Backlash*", Mechanisms and Robotics, v 5, pp. 1-7.

Liu, C., Tian, Q., Hu, H. 2012. "*Dynamics and Control of a Spatial Rigid-Flexible Multibody System with Multiple Cylindrical Clearance Joints*", Mechanism and Machine Theory, v 52, pp. 106-129.

Luo, B., Huang, H., Shan, J., Nishimura, H. 2013. "*Active Vibration Control of Flexible Manipulator Using Auto Disturbance Rejection and Input Shaping*", Journal of Aerospace Engineering, pp. 1-14.

Magee, D.P., Book, W.J. 1992. "*The Application of Input Shaping to a System with Varying Parameters*", Japan-USA Symposium on Flexible Automation, July 13-15, San Francisco, California.

Olabi, A., Damak, M., Bearee, R., Gibaru, O., Leleu, S. 2012. "*Improving the Accuracy of Industrial Robots by Offline Compensation of Joints Errors*", IEEE International Conference on Industrial Technology.

Pandilov, Z., Dukovski, V. 2014. "*Comparison of the Characteristics Between Serial and Parallel Robots*", ACTA Tehnika Corviniensis, pp 143-160.

Parenti-Castelli, V. and Venanzi, S. 2005. "*Clearance Influence Analysis on Mechanisms*", Mechanism and Machine Theory, v 40, pp. 1316-1329.

Ravn, P. 1998. "*A Continuous Analysis Method for Planar Multibody Systems with Joint Clearance*", Multibody System Dynamics, v 2, pp. 1-24.

Robots WEB Site. http://www.robots.com/ (accessed January, 2015)

Robot Palletizing WEB Site. http://robotpalletizing.co.uk/ (accessed February, 2015)

Schwab, A.L., Meijaard, J.P., Meijers, P. 2002. "*A Comparison of Revolute Joint Clearance Models in the Dynamic Analysis of Rigid and Elastic Mechanical Systems*", Mechanism and Machine Theory, v 37, pp. 895-913.

Shan, J., Liu, H., Sun, D. 2005. "*Modified Input Shaping for a Rotating Single-Link Flexible Manipulator*", Journal of Sound and Vibration, v 285, pp 187-207.

Singer, N.C., Seering, W.P. 1990. "*Preshaping Command Inputs to Reduce System Vibration*", ASME, v 112, pp 76-82.

Singhose, W.E., Seering, W.P., Singer, N.C. 1996. "*Input Shaping for Vibration Reduction with Specified Insensitivity to Modeling Errors*", Proceedings of the 1996 Japan-USA Symposium on Flexible Automation.

Singhose, W.E., Singer, N.C. 1996. "*Effects of Input Shaping on Two-Dimensional Trajectory Following*", IEEE, v 12, no 6, pp. 881-887.

Subsea World News WEB Site. http://subseaworldnews.com/ (accessed January, 2015)

Ting, K., Zhu, J., Watkins, D. 2000. "*The Effects of Joint Clearance on Position and Orientation Deviation of Linkages and Manipulators*", Mechanism and Machine Theory, v 35, pp. 391-401.

Tsai, M., Lai, T. 2004 "*Kinematic Sensitivity Analysis of Linkage with Joint Clearance Based on Transmission Quality*", Mechanism and Machine Theory, v 39, pp. 1189-1206.

Tsai, M., Lai, T. 2008 "*Accuracy Analysis of a Multi-Loop Linkage with Joint Clearances*", Mechanism and Machine Theory, v 43, pp. 1141-1157.

University of Leeds WEB Site. https://www.leeds.ac.uk/ (accessed February, 2015)

Wikipedia WEB Site. http://en.wikipedia.org/wiki/Backlash_%28engineering%29 (accessed December, 2014)

Wikipedia WEB Site. http://en.wikipedia.org/wiki/Stewart_platform (accessed February, 2015)

Xu, L., Yang, Y., Li, Y., Li, C., Wang, S. 2012. "*Modeling and Analysis of Planar Multibody Systems Containing Deep Groove Ball Bearing with Clearance*", Mechanism and Machine Theory, v 56, pp. 69-88.

Zhang, X., Zhang, X., Chen, Z. 2014. "*Dynamic Analysis of a 3-RRR Parallel Mechanism with Multiple Clearance Joints*" Mechanism and Machine Theory, v 78, pp.105-115.

Zhao, D., Yi, J. 2003. "*Swing Up Pendubot with a GA-Tuned Bang-Bang Controller*", IEEE International Conference on Robotics, Intelligent Systems and Signal Processing, Changsha, China, pp 752-757.

Zhao, Y., Bai, Z.F. 2011. "*Dynamics Analysis of Space Robot Manipulator with Joint Clearance*", Acta Astronautica, v 68, pp. 1147-1155.

Zhu, J., Ting, K. 2000. "*Uncertainty Analysis of Planar and Spatial Robots with Joint Clearance*", Mechanism and Machine Theory, v 35, pp. 1239-1256.

APPENDIX A

DRIVER CONNECTIONS AND SET-UP

To drive the system for different operation modes some arrangements should be done. In this section, these arrangements and the cabling are described. Figure A.1 shows the control panel from the top. In this figure, five drivers and six electrical terminals are shown. The drivers as it mentioned in Chapter 3, drive the servomotor. Moreover, the electrical terminals transmit the signals from DAQ card to the driver.

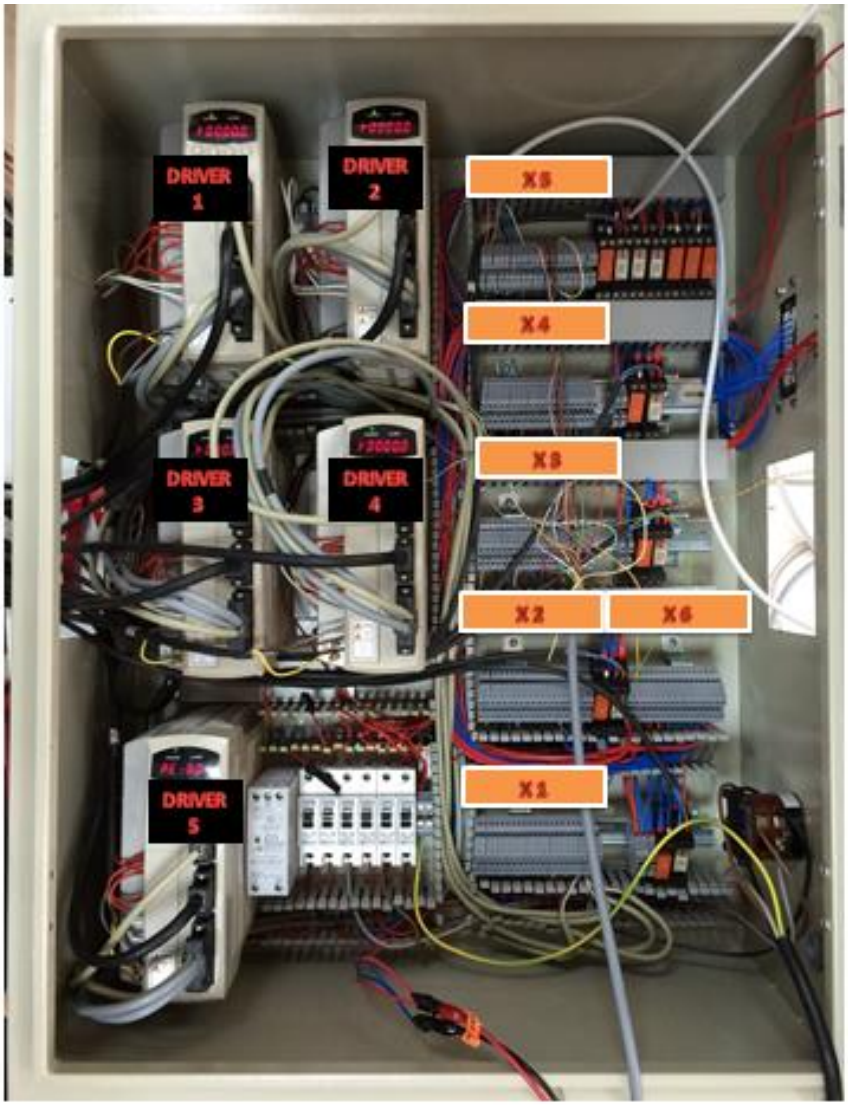

Figure A.1. Control Panel

In Figure A.1 electrical terminals, which are described as X, are shown. Each driver works with own electrical terminals, besides, the first two pins of the electric terminal X6 transmits the 5V from DAQ card to the control panel. For this reason, first and second pins of electrical terminal X6 attaches, independently from the other drivers. In Table A.1 electrical terminal X6 connections are listed.

Table A.1. Electrical terminal X6 connections

Electrical Terminal	Pin Number	Description	DAQ Pin Number
X6	1	5V +	28
X6	2	5V -	29

In this study, single DoF mechanism is driven by using 5^{th} driver and its electrical terminal X5. The connections of the electrical terminal X5 are listed in Table A.2.

Table A.2. Electrical terminal X5 connections

ELECTRICAL TERMINAL	Pin Number	Description	
X5	1	AO	ENCODER OUTPUTS
X5	2	/AO	
X5	3	BO	
X5	4	/BO	
X5	5	ZO	
X5	6	/ZO	
X5	7	OPC ZO	
X5	8	GND	
X5	9	SPDLMT	ANALOG OUTPUTS
X5	10	TRQLMT	
X5	11	GND	
X5	12	MON1	ANALOG INPUTS
X5	13	MON2	
X5	14	GND	
X5	15	PF+	LINE DRIVE FOR POSITION OPERATION MODE
X5	16	PF-	
X5	17	PR+	
X5	18	PR-	
X5	19	SVON	SERVO ON
X5	20	Internal usage	
K13	14	BRAKE +	BRAKE CONNECTIONS
K13	24	BRAKE -	

In every electrical terminal, same attachments aare used. The first 8 pins of the electrical terminal are used to encoder outputs. From 9 to 11 pins are used to analog outputs which are speed and torque outputs. From 12 to 14 pins are used to analog inputs. In addition to that, the pins from 15 to 18 are used to servo line drive, for this reason these pins are just used when the system is driven in position operation mode. Moreover the 19th pin are used to system servo on.

For encoder output attachements, because of using quadrature encoder, three signals are attached which are A,B and index input. The connections between the

electrical terminal and Humusoft 614 DAQ card are listed in Table A.3. Note that these connections are attached on the X2 connector.

Table A.3. Encoder connections

ELECTRICAL TERMINAL	ENCODER OUTPUTS	PIN NUMBER
AO	IRC2A+	13
/AO	IRC2A-	14
BO	IRC2B+	15
/BO	IRC2B-	16
OPC ZO	+5V	28
GND	GROUND	29

The speed and torque analog outputs are attached in Table A.4. These connections are attached on the X1 connector.

Table A.4. Analog output connections

ELECTRICAL TERMINAL	ANALOG OUTPUTS	PIN NUMBER
SPDLMT	DA2	24
TRQLMT	DA3	23
GND	GND	29

The speed and torque analog inputs are attached in Table A.5. These connections are attached on the X1 connector.

Table A.5. Analog input connections

ELECTRICAL TERMINAL	ANALOG INPUTS	PIN NUMBER
MON1	AD3	4
MON2	AD6	7
GND	GND	29

After these connections are attacheed, servo on/off connection is executed. Since lack of current, voltage is not reached the desired level. To solve this problem, H bridge is used. H bridge connections are illustrated in Figure A.2.

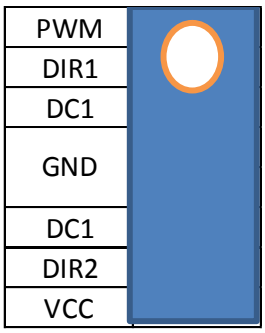

Figure A.2. H bridge connections

VCC and GND are the power pins of the H bridge. +5V is attached to the VCC and ground is attached to the GND. Then two ground pins are attached to each other. In addition, DIR2 pin is attached to the PWM pin. Then digital output signal, DOUT3 which is the pin number 33, is attached to the PWM pin of the H bridge. And finally, DC1 pin of the H bridge is attached to the Servo ON.

After cables are attached to the right places in the control panel and DAQ card, the driver is calibrated for the purpose. To calibrate the driver, first operation mode is selected in the driver menu PE-601 and it is listed in Table A.6.

Table A.6. Operation Mode

PE-601	0	Torque Op. Mode
	1	Speed Op. Mode
	2	Position Op. Mode
	3	Speed/Position Op. Mode
	4	Speed/Torque Op. Mode
	5	Position/Torque Op. Mode

After the operation mode is determined, rated speed is edited in the menu PE-216 as 3000 rpm. Then encoder type is selected in PE-203. Next, encoder pulse are entered in PE-204 as 3000 p/r . After that input signal type is selected in PE-701 as in the Figure 3.6 in Chapter 3. At last, electronic gear ratio is calibrated by using PE-702 and PE-703.

APPENDIX B

MEAN of the IMPROVEMENTS

The results of the improvements of the mean deviation in position operation mode when using input shaping ZVDD method is listed in below. As an experimental test, step and double step inputs are used. Step inputs are separated in two classes: low jerk value step inputs and high jerk value step inputs. As high jerk value step input, three different step inputs, 20°, 10°, 5°, are tested. The improvement of the mean deviations of these inputs is listed in Table B.1, Table B.2 and Table B.3 respectively.

Table.B.1. Mean deviations of the steady-state responses of the system for step input 20° degrees

	without is	with is
1	0.270	0.014
2	0.307	0.007
3	0.307	0.011
4	0.308	0.015
5	0.318	0.016
6	0.334	0.014
7	0.271	0.010
8	0.302	0.013
9	0.283	0.011
10	0.332	0.018
mean	0.303	0.013

Table.B.2. Mean deviations of the steady-state responses of the system for step input 10° degrees

	without is	with is
1	0.138	0.014
2	0.110	0.009
3	0.148	0.008
4	0.142	0.025
5	0.151	0.021
6	0.127	0.008
7	0.163	0.013
8	0.145	0.021
9	0.115	0.025
10	0.171	0.016
mean	0.141	0.016

Table.B.3. Mean deviations of the steady-state responses of the system for step input 5° degrees

	without is	with is
1	0.105	0.014
2	0.081	0.038
3	0.086	0.035
4	0.080	0.040
5	0.064	0.014
6	0.088	0.024
7	0.103	0.010
8	0.078	0.033
9	0.090	0.020
10	0.078	0.026
mean	0.085	0.025

In Table B.4, the results of a mean deviation of the 56° degrees low jerk value step input are shown.

Table.B.4. Mean deviations of the steady-state responses of the system for step input 56° degrees

	without is	with is
1	0.242	0.055
2	0.242	0.050
3	0.242	0.050
4	0.290	0.022
5	0.226	0.029
6	0.219	0.073
7	0.295	0.046
8	0.219	0.015
9	0.236	0.066
10	0.284	0.019
mean	0.249	0.042

After the results of the mean deviations are given for step input, the results of the double step input are listed in Table B.5.

Table.B.5. Mean deviations of the steady-state responses of the system for double step input 16° degrees

	without is	with is
1	0.273	0.027
2	0.266	0.019
3	0.288	0.018
4	0.265	0.026
5	0.288	0.020
6	0.286	0.020
7	0.277	0.025
8	0.284	0.022
9	0.263	0.023
10	0.281	0.023
mean	0.277	0.022

The improvement is percentage comes out to be at (0.303-0.013)/ 0.303=95.7% for 20° step input, the improvement is percentage comes out to be at (0.141-0.016)/ 0.141=88.6% for 10° step input, the improvement is percentage comes out to be at (0.085-0.025)/ 0.085=70.5% for 5° step input. For low jerk value step input, 56°, the improvement is percentage comes out to be at (0.249-0.042)/ 0.249=83.1% and the improvement is percentage comes out to be at (0.277-0.022)/ 0.277=92.1% for the double step input. The all mean of the improvements values are listed in Table B.6.

Table B.6. Mean of the improvements

Outputs	Mean of the improvements
Step output 20° degrees	95.7
Step output 10° degrees	88.6
Step output 5° degrees	70.5
Step output 56° degrees (low jerk value)	83.1
Double step output 16° degrees	92.1